UNIVERSITÀ DEGLI STUDI DI PALERMO
DEPARTMENT OF ENGINEERING
Doctorate in AIM HIGHEST

Fractional Calculus in Cellular Processes: A Caputo Approach to Endocytosis

SSD CEAR-06/A

PH.D. THESIS OF
ENG. GIANMARCO NUZZO

DOCTORATE COURSE COORDINATOR
PROF. GIUSEPPE CAMPIONE

TUTOR
PROF. MASSIMILIANO ZINGALES

XXXVI CYCLE ACADEMIC YEAR 2023-2024

 olti di quelli che vivono meritano la morte,
e molti di quelli che muoiono meritano la vita.
Tu sei in grado di valutare, Frodo?
Non essere troppo ansioso di elargire morte e giudizi.
Anche i più saggi non conoscono tutti gli esiti.

Gandalf, *Il Signore degli Anelli: La Compagnia dell'Anello*,
diretto da Peter Jackson, 2001.

Contents

Chapter 1

Introduction

This chapter aims to provide a brief overview of the research done during the three years of doctoral studies. First, a brief introduction of the problem addressed will be made, in order to fully understand the reasons and motivations behind this work, the need and possible clinical applications that may be done. Next, the state of the art will be presented and then the achieved studies over the decades by researchers on the topic, which have helped to shed light on ongoing research and what it's still missing. Finally, the results obtained will be presented.

1.1 Problem description

Over the centuries, biology, i.e., the science that studies living systems, has been of extreme interest because of it we have been able to understand how organisms function, their biochemistry, anatomy and physiology. As technologies have advanced, it has been possible to obtain more and more information about species, especially humans.

For example, several investigations exist through which the human genome is being studied to progressively obtain knowledge about human DNA with the goal of understanding the diseases that may affect people. Here, engineering also plays a key role. There are many mathematical models that from an engineering perspective lead to an understanding of the biological functions of the cells that make up the human body [1]. Specifically, the focus of this research work was on the mathematical modeling behind the processes of endocytosis that occur across the cell membrane.

The cytoplasmic membrane, common to every cell type, delimits it from the extracellular matrix (ECM), i.e. the external environment. It consists of a phospholipid bilayer, in which a single component is distinguished by having a hydrophobic tail and a hydrophilic head. The membrane is the only means by which the cell receives nutrients from the outside, exchanges signals, which may relate to cell differentiation, tissue repair, or unfortunately if transmitted incorrectly, the onset of diseases such as cancer.

Endocytosis is a biological process by which the internalization of nutrients, particles and more generally extracellular material occurs through the passage

allowed by the cell membrane. The term "endocytosis" was coined by Christian de Duve in 1963, although the concept itself dates back to the late 19th century. The process of cell regulation is ensured precisely by endocytosis. This phenomenon also enables the removal of dead and aged cells, as well as also supporting immune regulation. If this biological process fails, pathologies can occur and interfere with normal human life. Several diseases that are widely spread in the population can be traced precisely to a malfunctioning of the endocytosis process, including cancer, neurodegenerative diseases, diabetes and cardiovascular diseases, and many others.

Therefore, endocytosis has a fundamental function in the therapeutic pathway: it is the vehicle by which the delivered therapies reach all the cells. Reason why endocytosis is a widely studied process, not only in biology and pharmacology, but also by the more technological and engineering areas [2]. The endocytic pathway is also of interest to accelerate the development of gene and drug delivery tools, as well as for assessing the potential hazard of nanotechnology on human health.

Biological processes involve different types of endocytosis pathways. One of the most important is the receptor-mediated endocytosis, among sereval others as diffusion and protein-canal trafficking, with which viruses and bioparticles can enter or leave an animal cell. Viruses and intra-cellular bacteria exploit the endocytosis process to access the protective cell micro-environment to grow and reproduce. They have thousands of different shapes and sizes with a characteristic size in the range of tens to hundreds of nanometers. Virus are equipped with a limited amount of nucleic acid, and they propagate by parasitizing host cells and multiplying their viral nucleic acid and protein capsid via the biochemical machinery of the host.

It takes only 20–40 min for many bacteriophages to finish one life cycle from infection to lysis. For most animal viruses entering and leaving a host cell are mediated by specific binding of outer coat proteins (such as hemagglutinin in the case of influenza viruses) to specific mobile receptors on the host cell surface. It has been generally assumed that the endocytosis of viruses is associated with the formation of a clathrin coat at the inner membrane leaflet [3].

Typically, clathrin coats can generate a membrane radius of curvature as small as 50 nm. The formation of such small buds has been explained in terms of the bending elasticity concept by considering topological defects of the clathrin network [4]. However, more recently it has been shown that influenza viruses can enter cells even if the formation of clathrin coats are inhibited. Indeed, there are several other kind of non-conventional endocytosis mechanisms involving multiple pathways that will be discuss in details in Chapter 2, such as caveolae, and macropinocytosis. Viruses have been shown to use all of these during the viral infection.

1.1.1 The rationale behind

In recent times, various researches have been conducted to understand the mechanisms involved in the uptake of biomolecules by cells, so that they can

be exploited, for example, to understand ageing, the controlled release of drugs, the development of tumours and possible metastases, and virus infection.

A present-day case example, so that demonstrates the need to study and investigate the processes behind endocytosis, comes from the global pandemic epidemic in 2020 caused by the SARS-CoV-2 virus, which has spread globally with more than 697.000.000 cases and close to 7.000.000 of deaths (Worldometers website, updated on November 2023).

This virus is the responsible for the acute respiratory disease COVID-19 (COrona VIrus DIsease 19), that led the world population to declare a state of health emergency, owing to the fast spread of the disease since it is highly contagious. In Italy, the state of emergency COVID persisted from March 2020 to March 2022. This period saw events that had never happened before: closure of industries, schools and universities, isolation of people at home, who were unable to go out unless to buy primary necessities (food, drinks, medicines...) or if they were medical workers for example [5][6][7]. The pandemic gave the initial idea for this thesis work.

During the early investigation of world-spreading infection of SARS-CoV-2, preliminary evidences suggest that infection with SARS-CoV-2 may begin in the upper respiratory tract, e.g. in the nasal epithelium, which expresses the highest levels of SARS-CoV-2 receptors18. The clinical pathological features of COVID-19 include cough, fever and pneunomia [8]. The most significant morbidity and indeed mortality, however, appears to be associated with a further, severe stage of the disease, when infection spreads to the lower airways of the lung, resulting in respiratory failure, and possibly multi-organ failure due to cytokine storm. In the upper respiratory tract clathrin-based endocytosis may be a good candidate to explain the cell infection, but, in the lower part of the respiratory duct a different mechanism to infiltrate the pneumocytes seems to be involved due to the lack of SARS-CoV-2 receptors along the cellular membrane.

Hence, SARS-COV-2 virus is responsible for employs the receptor-mediated endocytosis (see Figure 1.1), i.e., one of the mechanisms adopted by proteins to permeate the cell membrane and infect the host. Coronaviruses are enveloped and plus-strand RNA virus [8] that involve four different proteins in which the viral genomic RNA is encapsulated. These proteins are the: spike and membrane glycoproteins, nucleuocapsid and envelope proteins [8]. All of these components represent the major contributors of the endocytic pathway that lead to the infection of the host cells [9].

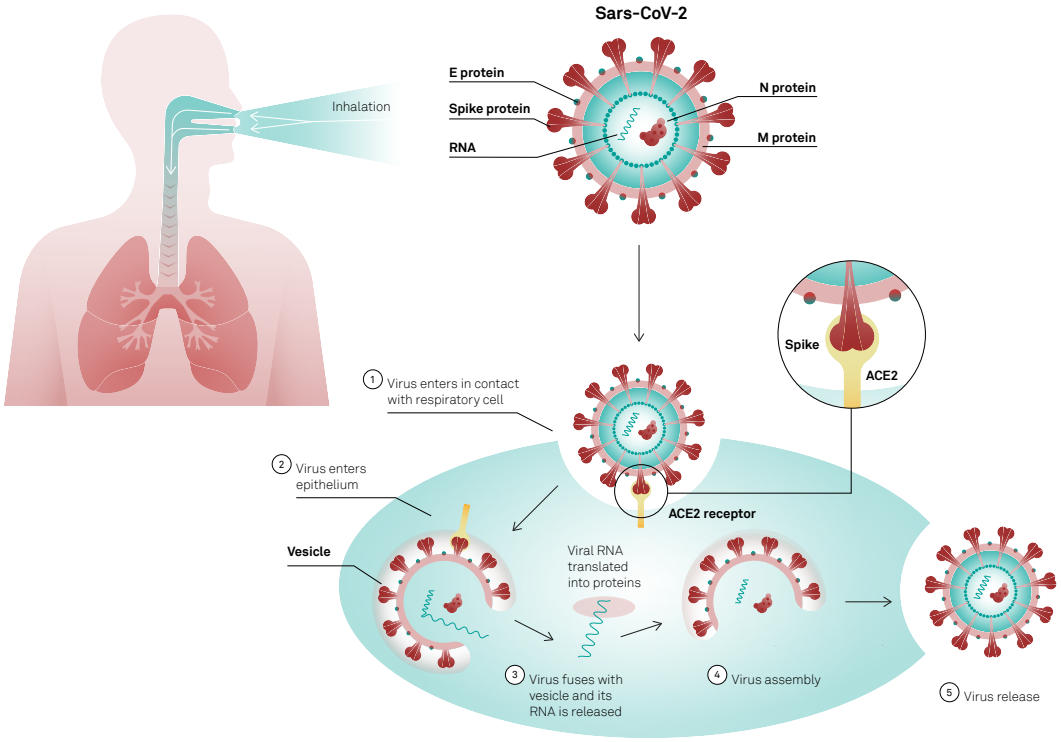

Figure 1.1: The steps of the entry mechanism via endocytotic pathways of the COVID-19: 1) The virus enters in contact with the respiratory cell through the airways. Here the ACE2 receptor allows to the virus to enter inside the host epithelial cell; 2) The virus enters inside the epithelium after that is fususes with a vesicle, 3) The vescicle is opened and the RNA of the virus is relleased. Here, the viral RNA is translated into proteins; 4) The virus is again assembled; 5) The virus is realised outside the host cell.

Specifically, the membrane protein (M protein) is a membrane integral, the most abundant one in the virus, whose function is going to organize the assembly between coronavirus virions through the protein-protein interactions that occur between the M proteins and the other three proteins in the virus. The N protein is responsible for the packing of the virus genome [10]. The E protein is one of the virus structural proteins whose function relates to the virus life cycle and the pathogenesis process. Many therapeutic agents that have been developed and are still under development are produced aiming to directly target these E proteins, hence proving to be the drug targets that could inactivate the virus [11].

Finally, the spike proteins (S protein) are the mainly responsible for the entry of the virus inside the host cells, by ensuring the receptor-binding and the membrane fusion process. They are composed by two functional sub-units, S1 and S2, where S1 is the responsible for the mediate receptor binding, while S2 is the responsble for the membrane fusion. The S proteins binds to the angiotensin-converting enzyme 2(ACE2) through adhesive strength and forces exchanging with each other [12] owing to the presence of its receptors-binding domain (RBD). These proteins, also, are one of the main target for neutralization antibody of the virus [13][14]. Indeed, considering the whole spike proteins,

RBD is the most immunologic zone of the virus, thus also representing the target for vaccination and antibody drug therapies [15].

The entry mechanism via endocytic pathways of the COVID-19 virus follow several steps [15][14]. After the virus nanoparticles are transmitted through the airways (even though the virus is able to infect by several ways, including via surfaces for example), it comes into contact with the cells of the respiratory tract (step 1, Figure 1.1). The virus enters into the cell membrane binding with the ACE2-receptor though the receptor-binding domain (RBD) of its spikes [15]. ACE2 is a cell surface membrane protein located on the surface of many cells. Its normal biological function is to provide an essential biochemical pathway for the regulation of processes such as blood pressure, wound healing and inflammation, called the renin-angiotensin-aldosterone system (RAAS) pathway [8][16], but it was found that ACE2 protein expresses not only in the heart and kidney, but also in the human lung epithelia and small intestine [17].

However, ACE2 acts as a key to the membrane access lock for the SARS-CoV-2 virus, thus ensuring that the virus can cross the cell membrane and enter inside the cell . Then, ACE2 works as a receptor for the virus, providing access to the cell. Hence, the virus is incorporated and enters into the epithelium (step 2, Figure 1.1). Subsequently, the virus fuses thorugh a vescicle with the host cell membrane [14], and releases its RNA (step 3, Figure 1.1). Here, the RNA is translated and read through complex biochemical processes. Once the virus is reassembled (step 4, Figure 1.1), it is released (step 5, Figure 1.1), and from here, then, the immune response of the human defense system will be triggered.

Indeed, understanding the role of the endocytic pathway in the viral entry or for a nanoparticle entry inside the host cells and then modelling the mechanics of the process might represent the breakthrough in the understanding of the virus infection. This could represent a great tool to be used in the clinical practice to develop new treatments of disease provoke for example, by COVID-19. Therefore, owing to the overwhelming importance of this biological process, which is not only physiological but also pathological, several biomechanical models have been proposed to describe the endocytosis process and understand how a virus or a functionalised particle comes into contact with the cell by being endocytosed, but none of them has been comprehensive enough, leaving out, for example, natural characteristics of the cell, such as its membrane non-homogeneity.

The aim of this study was to provide a new model in which a spherical-shaped virus, such as the coronavirus, or any generic nanoparticle exploits the mechanism of receptor-mediated endocytosis to enter the cell, considering the properties of a real membrane through the use of fractional calculus. The use of a reliable mathematical model to describe the mechanism beyond receptor-mediated endocytosis represents a good chance to predict with reasonable accuracy the spread of virus infection as well as the possible therapeutic interval.

1.2 State of the art

In the past two decades, several papers have been published that have attempted to capture the essence of the phenomenon of receptor-mediated endocytosis with their models about viruses or nano-particles. Below, a brief overview is done about the mathematical modelling of this biological process as reported in the literature. Therefore, the models considered relevant for this dissertation will be discussed in more detail in Chapter 3.

Several models have been established to elucidate the mechanism of virus budding on a host membrane. Simons and Garoff [18][19] suggested that the viral capsid may wrap itself in the host membrane via thermal fluctuations of the membrane where the host cell membrane proteins move from the viral glycoprotein patch simply for steric reasons, thus allowing the generation of virus specific patches.

In 1993, Lerner et al. proposed a mathematical modelling for several possible rate-limiting processes to explain virus budding and found that a nonzero spontaneous membrane curvature may be necessary to ensure a wrapping time in accordance with the experimentally observed upper limit of 20 min. They also observed that as the membrane wraps around the capsid, water must be removed between the membrane and the capsid itself. This phenomenon naturally slows down the speed of coiling, thus falling within the budding time of 10-20 min, which is within the experimentally determined upper limit.

Recently, van Effenterre and Roux [20] and Tzlil et al. [21] developed statistical thermodynamics models of virus budding. Their work was important in understanding how the membrane bending energy is apparently relevant for dynamic properties of bud formation, starting with the time when a nucleocapsid arrives at the cytoplasmic surface of the cell membrane and ending with its release coated by a membrane of lipid spikes, into the intercellular space. They derived a relationship between the volume concentration of viruses and the budding time, and they identified an optimal volume concentration of internalized particles for budding. Their model is valid in the case where the time spent by colloids on the surface is large compared to the time it takes for free receptors to diffuse to the surface and find a colloid. All of these models are based on the assumption of a specific particle size. The questions of whether and how particle size affects the dynamics of entry (endocytosis) or exit remains largely unresolved.

At the beginning of the last decade some papers attempted to shed light on this mechanism showing how a cell membrane containing diffusive mobile receptors wraps around a ligand-coated cylindrical or spherical particle. It was shown by Gao et al. [22] that particles in the size range of tens to hundreds of nanometers can enter or exit cells via wrapping even in the absence of clathrin or caveolin coats, and an optimal particles size exists for the smallest wrapping time. The ligands have been assumed to be immobile and uniformly distributed on the particle surface, whereas the receptors are mobile and undergo rapid diffusive motion in the plane of the cell membrane.

The receptors on the cell membrane diffuse to the wrapping site and bind

with the ligands on the particle surface to lower the free energy of interaction. Because cells are generally much larger than viruses, the particle was considered in its interaction with an initially flat membrane. The receptor-ligand binding causes the membrane to locally wrap around the viral particle at the cost of elevated elastic energy associated with increased local curvature of the membrane and reduced configuration's entropy associated with receptor immobilization.

Therefore, for such adhesive contact between cell membrane and particle, the mathematical framework developed in recent studies of curved biological membranes spreading on a flat substrate was adopted by Freud et. al [23] and Shenoy et. al [24], where results were found in good comparison with experimental observations [25][26] on spreading of giant vesicles on integrin-coated substrates. Freud's mathematical model [23] aimed to examine the role of binder mobility in the spontaneous adhesive contact of one surface with another. The phenomenon was characterized as spontaneous for a long time because there was the idea that the adhesive bond forms without the expenditure of external energy.

However, through his work Freud was able to show how this phenomenon evolves with a continuous expenditure of total free energy. The mathematical model, that pursued the idea of the evolution rate being controlled by the ligand mobility, was able to give an accurate representation of the adhesion process in animal cells. Insteed, Shenoy et al. [24] have considered the dynamics of adhesion fronts in cells and vesicles, which grow as a result of ligand flux that reaches the frontier by intramembrane diffusion. Their work allowed demonstrating how the front motion mediated by ligand diffusion is unstable to perturbations of its shape. Remarkably, from a mathematical perspective, the instability studied in this work was similar to other instabilities studied in non-equilibrium physics, in which the interface motion is determined by the solution of a partial differential equation (Euler or Navier-Stokes equation, Laplace equation, and heat equation).

The distribution of receptors in the membrane was determined by solving the problem of diffusion in a plane. In other recent studies [27][28] the effect of the elasticity of the particle uptake was accounted for in the analysis to achieve a more realistic endocytosis time. The analysis is always achieved accounting for the Helfrich-type membrane elasticity and some additional contribution related to the presence of receptors as well as to the membrane stress induced by moving receptors is included in the expression of membrane dissipation rate so that the governing equations have been obtained by stationary conditions.

Very recently a specific research that accounts the presence of the configurational change of receptors due to G-Reactive Protein (GPR) on cell membrane have been published by the stochastic structural biomechanics group of the University of Palermo Engineering Department in cooperation with research groups belonging to University of Carnegie-Mellon (USA), University of Trento (Trento, Italy), University of Pittsburgh (Pennsylvania, USA) and University of Naples "Federico II" (Naples, Italy).

The study, accounting for a modified version of the Helfrich membrane energy incorporates additional variables that are related to the change of state

order-disorder of the lipid bilayer that compose cell membrane and it is capable to capture the formation of lipids rafts in cell membrane. Lipid rafts are found, indeed, in presence of receptor clustering "receptors live on lipid rafts" after Nobel prize [29] and the mechanical model presented is capable to capture these important phenomena [30].

A very recent study from Nuzzo et. al [31] has focused on diffusion model which represents the membrane receptor motion with respect to viral endocytosis in the context of applied mechanics. The unexpected behavior of receptor density shifting from higher concentrations in the unbound phase to lower concentrations within the right-hand side of the virus surface is accounted by introducing a mechanical drift term into the governing mechanical equation, so that the concentration difference, higher in the bound phase and lower in the unbound phase, is bounded and the lower in the unbound phase is accounted for in receptor motion. In addition the authors added a non-Gaussian diffusion model in terms of fractional generalization of Fick's law.

1.2.1 Endocytosis models so far

Receptor-mediated endocytosis is one of those biological systems that can be handled by mathematical modeling. Several attempts have been made over the years to define, describe, and analyze the phases of this complex biological process with the help of mathematical models. Indeed, the two approaches through which the biological phenomenon can be described are from kinetical and mechanical perspectives [32].

One of the first models found in the literature was from 1997. Dee et al. [33] focused on quantitative understanding of virus trafficking aiming to help in the treatment of virus-mediated diseases, specifically in optimizing the production of vaccines and recombinant proteins. They have created a mathematical model that explains the multivalent binding formation of the virus with cell surface receptors. They were able to accurately mimic the virus trafficking that had occurred experimentally.

Specifically, the research work in this thesis for modeling receptor-mediated endocytosis was inspired by a few models which were considered appropriate and worthy, through which the research goal was then achieved. The pivotal article, from which later models were based, is from Gao et. al [22]. Their work started from the concept that the process of viruses entry and exit from animal cells is mediated by the binding interaction between viral capsid ligand molecules and their receptor molecules. Hence, their research question was related to how indeed could the size of a bioparticle affect receptor-mediated endocytosis? Hence, the authors studied how a cell membrane containing mobile diffusive receptors envelops a cylindrical or spherical ligand-coated particle.

They considered that during the process in which the virus permeates the host cell, there may be thermal fluctuations of the membrane itself and hydrodynamic interactions. In order to consider these factors, they introduced a simplified form of free energy, which completes the model whose solution is found numerically. It has been shown that the process is dependent on the

radius of the bioparticle, so that if this exceeds a threshold value, there is a limited number of receptors for which the nanoparticle cannot be phagocytosed. As conclusive remark, with their mathematical model, they demonstrated how particles ranging in size from tens to hundreds of nanometers can enter or exit cells through the envelope even in the absence of clathrin or caveolin coatings. However, they found that there is an optimal particle size to achieve the smallest coiling time. In addition, their model can be extended to include the effect of the clathrin coat.

Additionally, in subsequent study (Yi et al.)[27], they showed how the kinetics of receptor-mediated endocytosis of elastic nanoparticles is limited by receptor diffusion, and specifically about how the speed of uptake depends on the stiffness and size of the nanoparticle, membrane tension, and binding strength between membrane receptors and ligands. This established that soft nanoparticles are energetically less prone to complete coiling than rigid ones, the uptake rates for the first are kinetically faster than the second one.

The work of research group of Gao [22][27] is landmark because it allowed a mathematical interpretation of the receptor flux that mediates the endocytosis process as no one else had ever done, as well as determined the optimal size to terminate the coiling process in the shortest possible time. Owing to which, his work has since been a source of inspiration for many other researchers. Among them are Li et. al.[34] and Zhang et al. [35][36] whose investigated the topic on cellular uptake of biophysical factor-dependent nanoparticles (NPs) through receptor diffusion-mediated endocytosis, considering the topic's relevance on pathology, cellular immunity, and drug delivery systems. They focused on the role of the ligand distribution on the surface of nanoparticles in the endocytotsis process mediated by receptor.

Li et. al [34] used a statistical model of receptor diffusion-mediated endocytosis statistical dynamics, aiming to study cellular uptake dynamics dependent on ligand distribution. They considered that ligand-receptor complexes drive to overcome the membrane deformation resistance and changes in the receptor configuration entropy. Hence, they were able to show how the internalisation of nanoparticles is highly dependent on the distribution of ligands and how the process of uptake by the cell is more favoured when the distribution of ligands is more uniform. Their finding is quite important since it shows how endocytosis ensures a robust ability of virus infection to enter host cells.

Furthermore, their results have also shown that optimal ligand distribution is associated with maximum cellular uptake efficiency, which is slightly dependent on the ligand distribution pattern and receptor density itself. From here, they also highlighted how the location of the initial contact point is another influencing factor in dynamic packing, thus explaining why most enveloped viruses exhibit a nearly homogeneous distribution of ligands. This characteristic is key in controlled drug delivery systems.

Zhang et. al. [35][36] focused on the effect that nanoparticle shape and stiffness have in interacting with the cell in pathology, cellular immunity and drug delivery systems. Hence, their research questions were related to how the ligand distribution can influence the membrane envelopment of non-

spherical NPs under the influence of cytoskeleton deformation. The physical and biological problem was addressed by using a coupled elasticity-diffusion model to systematically study the role of ligand distribution in the cytoskeleton-associated endocytosis of ellipsoidal NPs for different shapes, sizes, cytoskeleton stiffness and initial receptor density.

In this model, they considered the effects of receptor diffusion, receptor-ligand binding, cytoskeleton and receptor-ligand deformations, cytoskeleton and membrane deformations, and changes in receptor configuration entropy. Their study results showing that the uptake process can be significantly influenced by the ligand distribution. They identified an optimal state of this distribution, which corresponds to the fastest uptake efficiency, proving how this depends on the aspect ratio of NPs and the stiffness of the cytoskeleton. Lastly, they also identified how the optimal distribution is sufficiently high in the region of large curvature and that the optimal state of NP entry into cells can tolerate slight changes from the corresponding optimal ligand distribution. Their study has been extremely important in providing guidelines for controlling NP-cell interactions and improving the efficiency of target drug delivery systems.

Another very remarkable research work is by Wiegold et. al. [37]. The work concerns receptor-driven endocytosis, which is typical of viral entry into a cell. They developed a two-dimensional model of a virus undergoing endocytosis. In their model, the virus is treated as a substrate with fixed receptors on its surface, while the host cell's receptors are free to move across its membrane, allowing a local variation in their concentration. They also considered the membrane bending, which inflects forming an envelope around the virus. The novelty of the model is the additional conditions added based on energetic considerations as the virus advances towards the membrane. Several factors such as mobility, receptor density and virus size play crucial roles in the duration of endocytosis. This study shows that the duration of the process increases considerably when the size of the virus reaches a critical value and that too high or low values of binding have negative consequences on the beginning of the process.

Other mathematical models worth mentioning are by Richards et. al [38], Shen et. al [39], Tang et. al [40] and Rismanian et. al [41]. Richards et. al mathematically modeled the virus encapsulation by the cell, but unlike literature studies, they utlized biologically relevant shapes outside of the spherical one such as ellipsoids, capped cylinders, and hourglasses. Based on the nanoparticle shape type to be encapsulated by the cell, they found different encapsulation behaviors and rates.

Hence, it is shown that drug treatments should take into consideration not only the process mechanics but also to particle shape considered. Concerning other mathematical modeling for this process, Rismanian et al [41] decided to develop an analytical model in which the receptor difussion process along the cell membrane was modeled as a non-Fickian process. This modeling brings novelty in the literature, although the modeling according to the classical Fick process always appears to be the best one to consider.

In addition, there are also numerical simulation studies of the receptor-mediated endocytosis processes, since from the experimental point of view it is

complicated, if not feasible in reality, actually to reproduce and simulate these biological processes.

Specifically, a relevant study is conducted by Shen et. al [39]. They proceeded with numerical dynamic simulations of the receptor-mediated endocytosis process of elastic nanoparticles (NPs) with different sizes (from 25 to 50 nm), also varying to the shape of them, using spherical, oblate and prolate shapes. Through their numerical simulation, they were able to demonstrate accurately and clearly how nanoparticle wrapping, during receptor-mediated endocytosis, results from the combined phenomena of receptor diffusion kinetics and thermodynamic driving force. Specifically, diffusion kinetics relates to the kinetics of receptor recruitment that are involved in the process and is dependent on the contact edge length between nanoparticle and cell membrane. While instead, the thermodynamic driving force relates to the free energy required for the nanoparticle to be incorporated inside the cell.

Another numerical simulation study of the endocytosis process is from Tang et. al [40]. In their study, other than simulating the wrapping process, they considered the rotation that the nanoparticle experiences as a result of the uptake. This phenomenon may be ignored when considering a spherical particle, but when more complex shapes are considered it becomes critically important. By including the rotational factor of the nanoparticles, they were able to create a model through which it is possible to evaluate how the incorporation rate of the NPs also depends on the rotation that occurs during the process. These types of numerical simulations represent an additional tool for understanding the mechanics behind this very complex biological process.

Therefore, the literature review has provided the groundwork necessary to understand how academics have engaged in modeling this complex biological process. As conclusive remark, there are multiple modelings of receptor-mediated endocytosis; however, none of these studies take into account the non-homogeneity of the cell membrane that influences endocytosis.

1.3 Results

In view of the neglected aspects a new mathematical modelling is needed. Hence, in this research work, we analysed receptor-mediated endocytosis by formulating a new model, in which a potential acts on the receptors, guiding them to the zone where the virus will be absorbed.

In addition, the fractional calculation tool took into account the inhomogeneity of the cell membrane during receptor influx. Given the complexity of the system, there is no analytical solution, so a numerical model was implemented. The method of fractional finite differences was used to mathematically solve the model, which is governed by a non-linear set of differential equations including a fractional partial differential equation. From the numerical solution, the trend of the membrane-virus interface as a function of time and the distribution of receptors for different orders of derivation of the fractional operator were obtained.

This work could be useful in understanding how virus and cell interact and

at what times the virus can be phagocytosed, taking into account the actual characteristics of the membrane. Furthermore, knowing the time taken for a particle with a certain radius to permeate the membrane could improve drug delivery for those patients where it is necessary for the active ingredient to act at the right time.

Chapter 2

Cellular Endocytosis

This chapter aims to provide an overview about the biology of the cellular membrane and the endocytosis processes under study. Owing to the focus of this research work, this overview is crucial to understand how the mathematical and engineering modeling of the endocytotsis process is done based on the biological knowledge. First, a brief introduction will be provided on the importance of the regulatory transport processes, and so, the endocytosis proceess occurring along the cell membrane. This will be followed by a detailed biochemical description of the cell membrane and all its components. After this, the chapter will include an in-depth description of the main endocytosis processes, i.e. phagocytosis, macropinocytosis, and caveaolae-mediated endocytosis. Specifically, the final target will be the receptor-mediated endocytosis process, as it is the one studied and mathematically modelled in this thesis work.

2.1 Uptake overview

The transport regulation of molecules within eukaryotic cells occurs at the cell membrane from which it follow that the cell membrane is the main mediator of the mechanisms underlying the process of endocytosis. It separates and delimits the internal environment (i.e., cytoplasm) of the cell from the external one, thereby governing the exchange processes of elements and chemical substances essential to the cell's maintenance in life [42][35][36].

The molecules to be transported may be small, such as amino acids, sugars, or ions, which can be carried through the action of membrane protein pumps or directly by channels or carriers. However, when large molecules, i.e., macromolecules, have to bypass and cross the membrane via other means that involve the invagination and pinch off of the cell membrane. The latter is nothing more than the process of endocytosis.

Endocytosis process involves the ingestion process of nanoparticles, virus or microorganisms, in which a series of mechanisms occur that bring the target from the outside of the cell or its outer membrane to the inside. The process is used by the cell as a source of nutrition, defense and homestasis maintenance.

The discovery of endocytosis dates back more than a century ago from studies done on white blood cells, for understanding how they defend and attack

external agents read as a threat, through the process of phagocytosis [42][43]. Besides the controlling of nutrient exchanges and cellular homeostasis, the endocytosis processe plays a key role in the receptor signaling, cell migration, and many other cellular mechanisms [44][45][46][43].

Several types of endocytosis exist:

1. **Phagocytosis.** Process of engulfing large foreign materials and destroying them, characteristic of white blood cells for the immune response to destroy bacteria and foreign materials.

2. **Macropinocytosis.** Type of pinocytosis, it is the process by which the cell is able to intake liquid substances from the external environment that are useful for its metabolism

3. **Endocytosis mediated by caveolae.** Invagination process using caveolae that is independent from receptors, followed by transport of the material to cellular apparatuses to modify it and then make it available for reuse.

4. **Receptor-mediated endocytosis.** Process for the uptake of material using membrane proteins mediated by receptors, which recognize the material to be internalized. Typically, the material is then invaginated through clathrin proteins.

Once the products transposed across the membrane within the cell cytoplasm, these are carried away from the membrane and fused through membrane compartments involving the endosomal membrane system. These include early/recycling endosomes, multivesicular bodies, late endosomes, and lysosomes.

Based on the membrane compartment type, the endocytosed substance destinations are different, depending on the specific type of endocytosis by which they have entered the cell interior [42]. A description of the specific types of endocytosis process will follow below.

2.2 Cellular membrane

Biological membranes are difficult to investigate, not only molecularly but also structurally and functionally. The cell membrane in eukaryotes is the load-bearing cell structure, as the main metabolic processes occur at it. It is a thin covering with a variable thickness, depending on the type of cell considered, between 5-100 nm, which delimits the cell by separating the cell's outer extracellular environment from the inner cellular one [42][47].

Cell membranes are complex structures involving multifold components. They are composed mainly of proteins and lipids, which help to allow the membrane to form a real barrier between the cells and their environment. Depending on the type of cell, the membrane differs in its composition according to the function it performs. Howevear, all biological membranes have in common

a fluid bilayer consisting of phospholipid molecules, integral membrane proteins that across the entire bilayer, and preriferous memnbrane proteins presented on both membrane surfaces.

In 1895 Overton was the first to introduce the concept of a phospholipid bilayer membrane. He proposed that the main structure of the membrane consisted precisely of a lipid bilayer, thus revolutionizing the understanding of biology at the time [42][35][36].

During the 1930s, physiologists concluded that the lipid bilayer alone could not be the only component of the cell membrane, as it alone was incapable of providing the adequate mechanical properties typical of the cell membrane. Therefore, they proposed the existence of a protein coating to support the phospholipid bilayer that would, therefore, contribute to the extraordinary properties of the cell membrane as well [42][35][36][47].

In later years, the issues behind the structure and function of the cell membrane were still further explored. In the early 1970s, an early approach based on the analysis of frozen and split membrane electron micrographs confirmed that there are proteins crossing the membrane, from the surface bordering the extracellular matrix to the surface in contact with the cytosol. This thus confirmed the physiologists' assumptions of 40 years earlier, showing how the structure of the cell membrane was conferred not only by the phospholipid bilayer but also by a membrane proteins, acting equally as the one of the main functional components [48][42][35][36][47].

In the same years, the Fluid-Mosaic Mmbrane (FMM) model was theorized in 1972. The FMM model was introduced to provide a general, schematic and simple picture for the basic organization and dynamics of biological membranes considered at the nanoscale.

This model schematizes how proteins and the phospholipid layer are arranged in the cell membrane. This kind of structure is possible thanks to the hydrophobic and hydrophilic non-covalent interactions that occur between membrane components, specifically thanks to lipids which exhibit dual behavior, hydrophobic at one end and hydrophilic at the other. Indee, the model assumes that transmembrane proteins flow in what is the fluid of the phospholipid bilayer. Therefore, this structural fluidity is the main key that ensures all the major transport functions of the membrane [49][50][48][42][51].

Indeed, it is possible to observe different behaviors of the proteins inside the cell membrane. Proteins may exhibit dynamic behavior on the cell surface. Thus, some of them may spread freely, while others may be partially confined and so this enables them to flow across the membrane at alternate times. Some examples of proteins that are partially confined are cadherins and transferrin receptors. Finally, there may be membrane proteins that are denied any movement, thus resulting in immobility by direct or indirect connection with the cytoskeleton [42].

Therefore, the cell membrane structure is extremely complex given also the complex functions it is dedicated to, and thus has different types of proteins, receptors, and many other components (Figure 2.1).

The main functions of the cell membrane is to act as a selective permeability

barrier that is conferred by the phospholipid bilayer. Therefore, the membrane acts as a real gate, thus by going to regulate the entry or exit of substances within the membrane or to block its access.

Acting as a barrier, the cell membrane is able to enable the passages of substances through it in multiple ways: passive diffusion, channel-mediated transport, active transport or passive transport. The patterns of passage through membranes are different from each other and very complex. Briefly, the passage is generally regulated by a difference in the concentration gradient of the substances itself, or electrochemical gradient, or is mediated by transport channels or through the action of ATP [52][53][48][42][36].

In the following decades, many proteins have been discovered that characterise the cytoplasmic membrane either on its surface or across it. Furthermore, it was found that there is a network of cytoplasmic proteins that restricts the movement of many integral membrane proteins. This affects the density of proteins in cell membranes, which is consequently much greater than that illustrated in a simplified manner in Figure 2.1.

A description of the cellular membrane components will now be provided in the next section.

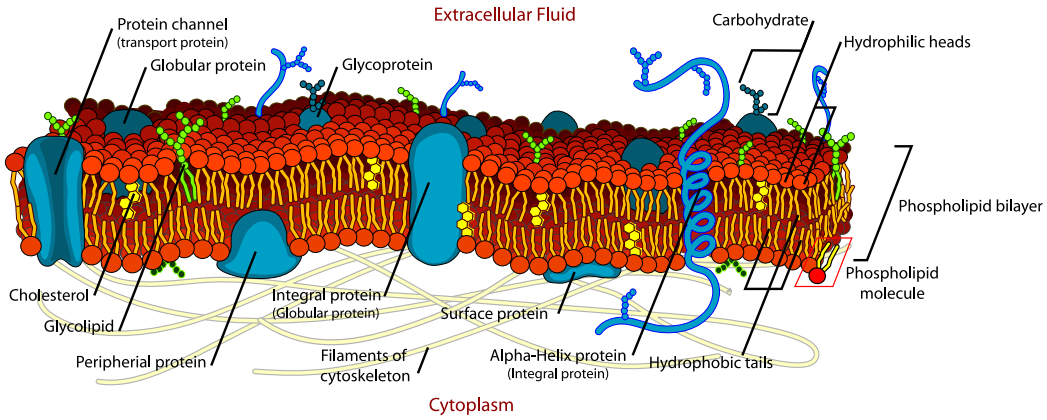

Figure 2.1: Representative composition of the cytoplasmic membrane of a eukaryotic cell. The main component are represented briefley: the extracellular fluid and the cytoplasm; the protein components, such as integral and peripheral proteins; the lipid components that create the phospholipid bilayer; the sterols components, such as cholesterol. [Source: Wikimedia Commons].

2.2.1 Lipids

Lipids are the building structure of the cell membrane. They play the important roles of anchoring proteins to the membrane surface, storing energy and transporting information in and out of the cell. Specific regions of lipids, so-called "lipid rafts" (see Fig. 2.2) in the cell membrane are recognized as an agglomeration of lipids and proteins.

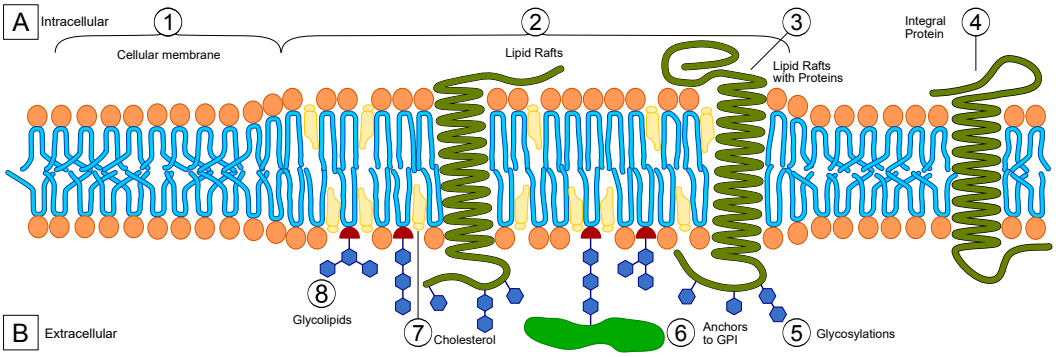

Figure 2.2: Representative organization of the lipid rafts: A) intracellular environment; B) extracellular environment; 1) Cellular membrane structure with phospholipid bilayer, without other components; 2) Lipid rafts; 3) Lipid raft with membrane proteins; 4) Integral protein; 5) Glycosylations, link between a protein and a molecule of glucose; 6) Glycosylphosphatidylinositol anchors to membrane protein; 7) Molecule of cholesterol; 8) Glycolipids. [Source: Wikimedia Commons].

The lipid rafts are identified by a small, heterogeneous, dynamic region (10-200 nm) composed of sterols, glycosphingolipids, and phospholipids. The lipid raft has the peculiar characteristic of being characterized by micro-domains in the phospholipid bilayer where areas with a higher density of packing of lipid molecules around specific lipids go [54][55][42][47].

The main membrane lipids include the following:

1. **Phosphoglycerides.** They are the major contributors to the arrangement of the cell membrane's phospholipid bilayer.

2. **Sphingolipids.** They support the maintenance of cell structure and also contribute in several fundamental biological processes such as cell differentiation, cell motility, apoptosis and cell proliferation.

3. **Sterols.** They influence membrane fluidity and also act in biological processes as secondary messengers.

Phosphoglycerides are the main constituents of the cell membrane from the lipid class, erroneously referred to as phospholipids, because other lipids possess the phosphate group. Deenen in 1966 was one of the first to investigate the chemical structure of the phosfolipids. Phosphoglycerides are amphiphilic since they possess a dual nature at their ends, one hydrophobic and the other hydrophilic.

Owing to their amphipathic nature at the extremities, they are able to arrange in a way that creates the phospholipid bilayer characterizing cell membranes. Its hydrophobic portion is a diacylglycerol (DAG), containing saturated or cis-unsaturated acyl chains having different lengths. Depending on the alcohol group present, they may have different properties. Among over a hundred phosphoglycerides that cells synthesise are: phosphatidylserine (PS), phosphatidylethanolamine (PE), phosphatidylinositol (PI) [53][56][48][57][42].

Besides phosphoglycerides, sphingolipids are the other lipid components of the cell membrane with a great role in its structure. They are synthesised from serine and a fatty acid. Most lipids that contain sugar are sphingolipids, as their heads may consist of one or more sugars; some of them have neutral charge, meanwhile others are negatively charged. Sphingolipids, along with cholesterol as well, are responsible for lipid rafts. The realization of these microdomains derives from the inherent ability of sphingolipids to self-associate and pack tightly together. These properties depend on the interactions established between the saturated acyl and alkyl chains that characterize them.

Hence, the main function of the sphingolipids is to contribute in regulating the raft formation and transport through it. The sphingolipids are longer than phosphoglycerides and more abundant than these in the cell membrane thickness than inside the cell itself. The main sphingolipids found in eukaryotic cells are sphingomyelin (SM) and glycosphingolipids (GSL)[58][53][59][48][57][42].

Lastly, the sterols represent the third group of membrane lipids, among which cholesterol is the most prevalent on the cytoplasmic membrane (it represents about 30% of the cell membrane in composition) with low concentrations on the inner side, contributing in the lipid raft formation. Cholesterol has an important metabolic role, as it is among the responsive components for the synthesis of steroid hormones, vitamin D and bile salts, for example [60].

The stability in the membrane structure also depends on the proportionate presence between sphingolipids and cholesterol for thus forming the lipid rafts essential for the proper function of cell membranes. Indeed, cholesterol and sphingolipids have a high affinity, and their interaction favours the formation of small domains on the outer layer of the membrane known as lipid rafts. Small grooves called caveolae are an example of rafts, which are believed to cooperate in the transmission of intracellular signals.

Depending on the type of cell being examined, the lipid composition varies considerably. In addition to the multitude of phosphoglycerides, the cell membranes of animals include 30-35% cholesterol and 10% sphingolipids.

On average, lipids are distributed asymmetrically between the two halves of the membrane. For example, in animal cells, sphingolipids are found on the outer part of the cell, whereas PS, PE and PI are more frequent in the middle of the membrane in contact with the cell cytosol. The asymmetry of PS results in the weakly negative cytoplasmic membrane.

2.2.2 Proteins

The membrane proteins ensure membrane functions and they may act as following:

- **Enzymes and regulators**, acting as catalysts of chemical reactions.
- **Transporters** of molecules across the membrane by pores, ion channels, ion pumps and specific carriers.
- **Adhesion molecules**, contributing in the formation of cell junctions;

- **Receptors**, thereby gaining recognition of signal molecules and activating phosphorylation signal cascades.

Indeed, there are a wide variety of proteins, which can be grouped into two categories as follows:

1. **Integral proteins.** They are so called because they cross the entire phospholipid bilayer.
2. **Peripheral proteins.** So-called because they can be found on the inner and outer surfaces of the membrane.

A total of 70% of membrane proteins are integral. Distinctive features can be identified through which the two types of membrane proteins can be distinct. A protein is defined as perifying when the following criteria are satisfied [49]:

- They can be molecularly dissociated from the membrane in the intact state by mild treatments, such as increasing the ionic strength of the medium or adding a chelating agent.
- They are able to dissociate without lipids.
- In the dissociated state they appear to be relatively soluble in neutral aqueous environments.

Hence, it can be concluded that peripheral proteins are characterized by rather weak non-covalent cell membrane bonds, and thus are not directly associated with lipids.

The binding mechanism between peripheral proteins and the cell membrane can be of different types, depending on the kind of peripheral protein considered. An example of binding mechanism is one where a hydrophobic acyl chain can anchor a protein to the membrane by inserting into the phospholipid bilayer, such as Myristate binding tyrosine kinase Src and other proteins to the membrane. However, this binding turns out to be very weak and requires electrostatic interactions between the base of the protein chains and phosphoglycerides to maintain protein anchoring.

Indeed, BAR (Bin/Amphiphysin/Rvs) domains, found on several proteins, positively charged, which bind to membrane phospholipids to keep proteins anchored, also exploit electrostatic binding. Specifically, BAR domains will actually see them as one of the main ones in some types of endocytosis (see following sections).

On the other hand, many other peripheral proteins form bonds with integral proteins. For example, catenins bind cadherins, transmembrane proteins for adhesion. Such a protein-protein interaction creates an even stronger affinity than the one established between the peripheral protein and the membrane itself. Therefore, it also can act as a medium of passage to transmit information.

On the other hand, the criteria to be fulfilled for integral proteins to be classified that way are as follows [49]:

- In order to be dissociated from the cell membrane, they require much more drastic treatments, with reagents such as detergents, bile acids, protein denaturants, or organic solvents.
- Even once isolated, in many cases they remain attached to lipids when isolated.
- Where they are totally isolated from lipids, they result in insolubility or aggregation in neutral aqueous environments.

Depending on their function, peripheral and integral membrane proteins may differ in their structure and mode of interaction.

Considering the intregral protein, also called Polytopic transmembrane proteins, they can have several type of structure, including a single α-helix protein, or α-helical, or a β-sheet (see Fig 2.3.

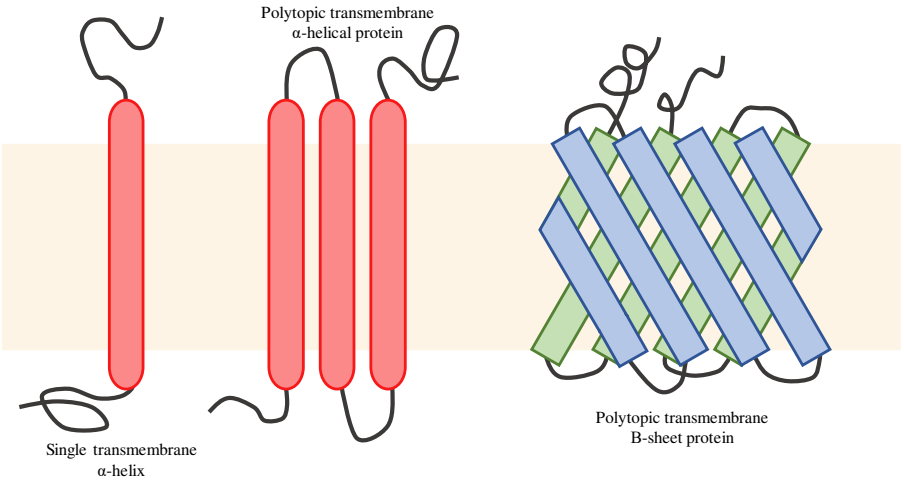

Figure 2.3: Representative organization of integral protein (so-called polytoipic transmembrane proteins): Single transmembrane α-helix protein; Polytopic transmembrane α-helical protein; Polytopic transmembrane β-sheet protein.

Most integral proteins are composed of a single peptide that, for energetic reasons, once it crosses the membrane assumes the form of α-helix, which interacts more favourably with lipid chains than with water.

Some examples of proteins having the α-helix form are bacteriorhodopsin, pumps, carriers and channels. Instead, a small proportion of proteins have the conformation of β-strands to cross the membrane. For instance, porins, i.e., transmembranous proteins, exploit this form to create channels, which cross the membrane, allowing substances to pass through. Such porins consist of a hydrophobic structure that surrounds a cone of water.

The transport function of the membrane protein is done from the protein channel. The channels in the cell membrane are generally ion-specific but passively transported, i.e. they allow ion fluxes or small amounts of solute to cross the membrane by electrical or concentration gradients. Ion channels are highly selective, and they are activated only if interaction with ligands,

for example, occurs. The ion influx regulates the electrical potential of the membrane, and the change in this potential produces electrical signals in the membranes of excitable cells, such as nerve and muscle cells.

Another important aspect is the membrane proteins' motion on the surface, which is vital for the proper cell functions. These include membrane receptors that accumulate in the coated pits to promote the uptake of particles and substances, or the transduction of many cellular signals from outside the cell depends on the formation of receptor dimers or trimers, as it will be discuss in the next section.

2.2.3 Membrane receptors

Among membrane proteins the most prevalent are receptors.

There are approximately 25 families of receptors. Membrane receptors possess many functions including responding to physical stimuli such as light absorption and chemical, or, for example, steroid hormones are capable of creating a chemical bond as a result of a physical stimulus with ligands.

In multicellular organisms, selective expression of certain receptors and transduction molecules promote cell interactions only with specific ligands and not with others, leading to the beginning of specific biological process. Therefore, the interaction between receptors and ligands is highly specific. Hence, this is the main mechanism of the receptor-mediated endocytosis process.

Energy derived from ligand binding is used to change the receptor configuration and transfer signals across the membrane to trigger a chain of signals within the cytoplasm. One or more enzymes may also participate in the transduction of these signals, whose job is to amplify the signal or speed up the process, for example.

The best-known families of receptors that conduct signals across the cytoplasmic membrane are the following:

- **G-Protein coupled Receptors.**
- **Receptor Tyrosine Kinase.**
- **Cytokine Receptors.**
- **Receptor Serine/Threonine Kinases.**
- **Guanylyn Cyclase Receptors.**
- **Tumor Necrosis Factor Receptors.**

The *G-Protein-coupled receptors family (GPCRs)* is the largest and most widespread family of cell membrane proteins. It is composed of transmembrane proteins that cross the plasmalemma. They transduce extracellular signals into physiological effects [42][8]. These types of receptors are employed, for example, in clathrin-mediated endopcytosis mechanisms (i.e, receptor-mediated endocytosis process, that it will be discussed in the next few sections) [61].

They activate proteins present on the intracellular side of the cell, the G-proteins, which possess the property of effecting hydrolyzing the GTP (guanosine triphosphate) nucleotide, in turn the G-proteins function as a conduit between the receptor and other proteins called effectors.

The G-Protein-coupled receptors have a serpetin form and they are shaped by seven α-helix proteins that develop within the phospholipid bilayer; meanwhile, on the cytosol-facing side it has three loops, in the last one there is the G-protein interaction domain. Whereas in the extracellular environment there is the so called N-terminal end to which the ligand will bind. Finally, concluding the structural composition of the protein, there is the C-terminal end facing the inside of the cell that has different regulatory sites [62][42].

Concerning *G-proteins*, they are trimeric proteins composed of three subunits: α, β, γ. In the steady state, the G protein forms a $\alpha\beta\gamma$ trimer, in which there is GDP (guanosine diphosphate) bound to α. When a ligand, which assumes the role of a first messenger, binds to the receptor the G protein changes conformation, exhibiting more affinity for GTP; therefore, the GDP separates and is replaced by GTP.

This new binding causes the α-GTP complex and the $\beta\gamma$ dimer to detach from the intracellular component of the receptor. The two aggregates formed can act distinctly on different effector proteins and act on several biological functions. When the hydrolysis of GTP, GTPase, by the α subunit occurs, the latter stops being active and regulates effector proteins. GTPase is catalyzed by the interaction of the α subunit with its target and the so-called RGS (regulators of G protein signaling) proteins.

Finally, GDP binds to the α subunit inactivating it and terminating its action. While the $\beta\gamma$ dimer can regulate proteins designed to phosphorylate receptors at a site rendering them inactive, such a dimer is able to play a negative feedback role and manage the upstream signaling pathway [62][42].

Effector proteins are enzymes that catalyze the formation of a second messenger that through signal transduction will lead to the cell's response. Two of the main effector proteins are: adenylate cyclase, catalyzing the conversion of ATP to cAMP; phospholipase C, capable of converting a membrane phospholipid into two distinct molecules that serve as second messengers.

These receptors are used by many drugs to be taken up by cells. Mutations in these types of receptors can cause the onset of manifestations at the physical level, for example, mutations in the melanocortin 1 receptor causes red hair and fair skin, or different diseases, as in the case of melanocortin 4, the cause of obesity.

Another noteworthy receptor family is *Receptors Tyrosine Kinase, RTKs*. RTKs are involved in endocytosis process like Macropinocytosis.

Membrane receptors having proteins with tyrosine kinase activity, by binding to polypeptide growth factors, allow those factors to regulate cell differentiation and proliferation. Among these factors, for example, we find epidermal growth factor (EGF), which stimulates the differentiation and proliferation of epithelial cells, or also platelet-derived growth factor (PDGF) responsible for the growth of smooth muscle, glial, and fibroblast cells.

About fifty genes belonging to the human genome have been found to encode RTKs, distinct in 20 different families, each with its own peculiarities. Most are characterized by a domain, responsible for contact with the ligand and different for each receptor depending on the family to which it belongs, on the outer side of the cell, which in turn is connected to an intracellular tyrosine kinase domain via a single transmembrane α-helix protein.

The ligand contact triggers the receptor by bringing together two kinase domains on the cytoplasmic membrane. The kinases' contact allows them to activate each other by direct interaction or by phosphorylating on tyrosine residues. Phosphorylation changes the kinase from inactive to active conformation. The juxtaposition of tyrosine and kinase domains by ligands can occur in three ways as following:

1. **First method.** Dimeric ligands, such as PDGF, recruit a pair of receptors from the set of membrane-flowing proteins and physically bind to them. This so called induced dimerization juxtaposes two kinase domains in the cytoplasm.

2. **Second method.** Once EGF binds to the membrane receptor, it allows a rearrangement of extracellular domains that promotes dimerization, bringing two kinases into contact. The kinases physically interact with each other, thus activating the membrane receptor.

3. **Third method.** Insulin causes a conformational change in a preformed dimeric receptor, this change brings into contact two kinase domains that activate each other by phosphorylation.

Mutations in the genes governing the expression of these receptors cause pathological disorders. Many tumors possess overexpression of EGF receptors [cit.]. Other mutations in the receptors responsible for fibroblast growth factor result in different congenital skeletal abnormalities, such as dwarfism or premature fusion of skull bones.

Cytokine are a family of polypeptide hormones and growth factors, which bind to receptors with tyrosine kinase activity. The kinases in turn activate transcription factors called STATs (signal transducer and activator of transcriptions), which are responsible for many cellular processes.

Example of cytokines may be somatotropin secreted by the pituitary gland. It regulates body growth and development in mammals. Hence, any mutations in this receptor will lead to a loss of the hormone's functions and the onset of the pathological condition of dwarfism. Other cytokines are interleukins, which are responsible for the body's defense and secreted by the immune system. Here, receptor mutations lead to immune deficiency of the subject.

Cytokine receptors are composed of a fibronectin III lingand-binding domain and a single α-helix transmembrane protein. While the inner end is composed of a kinase called JAK ("just another kinase") having a kinase domain and an inactive pseudokinase domain.

As a growth hormone ligand binds to the receptor, it causes the extra- and transmembrane domains to rotate from each other and activates the two JAK

kinases, thereby separating them. This action allows the JAKs to activate mutually by transphosphorylation. Then, the JAKs phosphorylate STATs that migrate to the nucleus in order to regulate gene expression.

Receptors belonging to the *Serine/Threonine Kinases* category exploit serine/threonine kinase domains present on the cytoplasmic membrane to enable signal transduction. The interacting ligands with these membrane proteins trigger the approach of the two receptor subunits in order to activate kinase activity. Subsequently, activated receptors phosphorylate transcription factors called Sma-related and Mad-related proteins (SMADs) and cause their migration from the cytoplasm to the nucleus, where they control cell proliferation and differentiation.

They bind to different growth factors, including those concerning embryonic development. Growth factors include transforming growth factor-β (TGF-β), which inhibits cell proliferation of most adult cells and instead stimulates the production of ECM, such as collagen and proteoglycans, and bone morphogenetic proteins (BMPs) are involved in osteoblast differentiation.

These receptors consist of two types of subunits, of which the human species has genes for the expression of seven type I and five type II. Four subunits, two type II and two type I, bind to a dimeric ligand, which presents with a high binding affinity toward type II receptors. These receptors through phosphorylation activate type I receptors, finally the latter phosphorylate serine threonine residues inducing the movement of SMADs factors toward the nucleus to promote the expression of the required genes.

Abnormal or misregulation of TGF-β via these receptors can induce overproduction of ECM and cause disorders of chronic inflammation and pathological fibrosis.

The *Guanylyn Cyclase receptor* family has two intracellular domains that promote the formation of cGMP (cyclic guanosine monophosphate) from GTP. The cGMP has several purposes such as regulation of ion channels, particularly for vascular smooth muscle and in the retina, vasodilation, retinal phototransduction, and regulation of cell growth and division.

These membrane receptors are homodimeric with an extracellular domain with the binding site for the ligand, a single transmembrane helix, and two cytoplasmic domains on the inner side of the cell: the inactive kinase domain and the guanylyl cyclase domain. Once there is no ligand bound to the receptor, the guanylyl cyclase domain remains inactive. As soon as ligand binding is formed, this action causes a movement, like that of a closing scissor, within the cytoplasmic part that stimulates guanylyl cyclase activity.

Guanylyl cyclase receptor A (GC-A) acts as a binding site for a polypeptide, atrial natriuretic factor, secreted by the heart for the purpose of regulating blood pressure. It stimulates the excretion of salt and water from cells by the kidneys and dilates blood vessels.

Since cGMP contributes to vasodilation by relaxing smooth muscle cells, it underlies the mechanism of taking certain drugs such as nitroglycerin and sildenafil, commonly known as Viagra, which used for erectile dysfunction.

Tumor necrosis factor receptors (TNFRs) together with Tumor Necrosis

Factor (TNFα) regulate gene expression for a wide range of developmental, inflammatory and cell death processes called apoptosis. TNFαs were discovered in 1975. TNFα has been intensively studied since it plays a significant role in both immunity and cancer. Indeed, these factors can trigger unique signaling mechanisms only through its two receptors: TNFR1 and TNFR2. Understanding how their signaling mechanisms work appears to be crucial, as this is key to further discovering its exact functions in many cancer diseases and perhaps to understand how to fight them.

The human body expresses two types of TNFRs that bind the same ligands but lead to different responses. Both types of receptors possess a similar structure, since they have a single transmembrane segment bound to different domains of the phospholipid bilayer; whereas on the cell surface there are the three receptor-forming subunits, which in the absence of the ligand are free to flow onto the cell.

The three finger-like parts forming the receptor bind to trimeric TNF through their interfaces. The clustering of the three receptor subunits allows it to carry you in the active form, generating an activation complex of adaptor proteins with the ultimate goal of achieving transcription factor activation [42][63].

TNF is one of the main contributors that play a key role in the inflammation of autoimmune diseases such as rheumatoid arthritis. Therefore, preventing TNF from joining its corresponding receptor would allow the inflammation caused by this disease to be attenuated.

2.3 Phagocytosis

Phagocytosis is the oldest mechanism of eukaryotic cells for the uptake of substances. This process involves the ingestion of large particles (500 nm or more) such as bacteria, foreign bodies, and dead cell remains (apoptotic cells). Therefore, this mechanism would have led the cells to incorporate the bacteria as a source of nourishment [42][43].

In mammals, this process characterises the three major groups of immune cells (e.e., macrophages, neutrophils and dendritic cells) which specialize in ingesting microorganisms through the phagocytosis process, thus initiating the immune and initial inflammatory response processes. Although, there are other types of cells that can exploit this mechanism such as fibroblasts, neurons and endothelial cells.

Phagocytosis process involves four steps regulated by the principal components of the cell membrane (cell surface receptors, polyphosphatidylinositides) and GTPases (Rho-family guanosine triphosphatases whose regulate the signaling cascades).

Schematically, the main steps are the following (Figure 2.4):

1. **Attachment.** It is the beggining of the process, involving the recognition and attachments of the phagocytic cell to the ingesting particle.

2. **Engulfment.** It is the ingestion phase, where the receptor of the phagocytic cell bind with receptors of the target particle which has to be ingested.

3. **Fusion with the lysosomes.** Once the target particle is incorporated, fusion with the lysosome starts, resulting in a vacuole called a phagolysosome where the target resides inside.

4. **Degradation.** It is the last phase of the process, where the ingested microorganism is killed and reduced in several products ready to be digested.

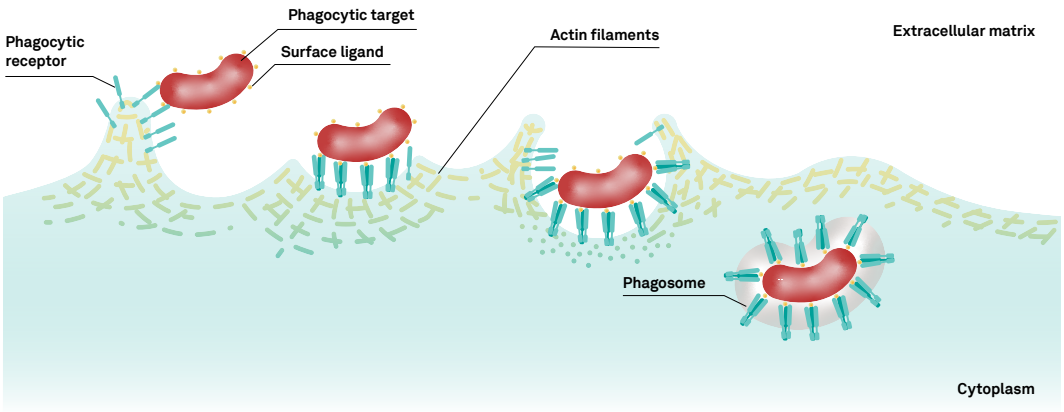

Figure 2.4: Phagocytocis process description, from left to right, of a macrophage: once the target to be phagocytosed has been identified, the macrophage starts the process; the macrophage's receptors are activated by binding with the bacteria; an actin filament activates the encapsulation process of the bacteria; after the bacterium has been encapsulated within the phagosome, the actin filament is removed; the bacterial degradation process begins.

As the particle is approached, it stimulates membrane proteins, which trigger a series of chain reactions leading to a microorganism being phagocytosed in the phagosome, and then digested within the cytoplasm cell. Hence, the phagocytosis is a process with signaling cascades mediated by GTPasess. Indeed, the actin has a major role in the process.

Actin monomers form short filaments on the membrane surface: the positive end is oriented towards the membrane surface; meanwhile the negative end grows towards the outside of the membrane. Therefore, the continuous assembly of actin filaments drives its assembly outwards from the cytoplasmic membrane.

The pivotal role of actin is shown due to that phagocytosis is sensitive to the widely used inhibitor cytochalasin D, which binds to the positive ends and inhibits their growth. Also latrunculin A, a fairly widely used drug, binds to actin monomers, blocking its polymerisation and conversely promoting its depolymerisation. Formins, proteins present in the cell cytoskeleton, are believed to promote the initiation of actin filament nucleation.

These proteins are able to nucleate actin monomers, insert the filaments into the positive end, and finally allow the negative end to detach further from the membrane to envelop the particle. Once the envelope within which the micro-organism is enclosed, i.e. the phagosome, is created, the actin filaments de-activate by detaching themselves from the phagosome. Afterwards, a series of digestive enzymes are activated, which will attack and split the bacterium into different components. The bacteria thus degraded will now be ready to be digested.

At the same time as actin polymerisation, a large number of molecules, forming part of signalling complexes, participate in the process of phagocytosis. Among theme, there are: lipids, cholesterol and also proteins such as kinase, phospholipase C,to mention merely a few. Throughout phagocytosis, the signalling mechanism involving multiple sites in the cell can be observed, a phenomenon also present in macropinocytosis (see Macrpinocytosis section).

Transmembrane processes such as phagocytosis involve many cellular components, but their reaction kinetics are too fast to be captured and observed experimentally. Therefore, there does not exist a full understanding of the internal process and all the proteins and enzymes involved in the mechanism.

2.4 Macropinocytosis

Macropinocytosis is a particular type of endocytosis that differs from the others according to what substances are ingested into the cell.

This process ingests extracellular fluids into the cell through the formation of large endocytotic structures called macropinosomes [42]. These are vescicles of heterogeneous size and filled with fluid substances to ingest with above 200 nm in diameter dimension, which are visible with a standard microscope.

In studies of macropinocytosis it is necessary to culture cells in-vitro to observe this biological phenomenon [43]. This is possible through the addition of a fluorescent marker, dextran, to the culture medium, thanks to which the formation of macropinosomes can be better appreciated.

Unlike the uptake in phagocytosis or caveolae or for foreign bodies surrounded by a clathrin coating, where distinct structures are noted under the electron microscope, both in cultured cells and tissues [42][43].

The macropinocytosis process involves several steps and actors (Figure 2.5). The actors in the macropinocytosis process are growth factors accompanied by other signals that are stimulated by actin-driven protrusions of the cell membrane. In this case, macropinocytosis is called "induced" since there is a sudden increase from an external stimulus, indeed, such as from the action of a growth factor [64].

The protrusions tend to then close around the fluid to be ingested, thereby forming the micropinosome. The micropinosome is then transported along the microtubules toward the core of the cell, allowing the complete internalization of the extracellular fluid, which will be useful for nutrient uptake of the cell. The created macropinosomes persist in the cytoplasm for 5 to 20 minutes, during which time their membrane components can be recycled by the cellular

membrane or they are directed to other organelles or can be then driven to lysosomes [65].

Other players in the process are PI kinases and GTPases recruit and activate proteins, who are involved in the process of assembling actin filamnets to support micropinosome formation.

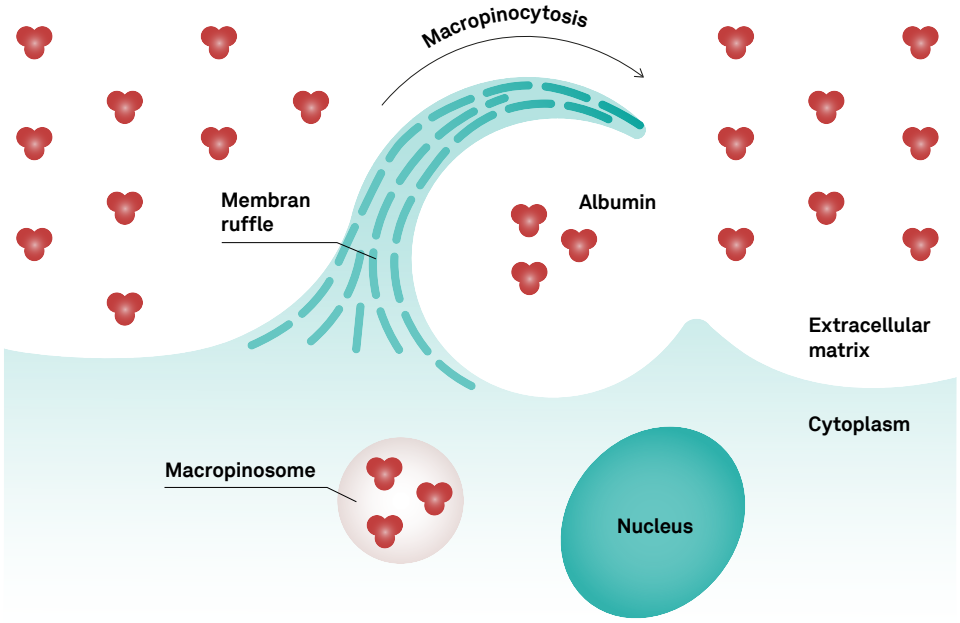

Figure 2.5: Schematization of the macropinocytotisis process. The cell membrane introfects to envelop a liquid substance and closes over it, forming an isolated vesicle within the cytoplasm, called a micropinosome. The contents of the micropinosome are then directed to other cellular structures or components to be either reused or degraded and digested.

Phagocytosis and macropinocytosis are related, whereas in the former, actin filaments envelop a solid particle, in the latter, only a certain amount of liquid is engulfed within the protuberances formed on the membrane by actin polymerisation [43].

It has been observed that the mammalian cells that exploit this process are the immature dendritic cells found in the skin epithelium and the mucosa of the respiratory tract. These cells can metabolise through macropinocytosis the equivalent of their volume in about 15 minutes. Due to the similarities between macropinocytosis and phagocytosis (actin polymerisation, membrane protrusion, signalling molecules and proteins), it is not always easy to unambiguously distinguish one from the other [42][43].

Conclusively, macropinocytosis is a crucial process for cell function. First, the process can regulate cellual functions such as the activation of certain cell surface receptors and nutrient absorption by amoebae, thyroglobulin by thyroid cells and bulk extracellular fluid by the dendritic cells for immune surveillance.

In addition, the macropinocytosis process is also utilized by innate immune cells, such as macrophages and immature dendritic cells, which therefore continuously process membrane protrusions a process called "membrane ruffling."

The mechanism is thus exploited to facilitate the functioning of the immune system by improving its efficiency. In this case it is referred to as constitutive macropinocytosis [64].

However, this process can also be used by specialized bacteria to enter inside the cell, where here they will attack the cellular system. One example is Samonella typhimurium, which is a pathogenic bacterium that injects toxins that trigger macropinocytosis and so ensuring a pathway to enter and then infect the cell [42][43].

A further example is the role that macropinocytosis plays in cancer-like diseases. This process ensures an endocytic pathway for the internalization of extracellular fluids through the macropinosome. It has been observed how macropinocytosis functions as a nutrient-scaveging pathway in Ras-driven cancer cells, caused by a mutation in RAS protein genes. The process ensures the uptake of extracellular proteins and their further degradation within endolysosomes, providing much-needed amino acids to cancer cells that feed their metabolism and promoting tumor growth.

2.5 Caveolae-mediated endocytosis

Endocytosis process can be mediated by Caveolae, which are small flask-like invaginations (60-80 nm) of the cell membrane, from which the clathrin-coated vesicles will be created to allow the uptake of small molecules. They are widespread throughout the membrane, but more present in muscle cells, endothelial cells, and adipocytes [42][43].

In caveolae-mediated endocytosis, plasma membrane proteins play a key role (Figure 2.6). These are associated with caveolae through interactions with caveolin and/or with cholesterol-enriched membrane components. The internalization process of caveolae requires a rearrangement of caveolae structure. Specifically, there will be a rearrangement of the actin cytoskeleton, requiring the action of the GTPase dynamin.

Specifically, EHD2 (Eps15 Homology Domain–containing 2), belonging to the dynamin-related ATPase protein family, are involved in membrane remodeling in the endosomal system. Its function is to drive intrinsic ATPase activity. EHD2 is not directly involved in clathrin-mediated endocytosis, but still has associated caveolae with the role of structure stabilizer [66].

The resulting caveolae will be small in size and transiently interact with endosomes or fuse with each other, retaining their cytoplasmic caveolin and cavin coatings. The role of caveolae in endocytosis is minimal in cells other than endothelial cells. However, they also help to store microdomain-associated lipids and regulate both non-cavaolar endocytic pathways and a variety of signaling pathways [42][43].

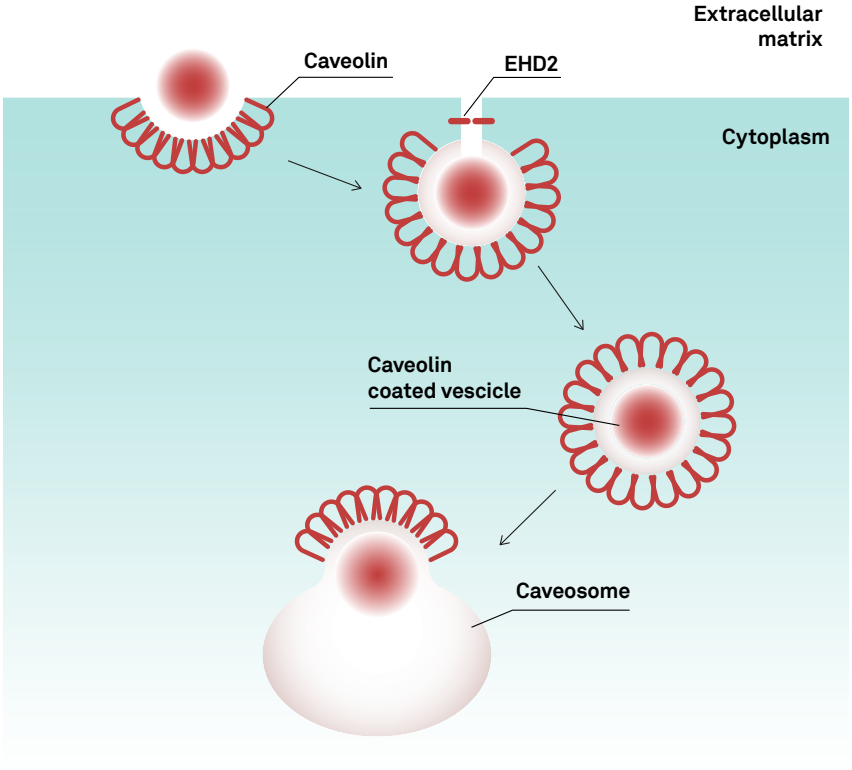

Figure 2.6: Endocytosis mediate by Caveolae. The caveolin along the cell membrane start the process to create the caveolin coated vescicle, that then will create the caveosome, ready to bring the transported material to cellular structure, where the material will be separated in other products to be reuse from the cell.

They are composed of oligomers of membrane proteins the caveolins 1-3, which work together with cholesterol and lipids. While caveolin 3 is limited to muscle, caveolins 1 and 2 are expressed in the majority of mammalian cells. Caveolae create homo-/hetero-oligomers by reacting with themselves and other lipids to form the typical flask-shaped caveolae sacs [42][43].

Cavaleolae involve also several signaling molecules, membrane transporters (calcium pumps) and glycosphingolipids. They might have several shapes invaginations of the cell membrane including simple flat and, also, flash-shape ones. The structure of caveolae is very complex and needs to be stabilized by coating proteins, such as caveolin and cavin, which consequently stabilize the microdomains of caveolae. Individual caveolae contain about 150 caveolin molecules, and caveins form string-like polymers that fit into the cell membrane. The caveolae density on the cell surface may vary depending on the type of cells considered.

For example, blood flow on the endothelial cells causes caveolae to flatten; or a change in membrane cholesterol can change the amount of caveolae. If caveolae collapse, cavins are degraded and caveolin and associated lipids redistribute along the plasma membrane. The distribution of caveolin and lipids depends on the physiological stresses and then increases the membrane surface area and membrane elasticity. Considering endothelial and muscle cells, these are

affected by physiological stretching and therefore this corresponds to an increase in the amount of caveolin within the plasma membrane [42][43].

Caveolae-mediated endocytosis differs from other types of endocytosis. Indeed, caveolae are involved in receptor-independent endocytosis. They differ, for example, from clathrin as they do not destine the coated material toward digestion by lysosomes, but instead they, in fact, transport the coated material (caveolin coated vescicle) to cellular apparatuses that modify it. Thus they allow its reuse [42][43].

This type of endocytosis is critical in mechanotransduction signal processes. Proteins in caveolae regulate cell growth and division, mitogen-activated protein (MAP) kinase signaling, and inhibition of cell-cell contact. Therefore, the main functions of cavealoe fall under signaling and endocytosis, although the relationship between the effects between the two phenomena is unclear. Caveolins or cavines are essential for the proper functioning of cavealoe-regulated processes; indeed, their mutation can result in human diseases, including lipodystrophy, muscular dystrophies, heart disease, and cancer [42][43].

2.6 Receptor-mediated endocytosis

Eukaryotic cells can employ the membrane receptor-dependent mechanism to internalize extracellular bodies.

Receptor-mediated endocytosis, or also called clathrin-mediated endocytosis (CME), involves the formation of a clathrin-coated vesicle (CCV) as the particle penetrates the cytoplasmic membrane until it finds itself in the cell cytosol and takes the name endosome (see Fig 2.7).

Schematically, the several step are the following:

1. **Initiation.** It is the beggining of the process. The process is triggered by the recruitment of AP-2 (Adaptor Protein Complex 2) and BAR domain proteins and ENTH (Epsin N-Terminal Homology protein domain) and ANTH (AP180 N-Terminal Homology domain) domains bind inositol phospholipids as well as proteins and they participate in nucleation and clathrin coat formation on membranes [67].

2. **Coat Assembly.** The second step involves the process of clathrin coat assembling at the nucleation sites of AP-2 proteins.

3. **Maturation and Scission.** Following the formation of the clathrin coat, a clathrin-coated pits (CCP) evolves into a dome-shaped invagination, which is subsequently reorganized into an Ω-shaped pit and separates from the plasma membrane to form a clathrin-coated vesicle. The reorganization process of the membrane is regulated by mechanical factors such as membrane tension, membrane stiffness.

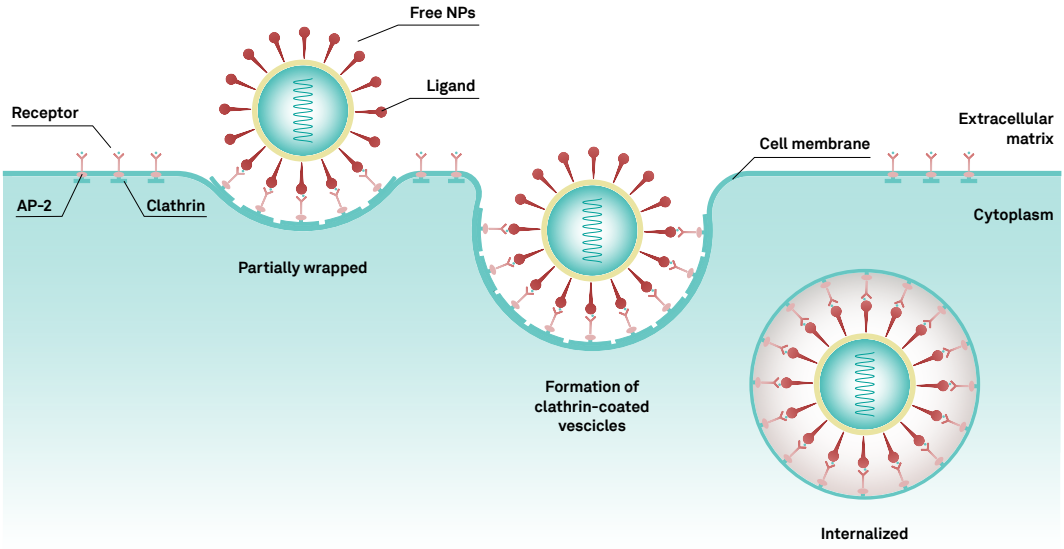

Figure 2.7: Endocytosis mediaed by receptor or clathrin-mediated endocytosis. The process is triggered by the recruitment of AP-2. In the second step, the clathrin coat is assembled at the nucleation sites of AP-2 proteins. Finally, the maturation and scission followed the formation of the clathrin coat, when a clathrin-coated pits (CCP) evolves into a dome-shaped invagination, which is subsequently reorganized into an Ω-shaped pit and separates from the plasma membrane to form a clathrin-coated vesicle.

Clathrin is a protein molecule that forms a polyhedral network around vesicles which transport protein molecules within the intracellular space. CME is used by most cells for the uptake of molecules and complexes about 100 nm in diameter. Indeed, the size of the clathrin-coated vescicles can be around 60-120 nm. Among these we can find nutrients, hormones, growth factors, signaling molecules and unfortunately also toxins and viruses.

The initiation phase starts when the CCV formation begins. CCV formation involves the interecation of the cytoplasmic membrane the receptors and PIP2 (phosphatidylinositol 4,5-bisphosphate, membrane component phospholipid) with AP-2, which in return recalls clathrin triskelions [68].

E/ANTH domains help in the nucleation and formation of the clathrin-coat. These domains work in the membrane curvature development through lipid remodeling during the formation of clathrin-coated vesicles. It was shown that E/ANTH proteins are functionally involved with adaptor protein-1 and GGA adaptors in the trans-Golgi network, which suggests that E/ANTH domains are universal components of the clathrin-mediated membrane budding machinery.

Process initiation has always been assumed to be a stochastic phenomenon, that is, a random phenomena. However, there are specific regions that can be considered as "hot spots" for initiating the process of CCP implementation. These points typically are in the presence of lipid or cargo proteins such as FCHo1/2 proteins that contain an F-BAR domain. FCHo1/2 assist in creating and maintaining the membrane curvature required for AP-2 nucleation. In this step, the mechanical properties of the membrane play an essential role. An

increase in membrane tension corresponds to a reduction in the initiation point of the process. Studies have shown that membrane tension goes to control the assembly of proteins that contribute to membrane curvature and the BAR domain. Thus increases or decreases in membrane tension go to speed up or slow down the process [69][70][68].

The second process is the coat assembly, where the clathrin triskelia are recruited for the formation of the cahe-like clathrin coat. The lifetime of CCV is on the order of one minute or less. After entering the cytosol and personating the clathrin coating, the foreign body is named early endosome. The subsequent stages can be multiple depending on the type of endosome. For example, the endosome may fuse with lysosomes, proteins that can degrade endocytosed material, exchange its contents with other endosomes, or in the case where the endosome is a virus release its nucleic acid to initiate viral replication.

Indeed, there is evidence that small viruses, with a diameter of up to 120 nm, can enter cells by exploiting the CCV. Viruses exploit membrane receptors, which usually bind to physiological substances needed by the cell, to permeate the mebrane. Viruses that adopt these mechanisms include parvoviruses, arenaviruses that bind to transferrin receptors to enter cells via CME or coronaviruses that bind to ACE2 (angiotensin-converting enzyme 2) receptors.

This endocytosis is mediated by mechanical stimuli due to the clathrin polumerization that is needed to stabilize the membrane invaginations. First of all, the deformation of the membrane is the main actor in the process. The mechanism that causes membrane deformation is still a matter of debate, and two theories are the most widely accepted. According to a first hypothesis, clathrin triskelions assemble on the membrane forming a flat hexagonal lattice, without changing the surface of the membrane on which the lattice is formed. Then the curvature is generated through remodeling of the coat by introducing pentagons into the lattice. Or, following a second explanation, the assembly of clathrin triskelions, already curved by themselves, shapes the pit, which later invaginates deep into the membrane. As mentioned above, assembly begins after the interaction of PIP2 with the AP-2 complex. Then AP-2 β_2, a subunit of the complex, recruits clathrin triskelions by initiating the assembly of the clathrin polyhedral lattice.

In addition, AP-2 acts as a recruiter for other proteins such as amphiphysin, Eps15 and sometimes actin in order to regulate CCV formation. When the particle has totally invaginated inside the membrane, it is necessary for it to detach, but it is not an autonomous operation. Then GTPase (family of enzymes that catalyze the hydrolysis of a chemical bond) dynamin intervenes, it binds to PIP2 on the neck of the formed pit and self-assembles to form a spiral structure.Through hydrolysis the dynamin collar is tightened, this causes the scission of CCV by releasing it into the cytoplasm.

Hence, the formation and assembly of the coat depends by the membrane tension and rigidity. More specific, the membrane rension acts as a inhibitory effector for the polymerization process of the clathrin coat, size and shape and it influencecs the shape stability curve of the membrane invaginations. Indeed, an increased membrane tension lead to the dissassembly of the clathrin coat.

Here, also the membrane rigidity can influence the clathrin coat formation, by slown down the rate of endocytosis process.

The last step of this process is the maturation and scission. Here, the clathrin coat formed involves the formation of hemispherical U-shaped CCPs, thus resulting in the transition from Ω to U shape, which occurs spontaneously. This shape transition is necessary to ensure internalization of the cargo molecules. The next step is membrane cleavage generated by the dynamin assembly into tight ligomers of initial radius 10 nm around the neck of a CCP to shrink the neck itself, thus ending the process [68].

Chapter 3

Membrane and Endocytosis models in literature

This chapter aims to provide a comprehensive overview of the relevant models in the literature for understanding the properties of cell membranes and the mathematical modelling of endocytosis.

The first section will first introduce W. Helfrich's 1973 work that provided the basis for understanding the elastic properties of lipid membranes. Next, a discussion will focus on Gerald Lim H. W. et al.'s 2002 study, about the human red blood cells, as this study brought important evidence for the lipid bilayer hypothesis of membranes. Furthermore, Tobias Baumgart et. al. studies from 2003 and 2005 studies will be presented, since these studies contributed significantly to further understanding of cell membrane dynamics and the coexistence of fluid domains in giant vesicles.

The last section will deal with the mathematical modelling of endocytosis present in the literature. Here, the chapter will present some of the most important models in the literature concerning the process on which the study of this thesis focused: receptor-mediated endocytosis. The starting baseline model is the Gao et al. [22] model, which will be explained in detail in the present chapter. Next, models of receptor-mediated endocytosis proposed by other authors, such as Yi et al. [27], Li et al. [34], Zhang et al. [36] and Wiegold et al. [37], will be briefly explained, which can generally be said to be derived directly from Gao's model.

3.1 Exploring Membrane Dynamics: From Theory to Experiments

3.1.1 Theory and simulation on cell membranes

In the field of the physics of biological systems, understanding the mechanical properties of biological membranes is crucial. These thin, flexible structures, mainly composed of lipids, play a crucial role in determining the shape and function of cells. The theory of elastic membranes, developed over the past

decades, provides a theoretical framework to describe the behaviour of these structures at the macroscopic level.

One of the most significant contributions in this field is Wolfgang Helfrich's 1973 article [71]. In this work, Helfrich developed a theory describing the elastic properties of lipid membranes in terms of energy. This theory had a profound impact on the understanding of the physical properties of biological membranes and paved the way for numerous experiments.

Helfrich paper introduces the idea that the elastic properties of lipid membranes can be described in terms of a free energy of deformation, which depends on the curvatures of the phospholipid membrane.

Considering a triplet of Cartesian axes and placing the origin at any point of the film, assumed to be infinitely thin, it is possible to identify the normal n relative to the layer.

This normal, parallel to the z-axis, is assumed to be dependent on the variables x and y, respectively the abscissa and ordinate of the plane, from which, thanks to the components of the vector $\mathbf{n}$ on the plane, it is possible to find the two principal curvatures through the partial derivatives:

$$c_1 = \frac{\partial n_x}{\partial x} \tag{3.1a}$$

$$c_2 = \frac{\partial n_y}{\partial y} \tag{3.1b}$$

The vector field $n(x, y)$ possesses the property of irrotationality, then the rotation of the vector must cancel as it is normal to a uniquely defined surface.

Then, the following relation of the partial derivatives in cross must hold:

$$\frac{\partial n_x}{\partial y} - \frac{\partial n_y}{\partial x} = 0 \tag{3.2}$$

Helfrich assumed that curvature is a quadratic function of the derivatives of n_x and n_y, and since the phospholipid bilayer is rotationally symmetrical, he only considered linear and quadratic shapes, independent of x- and y-axis orientation:

$$\frac{\partial n_x}{\partial x} + \frac{\partial n_y}{\partial y} \tag{3.3a}$$

$$\left(\frac{\partial n_x}{\partial x} + \frac{\partial n_y}{\partial y}\right)^2 \tag{3.3b}$$

$$\frac{\partial n_x}{\partial x}\frac{\partial n_y}{\partial y} - \frac{\partial n_x}{\partial y}\frac{\partial n_y}{\partial x} \tag{3.3c}$$

So the energy per unit area of the membrane can be written as:

$$e_H = \frac{1}{2}k\left(c_1 + c_2 - c_0\right)^2 + k_G\left(c_1 c_2\right) \tag{3.4}$$

Where c_0 represents the spontaneous curvature of the membrane, which takes into account the possible difference, chemically speaking, of the two sides of the membrane, a phenomenon that often occurs in biology because the

part of the membrane that communicates with the extracellular environment differs from its counterpart immersed in the cell cytosol. While k and k_G are the *bending modulus* and the *saddle splay modulus* or *Gaussian modulus*, respectively.

Helfrich energy can be used to study red blood cells (RBCs). The latter, also called erythrocytes, are fundamental cells for human life. They give blood its distinctive red colour and are responsible for transporting oxygen from the lungs to the tissues and carbon dioxide in the opposite direction.

Erythrocytes, unlike many other cells in the body, do not possess a nucleus, which allows them to accommodate more haemoglobin, the protein that binds to oxygen. In addition, their biconcave disc shape, which has also given them the name discocytes, increases the surface area available for gas exchange.

The shape and size of red blood cells are crucial to their function. Normally, they have a discocyte shape and a diameter of about $6 - 8\ \mu m$. This unique shape offers several functional advantages, including better gas exchange and the ability to pass through small capillaries.

However, the shape of erythrocytes can be altered by various factors, as certain pathological conditions can cause them to become deformed. For example, sickle cell anaemia is a genetic mutation that leads to the production of an abnormal type of haemoglobin that causes red blood cells to take on a sickle or crescent shape. These altered red blood cells can cause various problems, including occlusion of blood vessels.

Beyond pathologies, in the work of Lim H. W. et al. [72] it is reported how a different multitude of agents can interact to reversibly change the shape of red blood cells while keeping their area and volume constant.

On the one hand, there are anionic amphipaths, high salt concentrations as well as a high pH value, lack of ATP and cholesterol accumulations that can cause the erythrocyte to assume the form of an echinocyte, which has a convexity at its centre and protruding parts all around it.

By applying load to this shape, it was noticed how these protrusions become smaller and smaller as they increase in number; they then detach from the cell irreversibly, forming vesicles.

The cell, with reduced volume and area, takes on a spherical shape called a spheroechinocyte. On the other hand, cationic amphipaths, low concentrations of salts, acid pH and cholesterol gaps lead to the formation of a further form called stomatocyte. An increase in load in this case leads to the overproduction of convave forms that detach resulting in a cell called the spherostomatocyte.

RBCs have a composite membrane, i.e. formed by the combination of a cytoplasmic membrane and a membrane skeleton (MS), at the core of which is fluid. This suggests that the properties of the membrane are responsible for the shape changes of these cells. One of the mechanisms, which may be one of the plausible explanations, concerns the difference ΔA_0 of the relaxed area between the two layers, inner and outer, that make up the membrane.

A factor that expands, for example, the outer layer relative to the inner layer, increasing ΔA_0, results in the formation of convex structures on the cell membrane (such as those that characterise echinocytes. Conversely, the

expansion of the inner layer contributes to the production of concavities, typical of stomatocytes.

This hypothesis explains the stomatocyte-discocyte-echinocyte sequence (Fig. 3.1) by demarcating how external agents, whether chemical, physical or biological in nature, condition the shape of the cell through a modification of the ΔA_0. For example, cholesterol tends to favour the outer layer and expand the latter, while cationic amphipaths expand the inner one. This, however, remains a hypothesis that is not recognised by all.

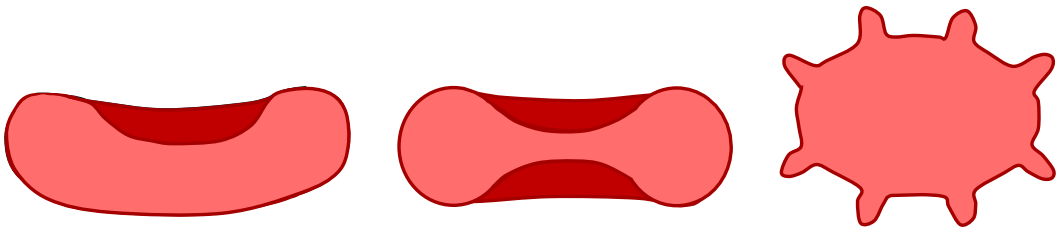

a) Stomatocyte **b)** Discocyte **c)** Echinocyte

Figure 3.1: Schematic outline of the evolutionary sequence of the erythrocyte, from stomatocyte to discocyte, typical red blood cell form, to echinocyte.

Another theory concerns the involvement of membrane-bound proteins, which are thought to play a dominant role in controlling the shape of the cell. In this context, the question is whether the shape of a cell analysed at a given value of ΔA_0 corresponds with that calculated through the implementation of a calculation model. Unfortunately, it is not possible to measure ΔA_0 directly, but the authors of this work [72], thanks to the formulation of such a model, have shown that it is possible to observe shape changes involving the sequence of RBCs.

The energy formulated by Helfrich, who was the first to realise that the cytoplasmic membrane can be regarded as a 2D fluid with a certain resistance to deformations caused by inflection, which causes the value of local mean curvature to deviate from the preferred value of $C_0/2$. Spontaneous membrane curvature C_0 is a parameter that is non-zero when there is asymmetry between the two membrane layers. A change in the value of ΔA_0 directly influences the shape to which C_0 is equivalent.

This equivalence comes from the fact that, if the membrane is not flat, a merely geometric difference ΔA between the two membrane layers must be introduced.

Therefore the Helfrich energy functional, called Area-Difference-Elasticity (ADE), which also takes this effect into account, has been expressed as follows:

$$E_{ADE}[S] = \frac{k}{2}\oint_S (2H - C_0)^2\, dA + \frac{k_G}{2}\frac{\pi}{AD^2}(\Delta A - \Delta A_0)^2 \tag{3.5}$$

Where D is the thickness of the membrane, A is the area of the membrane, and the integral is over the entire surface area S enclosing the vesicle. The mechanically stable shapes at fixed values of area and volume correspond to

a minimum of the energy functional. For the parameters used, this model leads to the discocyte form, while it becomes unstable and transforms into a stomatocyte if ΔA_0 is decreased. However, when ΔA_0 is increased, budding occurs instead of echinocytosis. Therefore, the previous model needs to be modified.

When the formation of the buds into the echinocyte shape takes place, the necks of these buds induce strong strech and shear in the MS. Incorporating the elasticity of the MS into the model will lead to an increase in the energy of the buds, but will allow the echinocytes to take a low-energy form for positive values of ΔA_0.

The new energy functional will be:

$$E_{RBC}[S] = E_{ADE}[S] + E_{MS}[S, S_0] \tag{3.6}$$

In which:

$$\begin{aligned} E_{MS}[S, S_0] =& \frac{K_\alpha}{2} \oint_{S_0} \left(\alpha_I^2 + a_3\alpha_I^3 + a_4\alpha_I^4\right) dA_0 \\ &+ \mu \oint_{S_0} \left(\alpha_{II} + b_1\alpha_I\alpha_{II} + b_2\alpha_{II}^2\right) dA_0 \end{aligned} \tag{3.7}$$

Where:

$$\alpha_I = \frac{dS}{dS_0} - 1 = \lambda_1\lambda_2 - 1 \tag{3.8a}$$

$$\alpha_{II} = \frac{(\lambda_1 - \lambda_2)^2}{2\lambda_1\lambda_2} \tag{3.8b}$$

α_I and α_{II} are the invariants of the local area and shear strain as a function of the principal stretches λ_1 and λ_2. K_α and μ are the linear and shear elastic moduli. The researchers included non-linear elastic terms of higher-order, i.e. a_3, a_4, b_1, b_2, because the principal stretches deviate far from unity for highly deformed forms such as some variants of echinocytes.

To proceed with the application of (3.7), it is also necessary to specify a relaxed shape S_0 at which the deformation energy is equal to 0. Oblate ellipsoidal shapes were chosen with area A of the RBCs but volume in the range from that of a sphere to the reduced volume $\nu_0 = V/V_{sphere}$.

The objective is to minimise the (3.6) functional for given values of ΔA_0 and S_0, in order to find the stable energies and shapes, the values of fixed area and volume of $A = 140\ \mu m^2$ and $V = 100\ \mu m^3$ were chosen.

The difference of the reduced effective area was calculated as:

$$\overline{\Delta a}_0 = \frac{\Delta A_0}{A} + \frac{k_G D C_0}{\pi k} \tag{3.9}$$

Combining the effects of both ΔA_0 and C_0. A first set of forms was obtained by varying the value of ΔA_0 from an initial negative value (stomatocyte) to a positive value (echinocyte), confirming that the entire sequence ($\nu_0 = 0.95$)

stomatocyte-discocyte-echinocyte could be obtained by adjusting only the variable ΔA_0. $\overline{\Delta a_0}$ was found to be in agreement with the experimental values found in the literature.

Despite this, a small ($\nu_0 = 1$) change in S_0 towards a more spherical shape leads no longer to the standard erythrocyte shape, i.e. discocytes, but to knizocytic shapes (triconcave cells). As such a live decrease in ν_0 has the effect of removing one of the potential stomatocyte shapes from the sequence.

Another set of simulations was conducted, varying slightly from the standard values ν_0 and $\overline{\Delta a_0}$, obtaining anomalous forms of red blood cells, such as the knizocyte and the triangular stomatocyte, found experimentally.

So, it was analysed how the stomatocyte-discocyte-echinocyte sequence can be obtained in accordance with the literature by controlling only one parameter, including other factors such as membrane elasticity and membrane skeleton stretch in the model. It is not always the case that the sequence always occurs this way, there could also be other mechanisms that condition the shapes.

For example, there could be reagents that influence the properties of the MS proteins and thus the shape of the RBCs through the S_0 and the elasticity modulus of the skeleton.

This work poses as a simple model, but could be further complicated by taking into account other aspects that condition RBCs such as differences in the density of lipid species present on the membrane and that would tend to influence the curvature of the membrane.

3.1.2 Study on two-phase membrane vesicles

Membranes are not perfectly homogenous but composed of multiple lipids separated laterally by liquid domains with different composition, this ordering conditions membrane properties such as elasticity and membrane shape. Through fluorescence imaging Baumgart et al. [73] showed a correlation between domain composition and membrane curvature.

This study focused on giant unilamellar vesiscles (GUVs), characterised by a ternary mixture of lipids: sphingomyelin (SM), dioleoyl phosphatidylcholine (DOPC) and cholesterol. The first two organics define a liquid phase with short-range order (L_o), while DOPC represents a disordered phase (L_d).

The shape, and thus the geometry, of vesicles can be obtained by minimising the bending energy functional of an axisymmetric lipid membrane and its sum over all the $i = L_o, L_d$ domains it possesses:

$$E_H^{(i)} = \int_{A^{(i)}} \left(\frac{1}{2} k^{(i)} \left(H - c_0 \right)^2 + k_G^{(i)} K \right) dA \tag{3.10}$$

A comparison of the first two images in Fig. 3.2, although the vesicles have the same shape but inverted domains, leads to the suggestion that the bending modulus is not responsible for the final shape assumed by the vesicles.

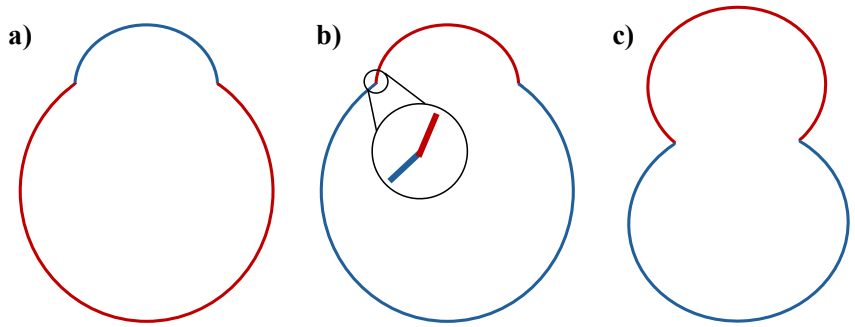

Figure 3.2: Simplified reproduction of images obtained by two-photon excitation microscopy in [73].

Therefore, a line tension σ, located between the two domains, has been theorised as a means of controlling deformation budding and fission. Above the boundary length limit value:

$$S_0 \approx \frac{8k^{(i)}}{\sigma} \approx 80\ nm \tag{3.11}$$

It was seen that the domain of a membrane, initially flat, could assume a spherical shape provided sufficient membrane area was present. It was shown how line tension leads vesicles to a boundary shape characterised by a minimum radius r_b of the boundary between the two phases Fig. 3.2c and the two dormers forming spherical caps.

The researchers observed that in the neck region (Fig. 3.2b), the L_d domains bend towards those of L_o, leading them to believe that the bending rigidity $k^{(L_o)}$ is greater than the $k^{(L_d)}$.

An algorithm was then set up to calculate the parameters deemed necessary to establish a correlation between domain composition and mechanical properties. The vesicle in Fig. 3.2c was chosen as the one on which to perform the analysis.

A line tension of $\sigma \approx 9 \pm 0.3 \times 10^{-13} N$ was obtained, with an order of magnitude smaller than Lipowsky's approximate estimate, which is based on the energy required to cross the lipid interfaces in a shear through the lipid bilayer at the phase boundary.

In other words, Lipowsky considered the energy associated with the voltage differences between the two sides of the lipid bilayer. The resulting lateral stresses $\Sigma^{L_d} \approx 8.2 \pm 0.1 \times 10^{-5} mNm^{-1}$ and $\Sigma^{L_o} \approx 1.06 \pm 0.01 \times 10^{-4} mNm^{-1}$ are balanced by a pressure difference $P \approx -1.83 \pm 0.01 \times 10^{-2} Nm^{-2}$. While the ratio between the bending moduli of the two phases $k^{L_o}/k^{L_d} = 1.25 \pm 0.6$, thus suggesting that the stiffness of the ordered phase is greater than the disordered one.

By increasing the surface-to-volume ratio through a rise in temperature, the formation of completely spherical vesicles was observed that originated from the fission of a vesicle that had the neck region.

The fission, therefore, occurred at the boundary between the two phases so that the new vesicles possessed a distinct and homogeneous lipid composition.

In addition to two-phase vesicles, vesicles with several ordered and disordered phases were also observed, but probably not in a minimum state of global energy because fused domains were observed, which reduced the total energy.

By raising the temperature to values several degrees below the mixing, or dissociation, transition temperature T_m, the circular domains of both phases oscillated laterally, indicating a reduction in line tension at higher temperatures. While further temperature increases led to the appearance of homogeneous membranes.

From a thermal point of view, the normal mean square amplitude of these movements, caused by temperature, is given by:

$$\left\langle u_n^2 \right\rangle = \frac{k_B T}{\pi r_o \sigma \left(n^2 - 1\right)} \tag{3.12}$$

Where k_B is the Boltzmann constant, T the temperature, r_o the mean radius of the domain and n the mode number.

Considering a $r_o \approx 5\ \mu m$, easily observed in its undulation with resolvable optical amplitudes, this leads to a line tension of the order of $\sigma \approx 10^{-14} N$ at elevated temperatures, two orders of magnitude smaller than that measured by researchers at room temperature. It is assumed that the line voltage decreases according to the proportionality $\sigma \propto (T_c - T)^{\lambda}$ where T_c is the critical temperature and $\lambda = 1$ is the critical exponent.

When the temperature is slightly lower than T_m, L_d phase domains are observed within a continuous matrix L_o. These wavy domains assume prolate elliptical shapes and, as the temperature increases, shape instabilities occur, leading to the formation of thin fluctuating stripes.

These stripes can extend over the entire surface of the liposome. Frequent fusions have been noted at the ends of the stripes, which as they cool, and thus raise the line tension, lead to circular ring-like domains across the entire vesicle.

Finally, homogeneous membranes were analysed by cooling them down from temperature T_m. This cooling caused the formation of small domains that merged to form recursive patterns, thus showing preferential bending between the two domains.

Furthermore, the disordered phase tends to prefer saddle shapes, a factor that again indicates how the value of the bending modulus is lower when compared to that of the ordered phase, which tries to concentrate in tubular areas with less curvature.

These experiments have been fundamental in understanding how the lipid domains of the membrane behave and how their shapes and properties may change when subjected to changes in temperature or even osmotic pressure.

In a second paper, Baumgart et al. [74] numerically inferred the shapes of the vesicles by comparing them with those obtained from experimental tests, showing that properties such as tension line, pressure, bending modulus and the difference in Gaussian moduli lead to different effects on the neck geometry of the vesicles, obtaining an estimate of these moduli and that Gaussian curvature strength intervenes at several stages in the vesicle melting process.

A closed axisymmetric lipid membrane with two balanced phases was considered (Fig. 3.3). The geometric description of the membrane was done by parameterisation of the arc length s and the tangent angle ψ.

The meridional curvature is denoted c_m, c_p the curvature along the circular parallels of the membrane and r the distance from the axis of revolution.

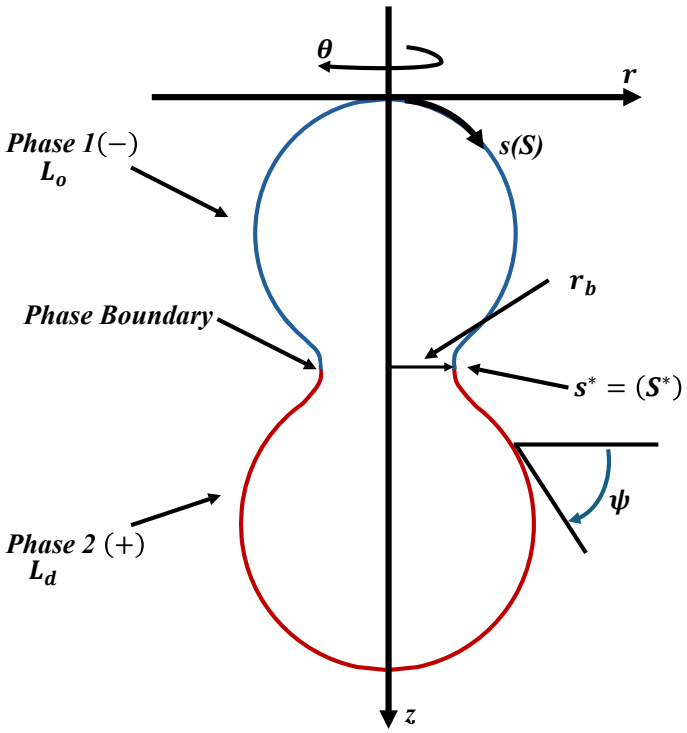

Figure 3.3: Representation of the coordinate system of the two-phase vesicle membrane [74].

The out-of-plane force balance equation can be written as:

$$\frac{dQ_s}{ds} + \frac{Cos\,(\psi)}{r}Q_s - T_s^s\frac{d\psi}{ds} - \frac{Sin\,(\psi)}{r}T_\theta^\theta - p = 0 \tag{3.13}$$

Q_s is the shear traction per unit length acting along the direction of the parallels, T_s^s and T_θ^θ are the stresses along the meridian and the parallels, while p is the net pressure per unit area of the membrane acting along the direction of the inward-facing surface normal.

The force balance equation in the plane results as:

$$\frac{dT_s^s}{ds} + \frac{Cos\,(\psi)}{r}\left(T_s^s - T_\theta^\theta\right) + Q_s\frac{d\psi}{ds} = 0 \tag{3.14}$$

The equation that links the two phases, the so-called jump condition:

$$T_s^{s+} - T_s^{s-} - \sigma\frac{Cos\,(\psi)}{r} = 0 \tag{3.15}$$

Where the jump (as shown in Fig. X, the sign $(-)$ and $(+)$ designate the phases before and after the jump, starting from the north pole) of the

lateral stress is equal to the line tension σ multiplied by the geodetic curvature $c_g = Cos\,(\psi)\, r^{-1}$.

In a similar way, the condition that binds the transverse shear in the two domains can be expressed:

$$Q_s^+ - Q_s^- - \sigma \frac{Sin\,(\psi)}{r} = 0 \tag{3.16}$$

Here, the jump of the transverse shear is equal to the line tension for the main bending along the boundary $c_p = Sin\,(\psi)\, r^{-1}$ whereas for completeness the meridional curvature is $c_m = -d\psi/ds$.

In addition, two other quantities have been defined, the ratio between the two bending rigidities:

$$\varepsilon = \frac{k^{(L_o)}}{k^{(L_d)}} \tag{3.17}$$

And a measure of the difference of the Gaussian curvature rigidities in the phases:

$$\Delta_G = \frac{k_G^{(L_d)} - k_G^{(L_o)}}{k^{(L_d)}} \tag{3.18}$$

The following representations, Fig. 3.4, are reproductions of the results obtained by the researchers using the two-photon fluorescence excitation microscope, in which the two lipid phases were stained differently, red the disordered one and blue the ordered one:

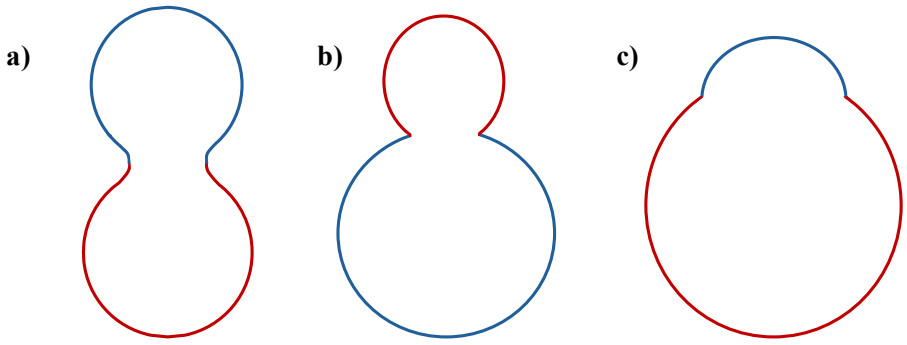

Figure 3.4: Graphical representation of images obtained by researchers using two-photon excitation microscopy. In blue is the ordered phase L_o, and in red the disordered phase L_d [74].

Vesicles with the presence of fluid domains present a more ordered arrangement in which the fluid tends to minimise its perimeter in order to reproduce circular domains, in contrast to the phase in which gel and fluid coexist, which is characterised by irregularly shaped domains and elongated perimeters due to the anisotropy of the line voltage and the high viscosity of the gel.

The image refers to vesicles whose domains depend on the composition of the vesicle itself, which in this case are 0.615:0.135:0.25 for Fig. 3.4a, respectively of SM, DOPC and cholesterol, Fig. 3.4b 0.584:0.103:0.313, Fig. 3.4c 0.25:0.5:0.25.

The mechanical analysis of the vesicle shape depends on the precision with which the neck of the vesicle itself is geometrically obtained, specifically the tangent of the southern trace of the boundary between the two phases, which is strongly influenced by the difference in the Gaussian moduli of the ordered and disordered phase.

Only the vesicle in Figure 3.4A was taken into account for the calculation of this tangent, as for the other vesicles only an estimation is possible.

In order to compare the area of the experimentally measured vesicle with the simulated one (with reference to Fig. 3.4A), the total area of the vesicle, after calculating the total arc length of the meridional section $S = 78.5\ \mu m$ by means of an algorithm, is obtained by:

$$A(s) = \int_0^S r(s)\ ds \approx 1205\ \mu m^2 \tag{3.19}$$

From which it appears that the radius of the undeformed sphere having this area is $R_o = 9.8\ \mu m$.

Knowing the radius, and consequently the volume, it is possible to know the reduction in volume using the following formula:

$$\nu = \frac{V}{(4\pi/3)\, R_o^3} \approx 0.76 \tag{3.20}$$

A high inverse value of meridional curvature was found in the area near the phase contour, while away from the contour, as the two domains are approximated by two spheres, the curvature was found to be constant.

Recalling that the meridional curvature is equal to $c_m = -d\psi/ds$, the derivative of the inverse function represents how quickly the curve moves away from its tangent at a specific point. Then it measures how quickly the curve 'bends' with respect to its local direction.

Near the neck region, it was noted how the disordered phase follows the shape of the spherical cap, then bends towards the ordered phase. The striation region in which there is this high curvature is predominantly formed by disordered phase.

The particular geometric shape of the neck can be explained by the difference in Gaussian moduli between the two phases, as theorised previously [73]. To confirm these hypotheses, different simulations were carried out and compared with experimental data.

First case: the vesicle is deformed by line tensions σ, gradually increasing, at the boundary of the biphasic domains, which possess the same saddle-splay or Gaussian modulus,$(\varepsilon = 1, \Delta_G = 0)$ and the volume of the vesicle is assumed to be freely adjustable, i.e. the fraction of area occupied by the disordered phase can be corrected up to the experimental value $x_{L_d} \approx 0.56$.

Comparison of the neck curvature obtained by simulation with the neck radius derived from the experimental test, $r_b \approx 0.34$, showed lower curvatures in the simulation.

If, on the other hand, the volume reduction is set to the previous value $\nu \approx 0.76$, the curvature of the neck increases as the line tension increases. The

imposed volume constraint leads to a limit shape to which a minimum radius in the contour area corresponds (again as the line tension increases).

For this boundary shape, by performing a force balance in the phase contour, a relationship between pressure and line tension was obtained:

$$\frac{\sigma}{p} = \frac{1}{2} r_b^2 \left(Cot\left(\psi_1\right) - Cot\left(\psi_2\right) \right) \tag{3.21}$$

Where angles ψ_1 and ψ_2 are tangent before and after the boundary.

In this case, the comparison between simulation and experimental test showed very similar neck curvatures, although the tangent angles of the simulated vesicle, with equal radius to the experimental one, do not fit well with the experimental data.

Second case: Another set of simulations provided that the vesicles had equal area fraction, volume and boundary radius r_b to the experimental tests, but with decreasing values of the bending moduli, $\varepsilon = 100, 10, 0.1, 0.01$, and equal Gauss moduli $\Delta_G = 0$.

From the figure below, it appears that the domain of the membrane with the lowest bending modulus takes the form of a spherical cap, while the region with the highest modulus that of a drop.

Comparing the simulation with $\varepsilon = 10$ (Fig. 3.5), second from the left, where it is assumed that $k^{(L_o)} > k^{(L_d)}$, with the experimental evidence, it can be confirmed that the bending modulus of the ordered phase is greater than that of the disordered phase.

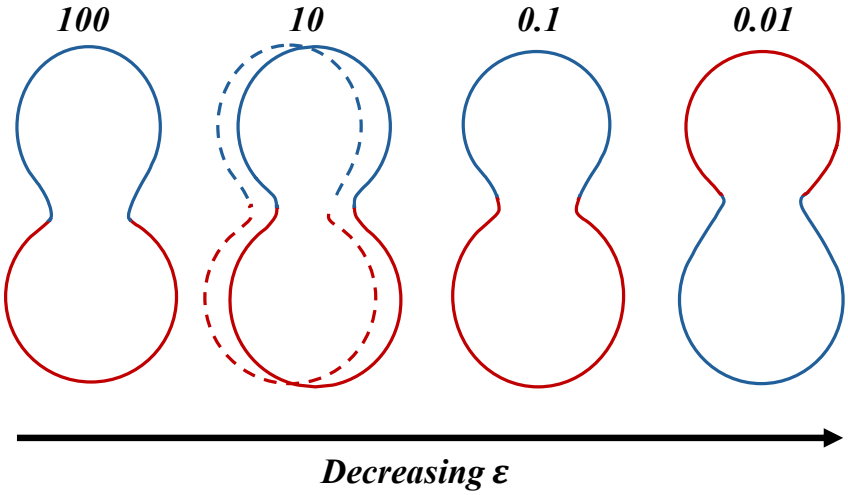

Figure 3.5: Vesicles with variable ε and $\Delta_G = 0$. In red the disordered phase L_d and in blue the ordered phase L_o [74].

To demonstrate the influence of different Gaussian moduli of the two phases on the neck geometry, simulations were conducted at $\Delta_G \neq 0$ and $\varepsilon = 1$.

The left and right vesicles in Fig. 3.6 refer to values $\Delta_G = -4$ and $\Delta_G = 4$ respectively, while the one in the centre is inferred from the experimental test.

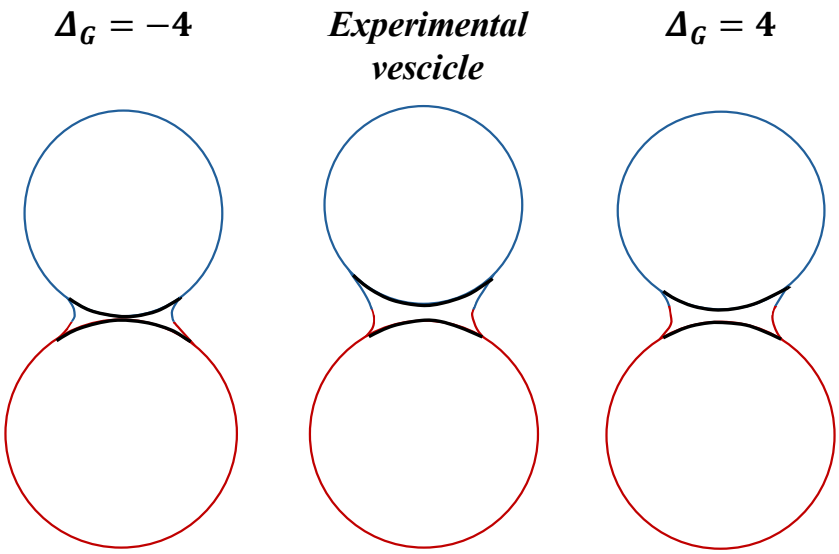

Figure 3.6: Vesicles with $\Delta_G \neq 0$ obtained from simulation and compared to the experimental vesicle.The black lines on the three vesicles are shown only to point out the spherical shape. [74].

The term $\Delta_G \neq 0$ tends to take the boundary between the two phases out of the neck striation, making it possible that the membrane domain with the higher value of $k_G^{(i)}$ predominantly occupies the neck. Thus, the variation of $\Delta_G \neq 0$ only affects the neck area, where the Gaussian curvature is greatest.

In order to obtain an estimation of the parameters ε, Δ_G, pressure p and line tension σ for the experimental test of the vesicle in fig2A, the experimentally obtained vesicle volume, r_b and phase contour angle ψ were taken as boundary conditions for the numerical solution of the vesicle shape equation problem.

A value of $\varepsilon = 5 \pm 1.56$ was obtained from the analysis of the vesicle fig.2A, from which a larger bending modulus of the L_o phase than the L_d phase can be deduced. Estimates of the ternary mixture characterising the vesicle, consisting of cholesterol, SM-saturated and DOPC-unsaturated chains, show that the ordered phase contains more cholesterol than the disordered one.

Cholesterol in membranes is known to increase the value of the bending modulus by up to a factor of five when compared to a membrane lacking it.

Microscopic models relate the bending modulus according to the following proportionality relationship with other quantities:

$$k \propto K_A \frac{l^\tau}{u^v} \tag{3.22}$$

Where K_A is the area compressibility modulus, l the membrane thickness, u the average cross-sectional area of a lipid molecule and the exponents $\tau, v \geq 1$. The value of K_A increases in direct proportion to the cholesterol content. A higher amount of this organic molecule leads to a thickening of the membrane and, simultaneously, to a decrease in the cross-sectional area in a single phase.

Atomic force microscope analysis revealed that the thickness l is greater in the ordered phase than in the disordered phase, which is also due to the

lipid-saturated chains present in the phase. The equation above, therefore, states that $k^{(L_o)} > k^{(L_d)}$, which is equivalent to saying $\varepsilon > 1$.

Measuring the Gaussian modulus, a parameter that describes how much a surface can be deformed, is a complicated task. This is because it is closely related to the intrinsic curvature of the surface, a property that remains constant when the surface is bent without stretching.

This concept is closely related to the Gaussian curvature energy, the energy associated with the deformation of a surface. This energy is 'topologically invariant', meaning that it does not change unless there is a change in the overall structure of the surface, such as the creation of a hole. This is a result of the Gauss-Bonnet theorem, a fundamental theorem in differential geometry that links the total curvature of a surface to its topology.

When discussing homogeneous bilayer membranes, such as cellular membranes, the situation becomes even more complex. These membranes consist of two layers of lipid molecules, and the Gaussian curvature energy cannot be determined directly just by looking at the shape of the surface. This is because Gaussian curvature is an intrinsic property that cannot be measured just by looking at the shape of the surface.

In spite of this, the researchers in this article measured the normalised difference Δ_G of the Gaussian moduli of the two phases of the vesicles with respect to the bending modulus. From the analysis, a value of $\Delta_G = 3.6 \pm 0.6$ was obtained, which designates a smaller, but more negative, value of $k_G^{(L_o)}$ than $k_G^{(L_d)}$.

It has been shown that the two modules are related to the values of the monolayer k_G^m:

$$k_G = 2k_G^m - 8k^m h_0^m \delta \tag{3.23}$$

Where h_0^m is the spontaneous curvature of the lipid monolayer and δ is the distance between the neutral surface of the monolayer, a surface that does not extend or contract, and the mid-plane of the bilayer, which is a two-layer structure.

In the literature, theoretical considerations place the relationship between k^m/k_G^m in the following range:

$$-1 \leq \frac{k^m}{k_G^m} \leq 0 \tag{3.24}$$

Asserting that this ratio is constant with respect to the variation of the microscopic parameters, i.e. that both the bending and the Gaussian modulus are similarly affected by the change in membrane parameters. Due to the minus sign, and that not only $k = 2k^m$, but also $\varepsilon > 1$, it is expected that the monolayers of the ordered phase have a more negative k_G^m than the disordered phase.

Furthermore, assuming that it is the first term that prevails in the (3.23) in the difference of the Gaussian moduli and that $k^m/k_G^m = -1$ it follows that:

$$\Delta_G = \frac{k_G^{(L_d)} - k_G^{(L_o)}}{k^{(L_d)}} = \varepsilon - 1 = 4 \tag{3.25}$$

This value is very close to that obtained by the researchers. However, h_0^m and thus the second term of (3.23) depends on parameters such as the membrane proteins, the geometric arrangement of the lipids and the temperature.

Thus, Δ_G may not always be positive. By replacing (3.25) with the experimentally derived value of $k^{(L_d)}$, we arrive at an absolute difference of the values of the Gaussian moduli equal to $\overline{\Delta_G} \approx 3.6 \times 10^{-19} J$.

The value of the line tension determined with the collected data is $\sigma \approx 6.7 \times 10^{-13} N$. The line tension depends on the sum of two factors: the inhomogeneity of the chemical composition on the boundary which results in a chemical line-tension, and a mechanical line-tension given by the differences in thickness between adjacent areas of the membrane, which causes the membrane to compress and tilt to avoid a misalignment that could be negative from an energetic point of view.

This value was found to be consistent and in line with values found in the literature, but always remembering that line tension is a function of the properties of both phases and temperature.

Finally, the pressure difference measurement across the membrane of the experimental vesicle gave the value of $p \approx -2.8 \times 10^{-2} N m^{-2}$ while the lateral mean tensions were $d(L_o) \approx -1.03 \times 10^{-4} m N m^{-1}$ and $d(L_d) \approx -0.91 \times 10^{-4} m N m^{-1}$.

The pressure difference must be balanced by the osmotic pressure:

$$\Pi = c_s R T \tag{3.26}$$

Where $c_s \approx 10^{-5} mM$ is the difference in solute concentration between the interior and exterior of the vesicle, R the gas constant and T the temperature. From the spherical shells of the experimental vesicle, imposing constant curvature, the radii of curvature of the two phases can be found, i.e. $R_{Ld} \approx 7.4 \mu m$ and $R_{Lo} \approx 6.5 \mu m$.

Using the Laplace equation:

$$p = \frac{2d}{R_i} \tag{3.27}$$

And substituting the corresponding values of lateral tensions and radii of curvature found, one finds a pressure difference consistent with the pressure found just before.

Lipid domains are of considerable importance because they characterise all cells and their ways of reacting with their environment, as in the case of endocytosis, and their properties, such as chemical inhomogeneity, can greatly influence the uptake of nutrients required for cellular sustenance.

It has been shown that cholesterol plays a fundamental role in influencing membrane stiffness; if a membrane were stiffer, for example, the time taken by the cell to phagocytose a biomolecule could be delayed.

Analysis of the membrane, its curvatures and the stress lines separating the domains, can be useful in shedding light on the processes that connect the cell with the external environment.

3.2 The basic model of receptor-mediated endocytosis

Gao et al. [22] based their work on the idea that the process of entry and exit of viruses from animal cells is mediated by the binding interaction between viral capsid ligand molecules and membrane receptors (Figure 3.7).

Their research question fell on the possible influence that the size of a bioparticle had on receptor-mediated endocytosis. Therefore, the authors' study focused on how a cell membrane with diffusible mobile receptors could envelop a ligand-coated particle.

Their considerations for the model realization concern that during the process in which the virus permeates the host cell, thermal fluctuations of the membrane itself and hydrodynamic interactions may occur. In order to consider these factors, they introduced a simplified form of free energy, which complements the model formulation, whose solution is found numerically.

Hence, it was assumed that the particle coming into contact with the cell has membrane proteins called spikes or ligands on its surface, which are immobile and evenly distributed throughout the process of endocytosis. Whereas the receptors on the cell membrane are mobile and move in a purely diffusive manner across the cell membrane, which is considered to be one-dimensional and semi-infinite.

Furthermore, since the particle size is far smaller than that of the cell, the membrane is considered flat.

Before the particle touches the cell, the density of the receptors on the membrane is assumed to be uniform and is equal to ξ_0 (Figure 3.7). In this state, the membrane has its highest level of entropy. Once the process has begun, the contact area under the particle, whose ligands and receptors have formed bonds, reaches the density of ξ_L.

The particle-membrane bonding leads to a reduction in free energy that drags the receptors towards the contact zone, leaving a depletion at the edge of the particle-membrane interface with density ξ_+ (Figure 3.8). The gradient that is created induces more and more receptors to go to the area where endocytosis is occurring. Receptor diffusion is governed by density function $\xi(x,t)$ that depends on space and time. Receptor flux can be expressed by Fick's first law, which is a key law in the field of transport phenomena and describes concentration changes in materials involving diffusion phenomena:

$$j\left(x,t\right) = -\lambda \frac{\partial \xi\left(x,t\right)}{\partial x} \tag{3.28}$$

Where λ is the membrane diffusivity with the following measuring unit $[\lambda] = L^2T^{-1}$.

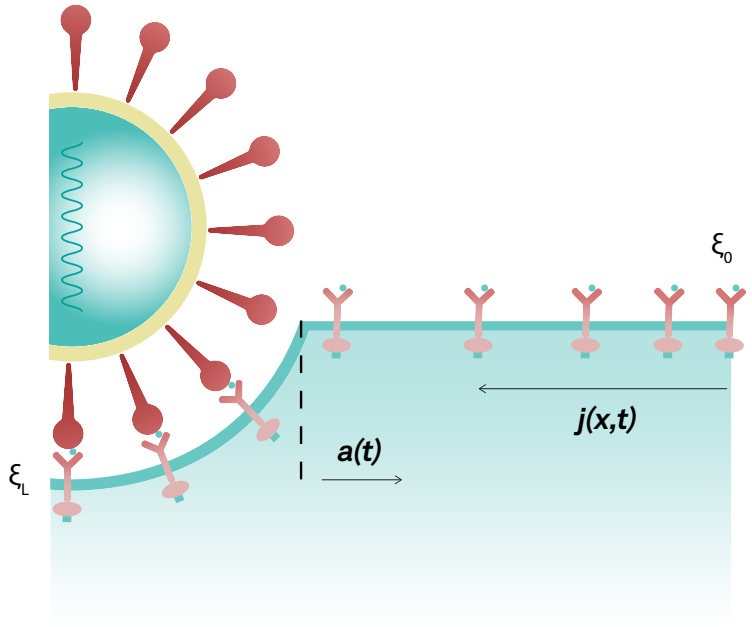

Figure 3.7: Receptor-mediated endocytosis schematized. The molecule to be incorporated into the cell makes contact with receptors that sit on the cell membrane initiating the process of endocytosis. The uniform receptor density before the contact with the molecule is ξ_0, while the receptor density in the contact zone is ξ_L. The schematic drawing represents the receptor flux $j(x,t)$ and the particle membrane interface $a(t)$.

As time passes, the particle-membrane interface $a(t)$ increases until the contact area reaches the maximum radius of the particle. Since the process is mirrored with respect to the y-axis of Figure 3.8 (schematic drawing of the process), only what happens in this first quadrant will be analyzed.

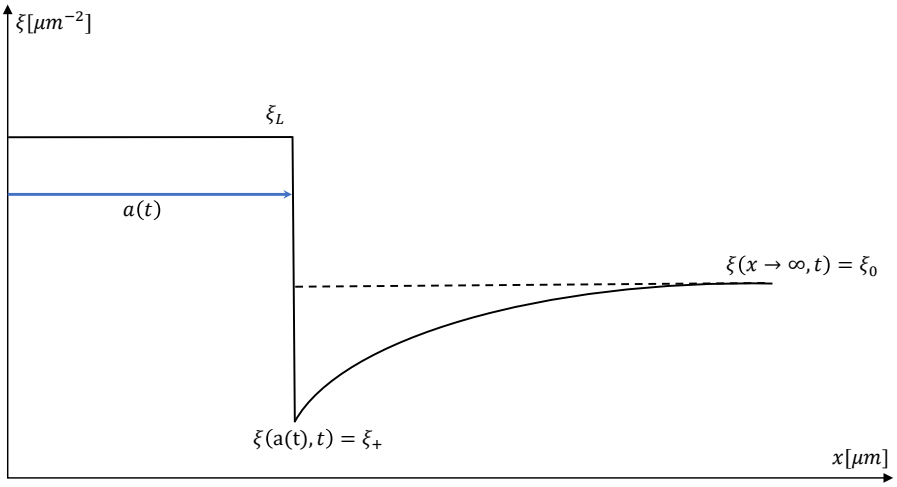

Figure 3.8: The graph represents the density of receptors with respect to space for a generic time. The receptor density assumes an uniform value ξ_0 at infinity. When the receptors flow, they reach the membrane-particle interface due to the depletion ξ_+ and finally they are consumed to form the ligand-receptor pairs under the particle with density ξ_L.

Substituting the flux (3.28) into the continuity equation, which is the differential equation that expresses in local form the conservation law of a given physical quantity using the quantity flow through a closed surface:

$$\frac{\partial \xi\left(x,t\right)}{\partial t} = -\frac{\partial j\left(x,t\right)}{\partial x} \tag{3.29}$$

Hence, the receptor diffusion equation is obtained:

$$\frac{\partial \xi\left(x,t\right)}{\partial t} = \lambda \frac{\partial^2 \xi\left(x,t\right)}{\partial x^2} \tag{3.30}$$

Where the spatial and time domains are the following: $a\left(t\right) < x < \infty\ ,\ t > 0$. Next, starting by the assumption that during the endocytosis process the total number of receptors remains unaltered, the conservation equation for receptor density can be written as follows:

$$\frac{d}{dt}\left[\int_0^{a(t)} \xi\left(x,t\right)\ dx + \int_{a(t)}^{\infty} \xi\left(x,t\right)\ dx\right] = 0 \tag{3.31}$$

Before make any considerations or modifications on the previous equation, it is necessary to fix the boundary conditions of the system. Hence, it can be supposed that, far away from the membrane, the flux of receptors is zero and consequently the density of receptors will be equal to the uniform distribution ξ_0. This is a mathematical assumptions that definitely differs form reality. In the particle-membrane contact zone $x < a(t)$, the receptors are bound to the ligands and there is no diffusive motion, here the density will be equal to ξ_L.

Finally, it is visible a depletion zone, where the receptor density will have reached a certain unknown value that is lower than the uniform density; this is indicated by ξ_+ (see Fig. 3.8).

In summary, the following equations represent the boundary conditions describing the system, for the sake of completeness the initial condition referring to the (3.30) is also given as follows:

$$\xi\left(x \to \infty, t\right) = \xi_0 \tag{3.32a}$$
$$\xi\left(x < a(t), t\right) = \xi_L \tag{3.32b}$$
$$\xi\left(a\left(t\right), t\right) = \xi_+ \tag{3.32c}$$
$$\xi\left(x, 0\right) = \xi_0 \tag{3.32d}$$

It is now possible to apply these boundary conditions and Leibniz's rule to the equation (3.31). Leibniz's rule is a useful tool for differentiation under the sign of the integral.

So for instance, considering a generic function $f(x,t)$ integrated with respect to the variable x with two time-dependent extremes and differentiated with respect to t, we will obtain:

$$\frac{d}{dt}\left[\int_{a(t)}^{b(t)} f\left(x,t\right)\ dx\right] = f\left(b\left(t\right),t\right)\frac{db(t)}{dt} - f\left(a\left(t\right),t\right)\frac{da\left(t\right)}{dt} + \int_{a(t)}^{b(t)} \frac{\partial f\left(x,t\right)}{\partial t}\ dx \tag{3.33}$$

In our specific case, applying the appropriate steps, the equation will result:

$$\dot{a}\left(t\right)=\frac{\lambda}{\left(\xi_{L}-\xi_{+}\right)}\frac{\partial\xi\left(a\left(t\right),t\right)}{\partial x} \tag{3.34}$$

The equation just obtained is called *Stefan condition*, meanwhile the system of differential equations constituted by (3.30),(3.32),(3.34) is a typical example of a non-linear mobile frontier problem called *Stefan's problem* (Appendix B), in which one extreme of the spatial domain varies at each temporal instant, expanding the domain or shrinking it.

For this kind of problem it is possible to find the solution through the application of a similarity variable (B.10) to (3.30). Also since the boundary condition (3.32c) is not known, only (3.32a) will be applied to the solution, leaving the other integration constant c_1 to be determined.

This will lead to the solution, and so the receptor density function will be obtained as follows:

$$\xi\left(x,t\right)=\xi_{0}-c_{1}\sqrt{\pi\lambda}\ Erfc\left(\frac{x}{2\sqrt{\lambda t}}\right) \tag{3.35}$$

Where $Erfc(y)$ is the complementary error function:

$$Erfc\left(y\right)=\frac{2}{\sqrt{\pi}}\int_{y}^{\infty}e^{-t^{2}}\ dt \tag{3.36}$$

Next, the equation (3.35) will be substituted into (3.34) obtaining as follows:

$$\dot{a}\left(t\right)=\frac{\lambda}{\left(\xi_{L}-\left(\xi_{0}-c_{1}\sqrt{\pi\lambda}\ Erfc\left(\frac{a(t)}{2\sqrt{\lambda t}}\right)\right)\right)}\frac{e^{-\left(\frac{a(t)}{2\sqrt{\lambda t}}\right)^{2}}c_{1}\sqrt{\lambda}}{\sqrt{\lambda t}} \tag{3.37}$$

The above equation can only be true if the interface assumes the form of:

$$a\left(t\right)=2\zeta\sqrt{\lambda t} \tag{3.38}$$

Where ζ is the *speed factor* that will be determined later.

The constant of integration is found by replacing (3.38) in (3.37). Consequently the receptor density function becomes:

$$\xi\left(x,t\right)=\xi_{0}-\frac{\zeta e^{\zeta^{2}}\left(\xi_{L}-\xi_{0}\right)\sqrt{\pi}}{1-\zeta e^{\zeta^{2}}\sqrt{\pi}\ Erfc\left(\zeta\right)}\ Erfc\left(\frac{x}{2\sqrt{\lambda t}}\right) \tag{3.39}$$

Therefore, the receptor density function is known, except for the β factor, which is not known. Hence, it is necessary to introduce a new equation. Following, the authors considered the free energy function $F(t)$ for cellular membrane in contact with a substrate:

$$\begin{aligned}F\left(t\right)=&\int_{0}^{a(t)}\left(-\xi_{L}k_{B}TC_{B}+k_{B}T\xi_{L}\ln\left(\frac{\xi_{L}}{\xi_{0}}\right)+\frac{1}{2}k_{B}TBk_{0}^{2}\right)dx\\&+\int_{a(t)}^{\infty}\xi\left(x,t\right)k_{B}T\ln\left(\frac{\xi\left(x,t\right)}{\xi_{0}}\right)\ dx\end{aligned} \tag{3.40}$$

Let us analyze the terms of the first in integral. The term on the left takes into account the energy of a single receptor-ligand bond. k_b is the Boltzmann constant, T is the absolute temperature in Kelvin, and C_b is the receptor-ligand adhesion energy coefficient.

Then there is the free energy per receptor associated to the loss of configurational entropy. Finally, the bending energy of the elastic membrane enveloping the particle with radius of curvature $k_0 = R^{-1}$ and bending modulus B coefficient.

The last integral represents the free energy associated with receptors that are unbound and free to move. Differentiating (3.40) with respect to time and assuming that the rate of energy reduction caused by the particle enveloping process precisely balances the dissipation energy spent on receptor transport, once some mathematical steps have been taken:

$$C_B - \ln\left(\frac{\xi_L}{\xi_0}\right) - \frac{1}{2}\frac{Bk_0^2}{\xi_L} + 1 - \frac{\xi_+}{\xi_L} = 0 \tag{3.41}$$

After placing the condition (3.32c) in the (3.39), it is possible to substitute the receptor function into the equation just derived to obtain an equation whose only unknown is the speed factor ζ:

$$\begin{aligned} &C_B - \ln\left(\frac{\frac{\xi_0}{\xi_L} - \zeta e^{\zeta^2}\sqrt{\pi}\ Erfc\left(\zeta\right)}{1 - \zeta e^{\zeta^2}\sqrt{\pi}\ Erfc\left(\zeta\right)}\right)\left(1 - \zeta e^{\zeta^2}\sqrt{\pi}\ Erfc\left(\zeta\right)\right) \\ &- \frac{1}{2}\frac{Bk_0^2}{\xi_L} + 1 - \frac{\xi_0}{\xi_L} = 0 \end{aligned} \tag{3.42}$$

Since ζ is now known, (3.38) can be exploited to calculate the final time it takes the interface to reach the radius of the R particle.

Until now, it has been assumed that the membrane with which the particle interacts is semi-infinite, so the cytoplasmic membrane could subject an infinitely large particle to endocytosis, which is not physically meaningful, so the right spatial extreme of the domain in (3.30) should be set equal to the length L of the membrane.

In this case, however, there is no analytical solution, so it is necessary to proceed numerically through the application of the finite difference method.

By knowing the receptor density vector $\boldsymbol{\xi(x, t^*)}$ and the position $a(t^*)$ of the particle-membrane interface at a certain time t^*, it is possible to calculate the interface speed by the equation (3.34) and then update the position of the particle by the relation $a(t^* + \Delta t) = a(t^*) + \dot{a}\left(t^*\right)\Delta t$. With the new position the left extreme of the domain of the (3.30) will be updated to find the vector $\boldsymbol{\xi(x, t^* + \Delta t)}$ and so the loop starts again until the radius of the particle is reached. As a boundary condition in L, the zero flow condition, the authors decided to set:

$$\frac{\partial \xi\left(L, t\right)}{\partial x} = 0 \tag{3.43}$$

Below there is a table with parameter values, curves of the receptor density and the interface trend between the particle and the membrane.

Table 3.1: Parameters of the model exploited to describe the receptor-mediated endocytosis process.

$\lambda[\mu m\ s^{-1}]$	$\xi_L[\mu m^{-2}]$	$\xi_0[\mu m^{-2}]$	$R[nm]$
0.01	5×10^3	50	25
C_B	B	$k_0[\mu m^{-1}]$	$L[\mu m]$
15	20	R^{-1}	10

The six receptor density curves in Figure 3.9 were extrapolated from the finite difference procedure to obtain the numerical solution. it is possible to note for each time the depletion at the particle-membrane interface and, by means of the magnification in the centre of the graph, the progress of the endocytosis process as the interface increases until the particle radius is reached.

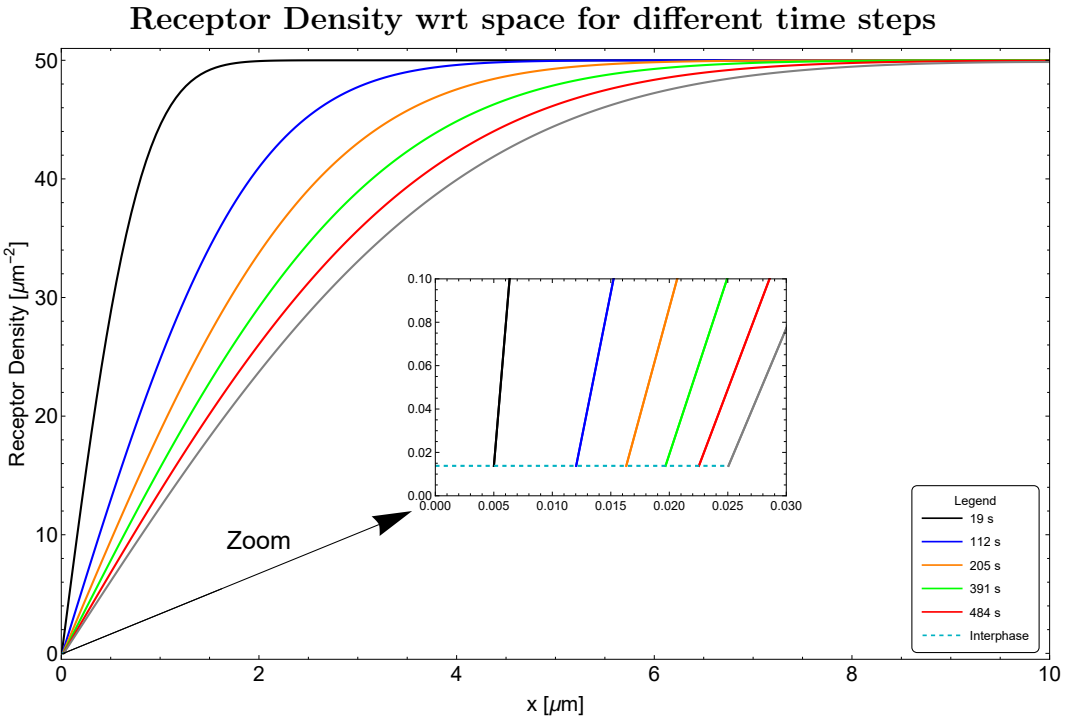

Figure 3.9: This graph shows six constant-time receptor density curves obtained by numerical solution using the finite difference method procedure. It is possible to notice the asymptote for all the curves, which is the value $\xi_0 = 50\ \mu m^{-2}$. While in the magnification in around zero,the progress of the interface for the different time intervals can be seen.

This second graph shows the progress of the interface from the initial interface value obtained from the analytical solutions for semi-infinite membrane.

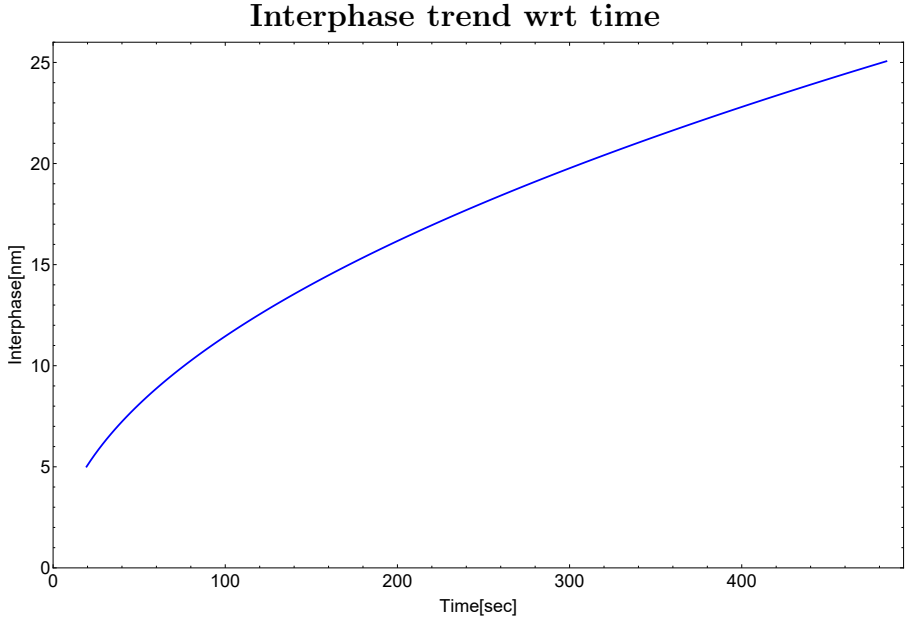

Figure 3.10: The particle-membrane interface calculated by the finite difference method is shown. The curve starts with a time value of $t_{start} \approx 19.5\ s$, which corresponds to an initial interface of 5 nm, obtained from the analytical solution, as does the starting vector of receptor density.

This procedure makes it possible to find the time required for a cell to endocyte a particle with a known radius. Although there are some limitations: first, the necessity of knowing the analytical solution and making the numerical computation start from a certain time interval, and second, the assumption of free diffusion of membrane receptors as if the membrane is perfectly homogeneous and there are only the receptors on its surface to move, a phenomenon that does not reflect reality, since on their way the receptors may encounter different obstacles and multiple proteins. This last aspect will be considered in the new formulation proposed in this thesis in Chapter 4.

3.3 Notes and changes of the later models

Other researchers over the years have modified or expanded the previous model, focusing their attention on new or previously neglected aspects. The following are examples of portions of successive models.

Li et al. [34] have focused their attention on how the nanoparticle might also not have ligands uniformly distributed on its supercific, and how this could affect the progress of the process.

Hence, the authors used a statistical model to study the dynamics of receptor diffusion-mediated endocytosis. Here, they considered how ligand-receptor complexes move to resist membrane deformation and changes in receptor configuration entropy. From here, they showed how the internalisation of nanoparticles depended on the distribution of ligands, and how the uptake process by the cell is enhanced when the ligand distribution is more uniform.

For this purpose, they performed numerical simulations where they considered different forms of ligand distribution: harmonic, linear periodic, and periodic piecewise, while the receptors always diffuse uniformly as described in the previous paragraph. An interesting case is the harmonic distribution:

$$\xi_L(x) = \xi_{L0}\left(1 + A\ Sin\left(\frac{2\lambda x}{R} + \frac{\pi}{2}\right)\right), \quad x \leq 2\pi R \tag{3.44}$$

It has been observed that the fastest absorption of the particle occurs when the amplitude of the wave reaches $A = 0.1$, in the case of high receptor density, whereas if the receptor density is low, the amplitude drops to $A = 0.01$. At high frequencies, the wrapping time is independent of the ligand distribution.

They proved how in the case of low receptor density, the nanoparticle still be phagocytosed as long as the ligand density is sufficiently high, receptor diffusion influences the phenomenon by delaying the particle's engulfment. In the case where the ligand density is low, neglecting the amount of receptor density, the scarcity of ligands does not allow adequate endocytosis and thus the particle will not be absorbed. In addition, it was observed that the wavy frequency of the ligand distribution does not affect wrapping efficiency, whereas very high values of wavy amplitude can lead to higher uptake time.

In the recent modeling proposed by Wiegold et al. [37] receptor-mediated endocytosis diffusion is modelled in the same way of Gao et al. [22], with some modifications.

They developed a two-dimensional model of a virus experiencing endocytosis. They first decided to model the virus as a substrate with fixed receptors on its surface, while receptors in the host cell are free to move across its membrane, thus allowing local variation in their concentration.

In addition, they have also considered the curvature of the membrane in the wrapping process of the virus. The novelty of the model is the additional energetic considerations on when the virus advances toward the membrane and in other factors considered.

Hence, this research group changed the free energy of the system. Here, the difference of energies in front of and behind the intephace, i.e. in the nanoparticle-membrane contact zone, is equal to the kinetic energy of the interface itself:

$$E^- - E^+ = E_{kin} \tag{3.45}$$

In which the first term represents the energy of the contact zone, the second term the energy outside the endocytosis zone where the receptors flow freely and the last the kinetic energy of the interface.

The energy behind the interface consists of three terms:

$$E^- = E_b^- + E_e^- + E_k^- \tag{3.46}$$

Respectively the energy of receptor binding, the energy concerning receptor entropy and the membrane bending energy:

$$E_b^- = -k_B T C_B \xi_L \tag{3.47a}$$

$$E_e^- = k_B T \xi_L \ln\left(\frac{\xi_L}{\xi_0}\right) \tag{3.47b}$$

$$E_k^- = \frac{1}{2} k_B T B k_0^2 \tag{3.47c}$$

While the energy in front of the interface has three other members:

$$E^+ = E_e^+ + E_k^+ + E_v^+ \tag{3.48}$$

The first relates to entropy, similarly to what has been written above, the second to the curvature of the membrane (a term that will be equal to 0 because the authors assume that the curvature in the contact zone is smaller than that caused by the virus) and finally the kinetic energy caused by the movement of the receptors of mass m_r, which move with velocity v_r:

$$E_e^+ = k_B T \xi_+ \ln\left(\frac{\xi_+}{\xi_0}\right) \tag{3.49a}$$

$$E_k^+ = 0 \tag{3.49b}$$

$$E_v^+ = \frac{1}{2} m_r \frac{\lambda^2}{\xi_+} \left(\frac{\partial \xi_+}{\partial x}\right)^2 \tag{3.49c}$$

The difference between the two macro-energy in (3.46) serves as a driving force for the advancement of the interface, which will be characterised by the following kinetic energy:

$$E_{kin} = \frac{1}{2} m_{rr} \xi_L \dot{a}\,(t) \tag{3.50}$$

Where m_{rr} is the mass of a ligand-receptor pair. Putting all the energy terms together in the (3.46) gives the new form of energy:

$$-C_B + \ln\left(\frac{\xi_L}{\xi_0}\right) + \frac{1}{2}\frac{B k_0^2}{\xi_L} - \frac{\xi_+}{\xi_L} \ln\left(\frac{\xi_+}{\xi_0}\right) - \frac{1}{2}\frac{m_r}{k_B T}\frac{\lambda^2}{\xi_+ \xi_L}\left(\frac{\partial \xi_+}{\partial x}\right)^2 = \frac{1}{2}\frac{m_{rr}}{k_B T}\dot{a}\,(t) \tag{3.51}$$

This equation is a more complex case of the (3.41). Another important factor considered is cooperativity: when receptors bind to ligands, they "smooth out" the membrane surrounding them, making it easier for other receptors to form bonds and strengthening adhesion between the nanoparticle and the membrane.It has been observed that the duration of the endocytosis process strongly depends on cooperativity and specifically on the binding range; small initial binding ranges are preferred to complete the process as quickly as possible. However, if the binding range is too low, there will not be enough ligand-receptor pairs and uptake cannot begin. In contrast, for progressively greater binding ranges, the number of receptors required to create the proper adhesion between particle and cell increases; this results in higher endocytosis times.

Another numerical simulation study of the endocytosis process is from Tang et. al (2018)[40]. When a particle undergoes endocytosis, one phenomenon that can occur is the rotation of the particle itself during wrapping. This phenomenon is more pronounced when the outer body takes on shapes other than spherical, such as ellipsoidal.

Here, the authors analysed what happens if receptor diffusion is coupled with the rotation of an ellipsoidal nanoparticle, its shape and initial orientation, and how these factors influence the wrapping time.

They hypothesised that at an early stage the particle penetrates the membrane symmetrically without rotating, then either the phenomenon continues symmetrically, as seen in the previous section, or after reaching a critical wrapping fraction f_c the nanoparticle begins to rotate, changing its configuration to asymmetrical.

Simulations have shown that the total deformation energy of the membrane is less when the process is asymmetrical rather than symmetrical. For large particles and flexible membranes, the difference in strain energy is small and it is easier to overcome thermal fluctuations of the membrane, whereas for small particles and rigid membranes, the difference in strain energy is large and it is not able to overcome thermal fluctuations. Thus, particle rotation, which always occurs beyond a certain critical wrapping fraction, is energetically more favourable than symmetrical wrapping.

It has been seen that the higher the membrane tension, the higher the f_c will be, indicating that for membranes with a sufficiently large tension the nanoparticle will tend to assume a symmetrical configuration, furthermore a reduction in bending energy facilitates the rotation of the nanoparticle.

It would appear that rotation promotes the speed of wrapping, but since wrapping proceeds in a specific direction in the asymmetric stage the total time is longer than that taken by an endocytosed particle with symmetric wrapping.

These numerical simulations represent an additional tool for understanding the mechanics behind this very complex biological process.

Chapter 4

Anomalous receptor diffusion

In this chapter, the movement of receptors on the membrane subject to the action of an external potential will be analysed and a generalised form of the diffusion equation, Smoluchowski equation, will be derived, which describes how the density of receptors varies during the process of endocytosis.

4.1 Smoluchowski equation

The Smoluchowski equation is named after Polish physicist Marian von Smoluchowski who studied the Brownian motion of particles subjected to external forces [75].

In 1915 he published a paper with his equation as a generalization of the diffusion equation with the addition of a damping term due to viscous friction. The equation describes the motion of particles in space and time in the presence of a potential that tends to move them toward regions of minimum energy.

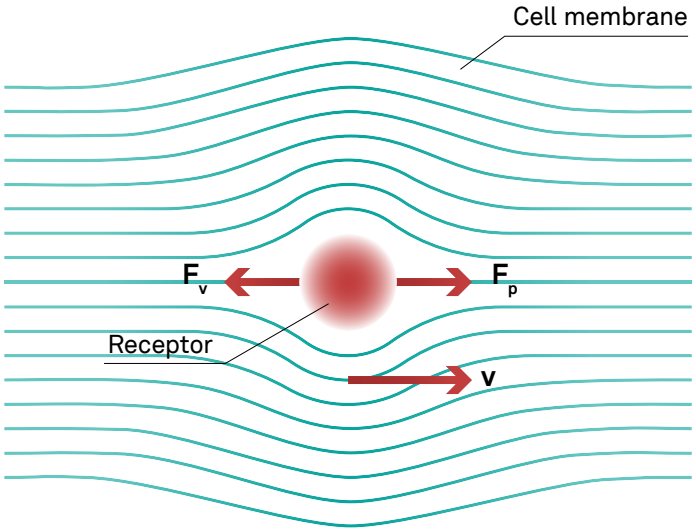

Figure 4.1: Membrane Receptor flowing on the cell membrane with a velocity v and subjected to a potential $U(x)$ from which the drag force F_p arises, and a friction force given by the membrane F_v.

To derive Smoluchowski equation we consider a potential acting on a receptor suspended in a fluid membrane.

The force balance on the receptor (Figure 4.1) will be given by:

$$m\frac{dv}{dt} = -F_v + F_p \tag{4.1}$$

In which m is the mass of the receptor, F_v the friction force and F_p the drag force. The terms after the equal can be expressed as:

$$m\frac{dv}{dt} = -\frac{v}{\mu} - \frac{dU(x)}{dx} \tag{4.2}$$

Where v is the velocity, μ is the mobility $[\mu] = TM^{-1}$ and $U(x)$ the potential.

Assuming that the receptor is in steady state, and therefore the velocity is constant, the first term on the left is zero. So the velocity can be found as:

$$v = -\mu\frac{dU(x)}{dx} \tag{4.3}$$

If we want to analyze receptors flow, we must take into account that Fick's law will not only consist of a diffusive term, but also the addition of a convective term that takes into account the velocity of these proteins:

$$j\left(x,t\right) = -\lambda\frac{\partial\xi\left(x,t\right)}{\partial x} + v\xi\left(x,t\right) \tag{4.4}$$

In which the diffusivity coefficient is expressed through Einstein's relation $\lambda = \mu k_B T$, k_B is the Boltzmann constant $[k_B] = ML^2T^{-1}K^{-1}$ and T the temperature in Kelvin.

By replacing the speed in Fick's law:

$$j\left(x,t\right) = -\lambda\frac{\partial\xi\left(x,t\right)}{\partial x} - \mu\frac{dU\left(x\right)}{dx}\xi\left(x,t\right) \tag{4.5}$$

Finally, by substituting Fick's law into the continuity equation, we obtain the modified diffusion equation or Smoluchowski equation, which accounts for the diffusive motion of the receptors and the action of the external potential:

$$\frac{\partial\xi\left(x,t\right)}{\partial t} = \lambda\frac{\partial^2\xi\left(x,t\right)}{\partial x^2} + \mu\left(\frac{\partial\xi\left(x,t\right)}{\partial x}\frac{dU\left(x\right)}{dx} + \xi\left(x,t\right)\frac{d^2U\left(x\right)}{dx^2}\right) \tag{4.6}$$

4.2 Time-fractional Smoluchowski equation

The discussed models in Chapter 3 describe the motion of receptors in a purely diffusive manner. In order to move in this way, it is necessary for the receptors to move from high-density zones to low-density regions, as can be seen in Figure 3.8.

This implies that between the bound and unbound phase the density function of the receptors has a discontinuity of the first kind, which is unexplainable from the physical point of view of the phenomenon.

In this perspective the aim of this research work is to propose a new model to more rigorously explain the phenomenon of endocytosis.

We hypothesized (Figure 4.2) that receptor flux is promoted by a potential that carries receptors from areas of low density and high potentials (green arrows), where receptors are unbound ξ_U and free to move, to areas of high density and low potentials (red arrows), where receptors are bound to ligands ξ_B.

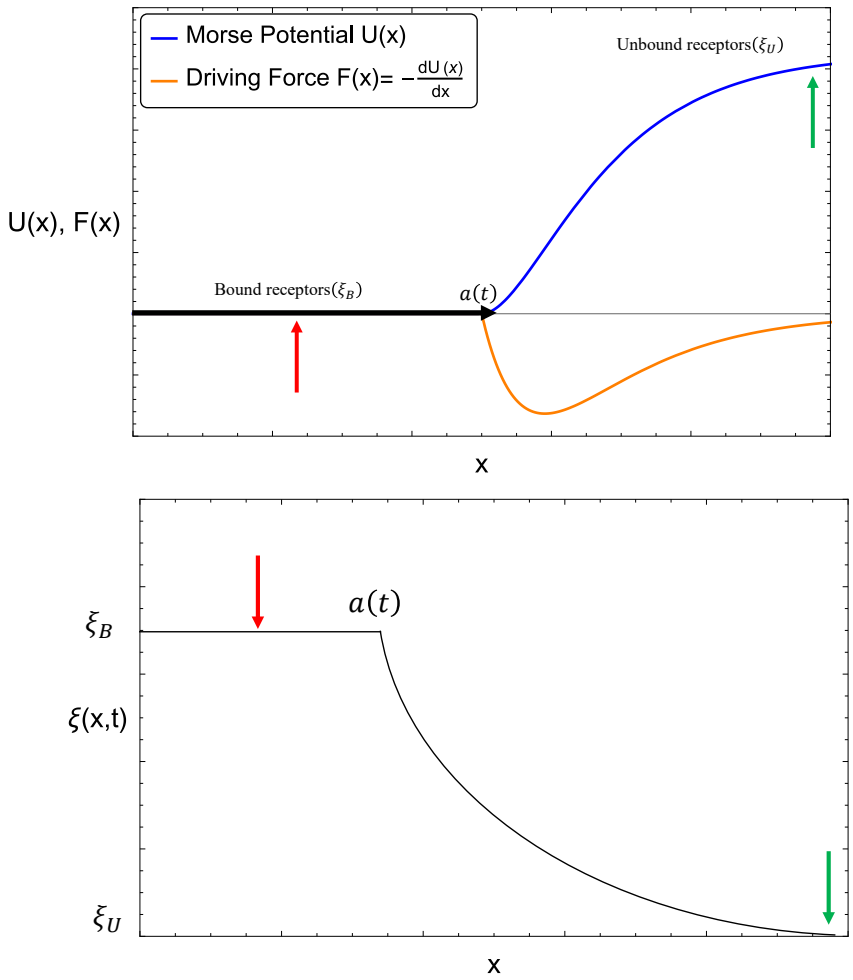

Figure 4.2: Top: the action of the Morse potential exerted on free receptors, leading them to low potentials, where the receptors are bound to ligands. Bottom: the distribution of receptors assumed at a certain time during the process.

The following modified and shifted form of the Morse potential was chosen as the acting potential on receptors [76]:

$$U(x,t) = 1.5\ k_B T \left(1 + e^{-2g(x-a(t))} - 2e^{-g(x-a(t))}\right) \tag{4.7}$$

$U(x,t)$ has the dimensions of an energy and g is the width of the potential

$[g] = L$.

This allows us to use the (4.5) and the Smoluchowski equation (4.6). To complete the system we need to derive a new Stefan condition that binds the speed intephase at receptor density, but first we need to set the boundary conditions.

Considering the right graphic in Figure 4.2, we assume that below the membrane-particle contact zone the density of ligand-bound receptors is a known quantity $\xi(a(t), t) = \xi_B$ and that there is no flux in this region, while considering the semi-infinite spatial domain we suppose that membrane areas sufficiently far from the zone of endocytosis are not involved during the process, so there the density is that of unbound receptors $\xi(x \to \infty, t) = \xi_U$.

Lastly, at the initial time the receptors are unbound and distributed on the membrane $\xi(x, 0) = \xi_U$.

Due to the previous boundary and initial conditions, and taking into account the conservation of receptors during the endocytosis process (3.31), with the appropriate mathematical steps we obtain:

$$\dot{a}(t) = -\frac{\frac{\partial^2 \xi(a(t),t)}{\partial t \partial x}}{\frac{\partial^2 \xi(a(t),t)}{\partial x^2}} \tag{4.8}$$

The model described so far, as well as the previous ones, bases the diffusion of receptors on a perfectly homogeneous phospholipid bilayer membrane, such as an artificial micelle membrane. But in reality, cells have several elements and proteins with different functionalities on their surface, as illustrated in section 2.2.

These proteins, during endocytosis, actively contribute to the recruitment of membrane receptors making it faster, e.g. PI3K (PhosphatidylInositol-3-Kinase) by activating various intermediate proteins stimulates actin reorganisation near the membrane, facilitating the migration of receptors to the endocytosis site [77]. Other proteins (section 2.6) are responsible for the recruitment of AP-2 receptors that interact with the Eps15 protein, which, through specific domains, helps to coordinate the collection of receptors and concentrate them in the areas of the membrane where invagination will occur [78].

Furthermore, it could happen that the outer body, depending on its size and the type of cell being targeted, is endocytosed in a shorter time due to the rapid movement of receptors, which is a negative aspect if the nanoparticles are viruses. this is the so-called fast endocytosis [78]. This implies that receptor flow is no longer Brownian, and simple Fick law fails to capture this.

To consider this phenomenon, we thought of introducing Caputo fractional derivative (Appendix A) of β order to modify the diffusive component of Fick's law (4.5):

$$j(x,t) = -\lambda_\beta \left({}_0^C D_t^\beta \frac{\partial \xi}{\partial x} \right)(x,t) - \mu \frac{dU(x,t)}{dx} \xi(x,t) \tag{4.9}$$

Where λ_β is the anomalous diffusivity coefficient $[\lambda_\beta] = L^2 T^{-(1-\beta)}$.

We can interpret the (4.5) as a special case of fractional Fick's law in which $\beta = 0$:

$$
\begin{aligned}
j\left(x,t\right) &= -\lambda_0 \left({}_0^C D_t^0 \frac{\partial \xi}{\partial x}\right)\left(x,t\right) - \mu \frac{dU\left(x,t\right)}{dx}\xi\left(x,t\right) = \\
&= -\lambda \frac{\partial \xi\left(x,t\right)}{\partial x} - \mu \frac{dU\left(x,t\right)}{dx}\xi\left(x,t\right)
\end{aligned}
\tag{4.10}
$$

Consequently by substituting the (4.9) into the (3.29), the new fractional system for receptor diffusion:

Fractional receptor diffusion:

$$
\begin{cases}
\dfrac{\partial \xi\left(x,t\right)}{\partial t} = \lambda_\beta \left({}_0^C D_t^\beta \dfrac{\partial^2 \xi}{\partial x^2}\right)\left(x,t\right) + \\
\qquad \mu\left(\dfrac{\partial \xi\left(x,t\right)}{\partial x}\dfrac{dU\left(x,t\right)}{dx} + \xi\left(x,t\right)\dfrac{d^2U\left(x,t\right)}{dx^2}\right), & (4.11a) \\
\qquad a(t) < x < \infty, t > 0 \\
\qquad\qquad \xi\left(x,0\right) = \xi_U & (4.11b) \\
\qquad\qquad \xi\left(a(t),t\right) = \xi_B & (4.11c) \\
\qquad\qquad \xi\left(x \to \infty, t\right) = \xi_U & (4.11d)
\end{cases}
$$

Stefan condition:

$$
\begin{cases}
\dot{a}(t) = -\dfrac{\frac{\partial^2 \xi(a(t),t)}{\partial t \partial x}}{\frac{\partial^2 \xi(a(t),t)}{\partial x^2}} & (4.12a) \\
a\left(0\right) = 0 & (4.12b)
\end{cases}
$$

However, for the given system there is no analytical solution, so we proceeded numerically through the application of the fractional finite difference method as will be explained in the following chapter.

Chapter 5

Fractional finite differences method

Given the new fractional system for receptor diffusion does not have analytical solution, this chapter will address the discretization and numerical solution of the following problem (4.11a)-(4.12b).

5.1 Setting the numerical solution

Before applying the method of fractional finite differences, we can make an argument.

As the particle-membrane interface advances, the density of receptors near the zone of endocytosis changes. It is possible to think that as the interface progresses, the spatial domain of the (4.11a) shrinks, consequently, if we discretize the space into a number of nodes their position will depend on time, as so will the density of receptors:

$$\xi(x(t), t) \tag{5.1}$$

Suppose we follow a given node $x(t)$ (Figure 5.1):

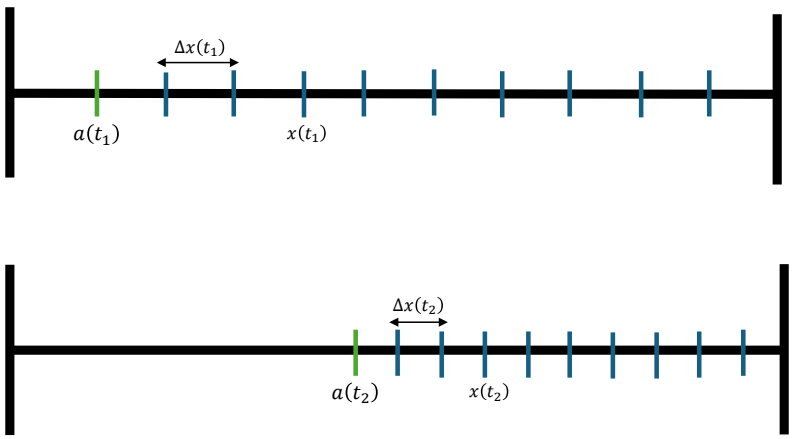

Figure 5.1: Movement of the interface (green) and spatial nodes (blue) in the grid at two different times t_1 and t_2.

At a certain instant the density of receptors will have a specific value, different from that at the next time.

To follow the change in density along the motion of the node, it is possible to apply the total derivative to the receptor density function:

$$\frac{d\xi\left(x\left(t\right),t\right)}{dt}=\frac{\partial\xi\left(x\left(t\right),t\right)}{\partial t}+\frac{dx\left(t\right)}{dt}\frac{\partial\xi\left(x\left(t\right),t\right)}{\partial x} \tag{5.2}$$

In which the first partial derivative represents the change in density over time of a fixed node in space. The second term takes into account that the spatial node at which the density is being measured may change over time, the first derivative representing the speed with which the node moves through space, while the partial derivative indicates how much the density changes with movement through space.

Finally, the product of these two functions gives the change in density due to the movement of the node in space. Through a proportion we can express the velocity of $x(t)$ as a function of the interface:

$$\frac{\frac{dx(t)}{dt}}{L-x(t)}=\frac{\frac{da(t)}{dt}}{L-a(t)} \tag{5.3}$$

Where L, the membrane length, is a sufficiently large number relative to the interface and will be the extreme right-hand side of the spatial domain.

By replacing the (5.2) and (5.3) in the (4.11a) and grouping the terms:

$$\begin{aligned}\frac{d\xi\left(x\left(t\right),t\right)}{dt}=&\lambda_{\beta}\left({}_{0}^{C}D_{t}^{\beta}\frac{\partial^{2}\xi}{\partial x^{2}}\right)\left(x(t),t\right)\\&+\frac{\partial\xi\left(x\left(t\right),t\right)}{\partial x}\left(\frac{L-x\left(t\right)}{L-a(t)}\frac{da\left(t\right)}{dt}+\mu\frac{dU\left(x,t\right)}{dx}\right)\\&+\xi\left(x(t),t\right)\left(\mu\frac{d^{2}U\left(x,t\right)}{dx^{2}}\right)\end{aligned} \tag{5.4}$$

For convenience during discretization, it is worth to bring the Caputo derivative to the term on the left side of the equation.

To do this, we apply the Riemann-Liouville fractional integral (Appendix Aof β order to all terms:

$$\begin{aligned}\left({}_{0}I_{t}^{\beta}\frac{d\xi}{dt}\right)\left(x\left(t\right),t\right)=&\lambda_{\beta}\left(\frac{\partial^{2}\xi\left(x\left(t\right),t\right)}{\partial x^{2}}-\frac{\partial^{2}\xi\left(x\left(0\right),0\right)}{\partial x^{2}}\right)\\&+{}_{0}I_{t}^{\beta}\left(\frac{\partial\xi\left(x\left(t\right),t\right)}{\partial x}\left(\frac{L-x\left(t\right)}{L-a(t)}\frac{da\left(t\right)}{dt}+\mu\frac{dU\left(x,t\right)}{dx}\right)\right)\\&+{}_{0}I_{t}^{\beta}\left(\xi\left(x\left(t\right),t\right)\left(\mu\frac{d^{2}U\left(x,t\right)}{dx^{2}}\right)\right)\end{aligned} \tag{5.5}$$

The second derivative of the density with respect to space calculated at time $t=0$ is 0.

Let us focus our attention on the first fractional integral on the left, it can be replaced by a Riemann-Liouville fractional derivative:

$$\left({}_0I_t^{\beta}\frac{d\xi}{dt}\right)(x(t),t)=\left({}_0D_t^{-\beta}\frac{d\xi}{dt}\right)(x(t),t) \tag{5.6}$$

This allows us to apply the property (A.10):

$$\left({}_0D_t^{-\beta}\frac{d\xi}{dt}\right)(x(t),t)=\left({}_0D_t^{1-\beta}\xi\right)(x(t),t)-\frac{t^{-(1-\beta)}}{\Gamma(\beta)}\xi(x(0),0) \tag{5.7}$$

Lastly by exploiting the (A.9) we arrive at the Caputo derivative:

$$\left({}_0D_t^{1-\beta}\xi\right)(x(t),t)-\frac{t^{-1+\beta}}{\Gamma(\beta)}\xi(x(0),0)=\left({}_0^CD_t^{1-\beta}\xi\right)(x(t),t) \tag{5.8}$$

By substituting Caputo fractional derivative in the (5.5):

$$\begin{aligned}\left({}_0^CD_t^{1-\beta}\xi\right)(x(t),t)=&\lambda_\beta\frac{\partial^2\xi(x(t),t)}{\partial x^2}\\&+{}_0I_t^{\beta}\left(\frac{\partial\xi(x(t),t)}{\partial x}\left(\frac{L-x(t)}{L-a(t)}\frac{da(t)}{dt}+\mu\frac{dU(x,t)}{dx}\right)\right)\\&+{}_0I_t^{\beta}\left(\xi(x(t),t)\left(\mu\frac{d^2U(x,t)}{dx^2}\right)\right)\end{aligned} \tag{5.9}$$

Now we can implicitly discretize the obtained equation. The speed of the interface is named $v(t)=da(t)/dt$.

The discretised functions will have the temporal nodes n as superscript and the spatial nodes J as subscript, with the exception of the interface having the temporal node as subscript.

The spatial discretization step is given by:

$$\Delta x(n)=\frac{L-a_n}{N} \tag{5.10}$$

Where N is the total number of spatial nodes, which will be distributed as follows:

$$x_J^n=(J-1)\,\Delta x(n) \tag{5.11}$$

While the time step:

$$\Delta t=\frac{t_{end}}{M} \tag{5.12}$$

M is the number of time nodes, t_{end} the chosen time at which the numerical computation will stop.

Recalling the Morse potential (4.7), let us first present the discretization of the two fractional integrals (Appendix A.1) in (5.9) so that they can be written in a more compact form.

The first discretized integral becomes:

$$\frac{\Delta t^{\beta}}{\Gamma\left(1+\beta\right)}\sum_{k=0}^{n}p_{n,k,\beta}\left(\left(\xi_{J+1}^{k+1}-\xi_{J-1}^{k+1}\right)B_{1}\left(J,k+1\right)\right) \tag{5.13}$$

Where $p_{n,k,\beta}=(n-k+1)^{\beta}-(n-k)^{\beta}$. It is useful to set:

$$\begin{aligned}B_{1}\left(J,k+1\right)=&\frac{1}{2\Delta x\left(k+1\right)}\frac{L-x_{J}^{k+1}}{L-a_{k+1}}v_{k+1}\\&+1.5\ g\ \lambda\left(-2e^{-2g\left(x_{J}^{k+1}-a_{k+1}\right)}+2e^{-g\left(x_{J}^{k+1}-a_{k+1}\right)}\right)\end{aligned} \tag{5.14}$$

The same thing was carried out for the second integral:

$$\frac{\Delta t^{\beta}}{\Gamma\left(1+\beta\right)}\sum_{k=0}^{n}p_{n,k,\beta}\left(\xi_{J}^{k+1}B_{2}\left(J,k+1\right)\right) \tag{5.15}$$

$$B_{2}\left(J,k+1\right)=1.5\ g^{2}\lambda\left(4e^{-2g\left(x_{J}^{k+1}-a_{k+1}\right)}+2e^{-g\left(x_{J}^{k+1}-a_{k+1}\right)}\right) \tag{5.16}$$

Therefore, the discretized equation is:

$$\begin{aligned}&\frac{1}{\Delta t^{1-\beta}\Gamma\left(1+\beta\right)}\left(\sum_{k=0}^{n}b_{k,\beta}\left(\xi_{J}^{n-k+1}-\xi_{J}^{n-k}\right)\right)=\\&=\lambda_{\beta}\frac{\left(\xi_{J-1}^{n+1}-2\xi_{J}^{n+1}+\xi_{J+1}^{n+1}\right)}{\Delta x\left(n+1\right)^{2}}\\&+\frac{\Delta t^{\beta}}{\Gamma\left(1+\beta\right)}\sum_{k=0}^{n}p_{n,k,\beta}\left(\left(\xi_{J+1}^{k+1}-\xi_{J-1}^{k+1}\right)B_{1}\left(J,k+1\right)\right)\\&+\frac{\Delta t^{\beta}}{\Gamma\left(1+\beta\right)}\sum_{k=0}^{n}p_{n,k,\beta}\left(\xi_{J}^{k+1}B_{2}\left(J,k+1\right)\right)\end{aligned} \tag{5.17}$$

In which $b_{k,\beta}=(k+1)^{\beta}-(k)^{\beta}$.
By multiplying the terms in the equation by $\Delta t^{1-\beta}\Gamma(1+\beta)$ we get:

$$\begin{aligned}&\left(\sum_{k=0}^{n}b_{k,\beta}\left(\xi_{J}^{n-k+1}-\xi_{J}^{n-k}\right)\right)=\\&=\frac{\lambda_{\beta}\Delta t^{1-\beta}\Gamma\left(1+\beta\right)}{\Delta x\left(n+1\right)^{2}}\left(\xi_{J-1}^{n+1}-2\xi_{J}^{n+1}+\xi_{J+1}^{n+1}\right)\\&+\Delta t\sum_{k=0}^{n}p_{n,k,\beta}\left(\left(\xi_{J+1}^{k+1}-\xi_{J-1}^{k+1}\right)B_{1}\left(J,k+1\right)\right)\\&+\Delta t\sum_{k=0}^{n}p_{n,k,\beta}\left(\xi_{J}^{k+1}B_{2}\left(J,k+1\right)\right)\end{aligned} \tag{5.18}$$

As a further simplification we pose:

$$G_1(n+1) = \frac{\lambda_\beta \Delta t^{1-\beta} \Gamma(1+\beta)}{\Delta x (n+1)^2} \tag{5.19}$$

$$G_2(J, k+1) = \Delta t \; B_1(J, k+1) \tag{5.20}$$

$$G_3(J, k+1) = \Delta t \; B_2(J, k+1) \tag{5.21}$$

The simplified equation becomes:

$$\begin{aligned}
&\left(\sum_{k=0}^{n} b_{k,\beta} \left(\xi_J^{n-k+1} - \xi_J^{n-k} \right) \right) = \\
&= G_1(n+1) \left(\xi_{J-1}^{n+1} - 2\xi_J^{n+1} + \xi_{J+1}^{n+1} \right) \\
&+ \sum_{k=0}^{n} p_{n,k,\beta} \left(\left(\xi_{J+1}^{k+1} - \xi_{J-1}^{k+1} \right) G_2(J, k+1) \right) \\
&+ \sum_{k=0}^{n} p_{n,k,\beta} \left(\xi_J^{k+1} G_3(J, k+1) \right)
\end{aligned} \tag{5.22}$$

We bring out the terms at time $n+1$ in the sums, and then group the members having the same spatial subscript:

$$\begin{aligned}
&\xi_J^n - \left(\sum_{k=1}^{n} b_{k,\beta} \left(\xi_J^{n-k+1} - \xi_J^{n-k} \right) \right) = \\
&= \xi_{J-1}^{n+1} \left(-G_1(n+1) + G_2(J, n+1) \right) \\
&+ \xi_J^{n+1} \left(1 + 2G_1(n+1) - G_3(J, n+1) \right) \\
&+ \xi_{J+1}^{n+1} \left(-G_1(n+1) - G_2(J, n+1) \right) \\
&- \sum_{k=0}^{n-1} p_{n,k,\beta} \left(\left(\xi_{J+1}^{k+1} - \xi_{J-1}^{k+1} \right) G_2(J, k+1) \right) - \sum_{k=0}^{n-1} p_{n,k,\beta} \left(\xi_J^{k+1} G_3(J, k+1) \right)
\end{aligned} \tag{5.23}$$

In which there is the density vector at time n and time $n+1$, the matrix of coefficients and an additional vector that takes into account the sums derived from the fractional integrals.

If $\beta = 0$ is placed in the (5.23) the three sums vanish and a pattern similar to (B.35) would be obtained.

The boundary conditions will be set as follows:

$$\xi_0^n = \xi_0^{n+1} = \xi_B \tag{5.24a}$$

$$\xi_N^n = \xi_N^{n+1} = \xi_0 \tag{5.24b}$$

By placing $J = 1$ in the (5.23) and substituting the (5.24a):

$$\xi_1^n - \left(\sum_{k=1}^{n} b_{k,\beta}\left(\xi_1^{n-k+1} - \xi_1^{n-k}\right)\right) - \xi_B\left(-G_1\left(n+1\right) + G_2\left(1, n+1\right)\right)$$
$$- \sum_{k=0}^{n-1} p_{n,k,\beta}\left(\xi_B G_2\left(1, k+1\right)\right) = \xi_1^{n+1}\left(1 + 2G_1\left(n+1\right) - G_3\left(1, n+1\right)\right) +$$
$$\xi_2^{n+1}\left(-G_1\left(n+1\right) - G_2\left(1, n+1\right)\right) - \sum_{k=0}^{n-1} p_{n,k,\beta}\left(\xi_2^{k+1} G_2\left(1, k+1\right)\right)$$
$$- \sum_{k=0}^{n-1} p_{n,k,\beta}\left(\xi_1^{k+1} G_3\left(1, k+1\right)\right) \tag{5.25}$$

This equation represents the starting point of the computation, from which by knowing the vector ξ_j at the instant n, it is possible to proceed iteratively to know the subsequent ones.

Hence, the equation (5.25) represents the first row of vectors and matrixes of the computation, in which the interface was placed to the ghost node before the first space node.

As for the second boundary condition, it is simpler to set and one proceeds set the Dirichlet condition as in classical finite differences.

To complete the discretization of the system, only the interface condition (4.12a) remains, treated as shown below:

$$v_{n+1} = -\frac{\frac{1}{\Delta t}\left(\frac{-\xi_B + \xi_1^{n+1}}{\Delta x(n+1)} - \frac{-\xi_B + \xi_1^n}{\Delta x(n)}\right)}{\frac{\xi_B - 2\xi_1^n + \xi_2^n}{\Delta x(n)^2}} \tag{5.26}$$

In addition, through speed, it is possible to update the position of the interface via the equation:

$$a_{n+1} = a_n + \Delta t \; v_{n+1} \tag{5.27}$$

The algorithm loop, considering the time nodes $n = 0, 1, 2, ...M - 1$, will continue iteratively by calculating the parameters $\Delta x(n)$, v_{n+1}, ξ^{n+1} and a_{n+1}, and then restarting the loop, thus reaching the final numerical solution.

The diffusivity coefficient, assumed constant as β varies, will be calculated by means of Saffman-Delbrück theory [79][80], in which the mobility of a protein moving across the membrane is given by:

$$\mu = \frac{1}{4\pi\nu_m}\left(ln\left(\frac{\nu_m}{r\ \nu_w}\right) - \gamma\right) \tag{5.28}$$

Where ν_m and ν_w are the viscosities of the membrane and water respectively at 25 °C, r is the radius of the receptor approximated as dimenision to a sphere and γ is the Euler–Mascheroni constant.

After obtaining the mobility, the diffusivity will be calculated using Einstein's relation $\lambda_\beta = \lambda = \mu k_B T$. Below is a table with the data used for the computations:

Table 5.1: Parameters of the time-fractional model for the receptor diffusion.

$\nu_m[mPa\ s]$	$\nu_w[mPa\ s]$	$r[nm]$	$\mu[\mu m\ pN^{-1}s^{-1}]$	$\lambda_\beta[\mu m^2\ s^{-(1-\beta)}]$
255 [81]	0.905[81]	5	3.23	0.013
$g[\mu m]$	$L[\mu m]$	$\xi_U[\mu m^{-2}]$	$\xi_B[\mu m^{-2}]$	$t_{end}[ms]$
3[76]	10	1×10^3	5×10^3	10

The computational algorithm code was written on *Wolfram Mathematica® 14* software. For the computations, we decided to model endocytosis for 10 ms, as shown in the table, aiming to discover the values reached at the virus-membrane interface.

In the following plot (Figure 5.2), the trends of the particle(or virus)-membrane interface with respect to time have been plotted for different values of the derivation order β. Depending on the cell type, there may be different types of proteins, which may somehow vary the moving speed of the receptors exploited for the endocytosis process.

From this perspective, the β parameter is likely to be intended as a measure mirroring the action of the proteins that are involved in receptor recruitment. Indeed, for a higher β it will take less time for the receptors to reach the target area for endocytosis, therefore more easily the external body will be absorbed.

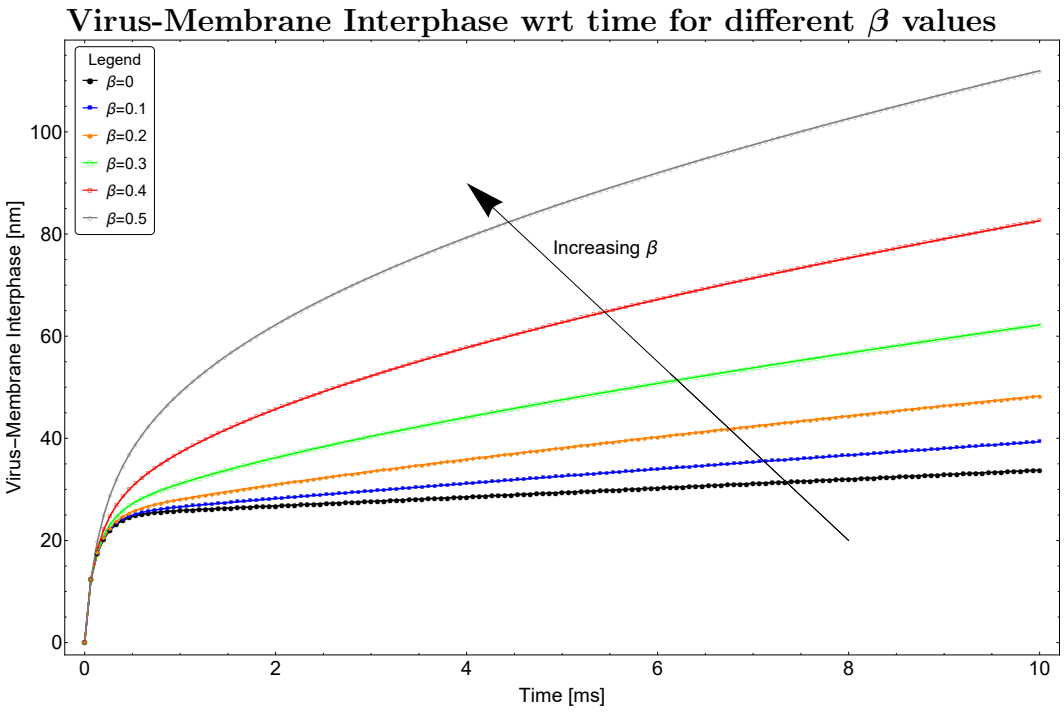

Figure 5.2: Virus-Membrane interface curves with respect to time for different values of β.

Under real biological conditions, cells are composed of numerous kinds of receptors (section 2.2.3) and depending on their function, some receptors, with different characteristics among them, may be more prevalent than others, thus conditioning the speed of the endocytosis process.

Figure 5.3 shows the trend of the virus-membrane interface curves, for a fixed β, corresponding to different values of the initial density of receptors which is responsible for binding to outer body spikes. It is possible to underline from these curves how the more free receptors are on the membrane, the faster the external body will be processed and internalized.

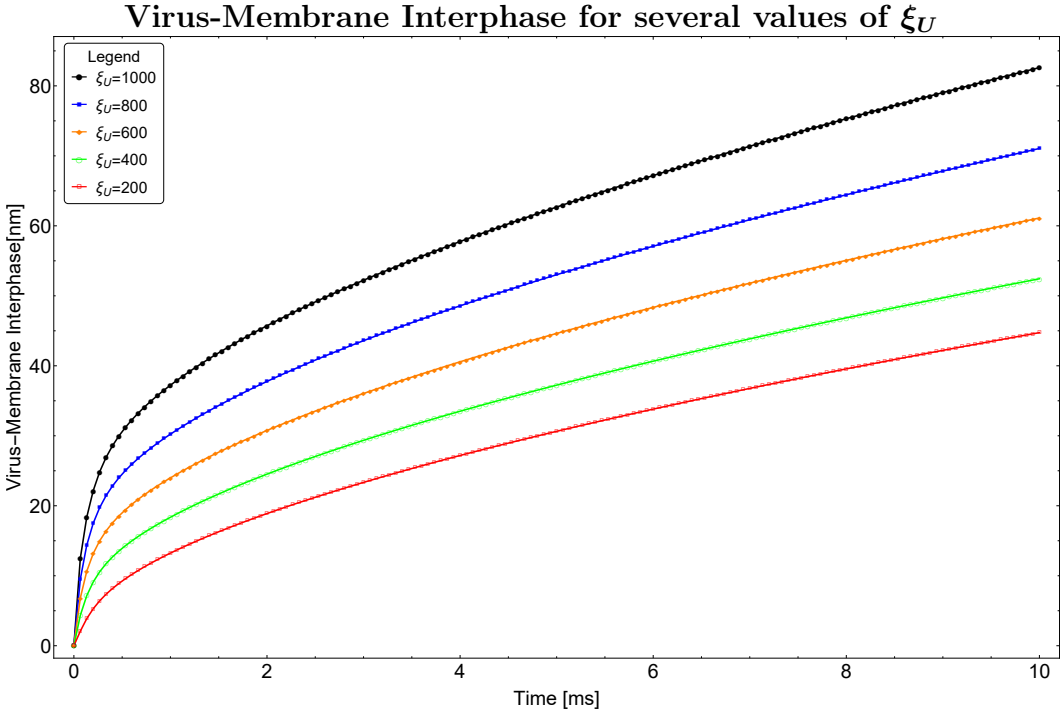

Figure 5.3: Interface with respect to time with $\beta = 0.4$ at different values of the initial number of available receptors ξ_U to promote endocytosis.

Figure 5.4 shows, for a fixed β, the progression of endocytosis from the beginning until a particle radius of 80 nm is reached.

By considering a simple virus, such as coronavirus, with a radius of 80 nm, this virus takes 10 ms to completely permeate the membrane if for example we consider the value of β fixed equal to 0.4.

Figure 5.4 shows an oscillating trend in receptor density. Since there are no other papers in the literature concerning the fractional calculus employed in endocytosis, being this thesis the first case to the authors' knowledge, or experiments analyzing receptor flux from this perspective, it remains for now without physical interpretation such oscillating trend and we allocate the investigations to future works.

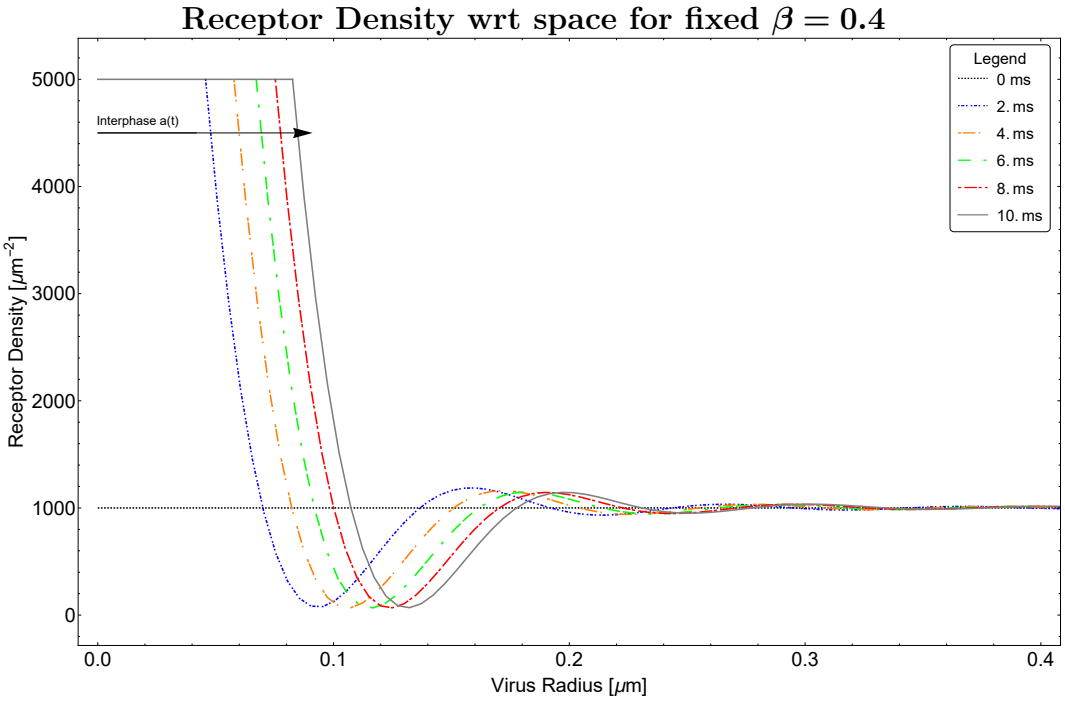

Figure 5.4: Receptor Density for fixed β.

On the other hand, Figure 5.5 represents the trend of the receptor density for a fixed time value at different β.

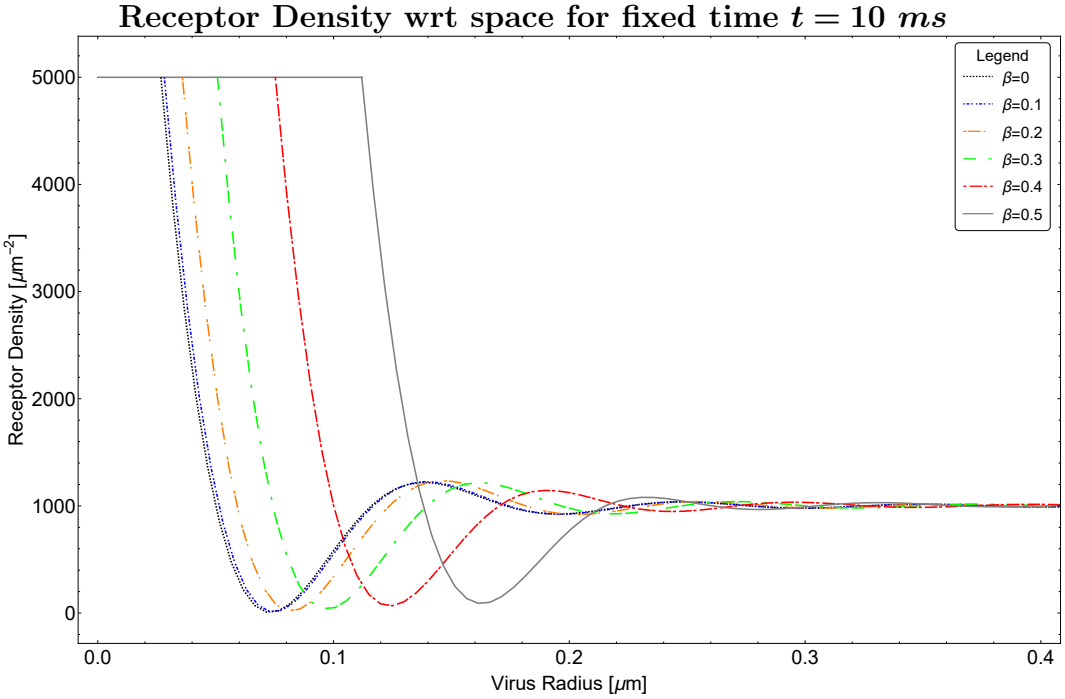

Figure 5.5: Receptor Density for fixed time.

From the Figure 5.5, we can conjecture that the β parameter may be interpreted as a mathematical parameter representing the ease through which

the virus is encapsulated during the uptake process, thereby possibly accounting for a sort of resistance of the medium in which the receptors flow. Hence it follows that the higher the β, the lower the resistance of the membrane and its proteins.

In previous simulations λ_β was considered equal to λ, but in a realistic biological phenomenon of endocytosis λ_β decreases with advancement of the process. Depending on the cell and its surface characteristics, the possible bonds that receptors can naturally form with ligands are saturated as the encapsulation process progresses. Indeed, cells possess a limited number of receptors which are available in order to form ligand bonds, and over time, these receptors have been already engaged, reducing the likelihood of further receptor-ligand interactions as the endocytosis proceeds. This phenomenon also limits the maximum engulfing size of the particle: as the surface area becomes saturated, the probability that the cell can fully envelop a large particle decreases.

From a mathematical point of view, we have described this behavior by modeling λ_β as a decreasing function with respect to time and β.

The following decay function was chosen:

$$\lambda_\beta(t) = \mu k_B T e^{-mt^{1-\beta}} \tag{5.29}$$

Where m is a constant(with dimension time to the power of $-(1-\beta)$) governing the rate of decay, which is regulated as β varies. By implementing this law, we obtain the following graph 5.6:

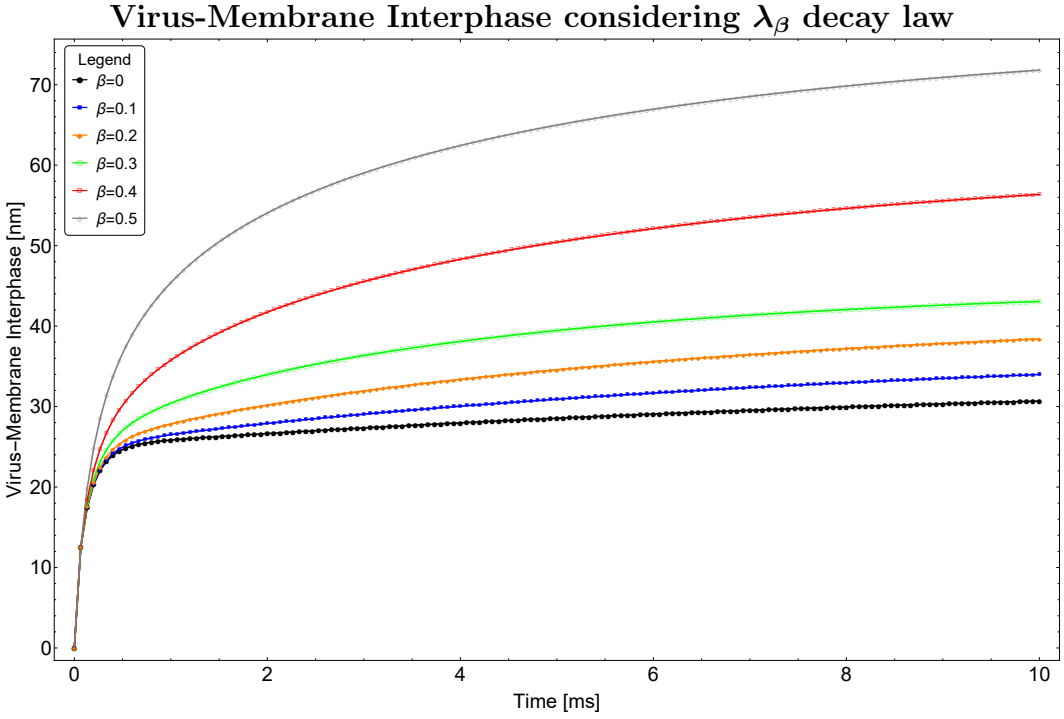

Figure 5.6: Trends of the virus-membrane interface obtained by exploiting the decay law of the anomalous diffusivity coefficient λ_β dependent on time and derivation order β. From the highest to the lowest β, m values are in the range of $8 - 100\ ms^{-(1-\beta)}$

The time-dependent interface curves are trending toward an asymptotic value that indicates the maximum effective radius that a cell can internalize through receptor-mediated endocytosis, having a given phospholipid bilayer composition dependent on β.

It should be pointed out that this represents simply one possible decay law for the anomalous diffusivity coefficient, and several different ones could be adopted based on experimental evidence on how receptors flow, which, up to the writing of this thesis, are not available in the literature.

This model could be at the root of the different epidemiological patterns, and thus why viruses infect people in a non-unique manner, or how the membrane slows down or catalyses the movement of the virus, which can be endocytosed and infect the host, or otherwise if too much time passes, it can be deactivated. The advantage of this model, compared with some previous models is that it is possible through β derivation order and other parameters, by associating the model with experimental evidence, to localize the model to specific case studies and thus analyze how receptor-mediated endocytosis occurs in, for example, muscle cells, nerve or epithelial cells. It could be possible to find several β parameters that characterize the surfaces of different cell types, making it easier to predict permeation by viruses to prevent and hinder infection, or optimizing the uptake of drug-functionalized particles for greater efficacy.

Chapter 6

Conclusion and final remarks

In this thesis, receptor-mediated endocytosis was examined, i.e. a membrane process in which membrane receptors flow onto the cell and bind to the ligands of the target to be endocytosed. This process not only allows the internalisation of nutrients needed by the cell, such as enzymes or biomolecules or nanoparticles in general, but is also a pathway used in recent times in the field of pharmacology for the production of drugs to be administered that have been appropriately functionalised in the laboratory. Unfortunately, this mechanism is also generally exploited in nature by viruses, which take advantage of it to infect the host cell and progenate the eventual emergence of disease.

It is therefore necessary and extremely useful to have a predictive model of how these viruses or nanoparticles are phagocytosed by cells. In the pharmocological field, the predictive model could be useful for optimising the timing and speed of drug release in an increasingly targeted manner for effective therapy. On the other hand, at the epidemiological level, predictive models of endocytosis processes can provide information regarding the virus and its behaviour, from which it is possible to identify how and how long it takes the hostile nanoparticle to permeate the membrane in order to inhibit its action.

Mathematical modelling is therefore necessary. Existing models in the literature treat the membrane as perfectly homogenous, when in fact it is composed of a large number of proteins with different roles. During endocytosis, some of these proteins contribute to the recruitment of receptors on the membrane, modifying their flux and increasing their speed in order to travel to the area where uptake of the parasite will take place. These models, due to physical limitations and mathematical simplifications considered, cannot explain and predict the actual process of endocytosis well.

Therefore, the aim of this work is the more rigorous formulation of a new model of receptor-mediated endocytosis, overcoming the physical limitations of previous models, such as the presence of a discontinuity without an appropriate physical meaning or the need to resort to the analyte solution in order to find the actual numerical solution of the system. The idea was to introduce a form of Morse potential, which leads the receptors from high potentials and low densities to areas of low potentials and high densities, i.e. the area where the nanoparticle will be absorbed. The Morse potential via the Smoluchowski

equation made it possible to eliminate the problem of first-species discontinuity of existing models in the literature.

The modelling involved taking into account the presence of proteins, each with its own role, that characterise the cell membrane, so that the membrane was no longer treated as homogeneous, thus coming closer to the real physical situation. These proteins influence the membrane in which the receptors flow and consequently their speed flow, no longer considered and modelled as Brownian. In order to take this important factor into account, the tool of fractional calculus, which is widely used today for the description and modelling of biological tissue behaviour, was used. Specifically, the Caputo derivative was used in the model by applying it to the diffusive component of Fick's law governing the motion of receptors.

The differential equation system modelling the endocytosis process was therefore transformed into a fractional system of differential equations. This set of differential equations does not have an analytical solution so the application of fractional finite differences was employed to numerically solve the mathematical system.

Numerical simulations of the new mathematical model predicting the process of nanoparticle endocytosis yielded interesting results. The phenomena that were evaluated included the development of the nanoparticle-membrane interface and how the flow of receptors on the space is affected. By adjusting different parameters, e.g. as a function of the order of the fractional derivative β or the availability of receptors on the cell surface or the diffusivity coefficient, it was possible to obtain a prediction of the time it takes for the external body to permeate the membrane. Furthermore, the implementation of this new mathematical model revealed an oscillatory behaviour inherent in the density of receptors never found in the literature that could be fundamental in understanding the complex mechanism of endocytosis.

The disadvantage of the model is the current impossibility of validation, as there is no other work in the literature on models of endocytosis coupled with fractional calculus. Therefore, at the time of writing this thesis, no experimental data from laboratory campaigns have been found or produced that would allow the advancement of the interface of a virus on a membrane to be examined. The lack of data mainly stems from the difficulty of carrying out an experimental setup such that it would be possible to appreciate phenomena occurring at measurement scales in the nanometre range and at very low timescales.

However, this model could be expanded for an even more accurate analysis by taking into account other different phenomena such as:

- The possibility that the particle does not simply 'fall' onto the membrane but arrives from the extracellular matrix with a certain rotational velocity that affects endocytosis, or that it penetrates the membrane in an asymmetrical way.

- The mechanics of the membrane could be taken into consideration. As the membrane deforms throughout the process, it could be treated as a

fractional visco-elastic material, certainly enriching the model in order to obtain a more accurate uptake time.

- It might be interesting to examine endocytosis in the case of multiple dimensions such as 2D or 3D.
- Introducing the mechanical action of dynamin after uptake in order to separate the endosome from the cell membrane.

Future developments could focus, first on improving the fractional model to overcome current limitations and then on the execution, with the right laboratory equipment if available, of an experimental campaign that could be used to validate this model of endocytosis.

Appendix A

Fractional calculus

Fractional calculus is an extension of the concept of derivative and integral, extending the order of derivation and/or integration to non-integer numbers β, while for $\beta = n$ we recollect the classical derivative or integral.

Some basic definitions and properties are explained below, for further details please refer to [82][83].

Euler's *Gamma Function* is defined as:

$$\Gamma(x) = \int_0^\infty \frac{e^{-t}}{t^{1-x}} dt, \quad \mathcal{R}(x) > 0 \tag{A.1}$$

The *Riemann-Liouville left-sided Fractional Integral*:

$$\left({}_0I_t^\beta G\right)(t) = \frac{1}{\Gamma(\beta)} \int_0^t \frac{G(\tau)}{(t-\tau)^{1-\beta}} d\tau \qquad n-1 < \beta < n, n = \lceil \beta \rceil \tag{A.2}$$

The *Riemann-Liouville left-sided Fractional Derivative*:

$$\left({}_0D_t^\beta G\right)(t) = \frac{d^n}{dt^n}\left({}_0I_t^{1-\beta} G\right)(t) = \frac{1}{\Gamma(n-\beta)} \frac{d^n}{dt^n} \int_0^t \frac{G(\tau)}{(t-\tau)^{\beta-n+1}} d\tau \qquad n-1 < \beta < n, n = \lceil \beta \rceil \tag{A.3}$$

While *Caputo Fractional Derivative* is expressed as:

$$\left({}_0^C D_t^\beta G\right)(t) = \left({}_0I_t^{1-\beta} \frac{d^n G}{dt^n}\right)(t) = \frac{1}{\Gamma(n-\beta)} \int_0^t \frac{G^{(n)}(\tau)}{(t-\tau)^{\beta-n+1}} d\tau \qquad n-1 < \beta < n, n = \lceil \beta \rceil \tag{A.4}$$

The Riemann-Liouville fractional derivative operator is the left-inverse to fractional integral, so the following property is valid:

$$\left({}_0D_t^\beta \, {}_0I_t^\beta G\right)(t) = G(t) \tag{A.5}$$

But it is not right-inverse, in fact:

$$\left({}_0I_t^{\beta}\,{}_0D_t^{\beta}G\right)(t) = G(t) - \sum_{k=1}^{m} \frac{t^{\beta-k}}{\Gamma(\beta-k+1)} \left({}_0D_t^{\beta-k}G\right)(0) \qquad (A.6)$$
$$m \in Z^+, m-1 < \beta < m$$

Also for Caputo derivative:

$$\left({}_0^C D_t^{\beta}\,{}_0I_t^{\beta}G\right)(t) = G(t) \qquad (A.7)$$

And:

$$\left({}_0I_t^{\beta}\,{}_0^C D_t^{\beta}G\right)(t) = G(t) - \sum_{k=0}^{m-1} \frac{t^k}{\Gamma(k+1)} G^{(k)}(0) \qquad (A.8)$$
$$m \in Z^+, m-1 < \beta < m$$

Between the two fractional derivatives there is a formula that binds them:

$$\left({}_0^C D_t^{\beta}G\right)(t) = \left({}_0D_t^{\beta}G\right)(t) - \sum_{k=0}^{m-1} \frac{t^{k-\beta}}{\Gamma(1+k-\beta)} G^{(k)}(0) \qquad (A.9)$$

Another property concerns the Riemann-Liouville fractional derivative of an integer-order derivative:

$$\left({}_0D_t^{\beta}\frac{d^m G}{dt^m}\right)(t) = \left({}_0D_t^{\beta+m}G\right)(t) - \sum_{k=0}^{m-1} \frac{t^{k-\beta-m}}{\Gamma(1+k-\beta-m)} G^{(k)}(0) \qquad (A.10)$$

A.1 Fractional operators discretization

A more complete explanation of the discretization algorithms discussed can be found at [84][85][86]. We report in the following only the discretization of Caputo fractional derivative, which is functional for solving the problem in Chapter 5.

First we consider the interval $0-t$ in which the fractional derivative of Caputo is expressed, choose a number of time instants $n = 0, 1, 2...N-1$ with which to discretize the interval, and then we can calculate the discretarization step as $\Delta t = t/N$, the position of each node can be easily calculated as $t_n = n\Delta t$.

Considering node $n+1$ and $0 < \beta < 1$, the discretization of the Caputo derivative can be expressed in the following way, without taking the remainder into account:

$$\left({}_0^C D_t^{\beta}G\right)(t_{n+1}) = \frac{1}{\Gamma(1-\beta)} \sum_{k=0}^{n} \int_{k\Delta t}^{(k+1)\Delta t} \frac{dG(\tau)}{dt} \frac{1}{((n+1)\Delta t - \tau)^{\beta}}\, d\tau \qquad (A.11)$$

We can discretize the first derivative inside the integral and take it outside:

$$\left({}_0^C D_t^\beta G\right)(t_{n+1}) = \frac{1}{\Gamma(1-\beta)} \sum_{k=0}^{n} \frac{G_{k+1} - G_k}{\Delta t} \int_{k\ \Delta t}^{(k+1)\ \Delta t} \frac{1}{((n+1)\Delta t - \tau)^\beta}\, d\tau \tag{A.12}$$

The solution of the integral is:

$$\left(\frac{((n-k+1)\Delta t)^{1-\beta} - ((n-k)\Delta t)^{1-\beta}}{1-\beta} \right) \tag{A.13}$$

After some simple mathematical steps and writing in a more compact form we get:

$$\left({}_0^C D_t^\beta G\right)(t_{n+1}) = \frac{1}{\Gamma(2-\beta)\Delta t^\beta} \sum_{k=0}^{n} b_{k,\beta} \left(G_{n-k+1} - G_{n-k}\right) \tag{A.14}$$

Where $b_{k,\beta} = (k+1)^{1-\beta} - k^{1-\beta}$. By means of this formula, exploiting the property (A.9), it is also possible to derive a discretized form of the Riemann-Liouville derivative. Similarly, one can proceed by following the same steps illustrated here to obtain the discretization of the Riemann-Liouville fractional integral. A small application of this method will be shown in the following subsection, comparing the numerical solution of a Fractional Ordinary Differential Equation (FODE) with its analytical solution.

A.1.1 Example of numerical solution of a FODE

Suppose we have the following FODE with an associated initial condition:

$$\begin{cases} \left({}_0^C D_t^\beta y_\beta\right)(t) = Sin(t) & \text{(A.15a)} \\ y_\beta(0) = 1 & \text{(A.15b)} \end{cases}$$

By applying the Laplace transform to both members of (A.15a), after some steps, the following solution is obtained:

$$y_\beta(t) = 1 + t^{1+\beta} E_{2,2+\beta}\left(-t^2\right) \tag{A.16}$$

In which $E_{2,2+\beta}(-t^2)$ represents a one-parameter Mittag-Leffler function. While for $\beta \to 1$ in (A.15a), we obtain a simple differential equation whose solution is:

$$y_1(t) = 2 - Cos(t) \tag{A.17}$$

In the case where $\beta \to 0$ in (A.15a), the Caputo fractional derivative is equal to the difference between the function $y_0(t)$ minus the function itself calculated in 0, hence 1, from which we can trivially write:

$$y_0(t) = 1 + Sin(t) \tag{A.18}$$

It is interesting to note that the (A.16) coincides perfectly with the (A.17) and (A.18), performing the corresponding limits. Let now proceed to the discretization of the (A.15a), which will have this form:

$$\frac{1}{\Delta t^{\beta}\Gamma(2-\beta)} \sum_{k=0}^{n} b_k^{(\beta)} \left(y_{n-k+1} - y_{n-k}\right) = Sin(t_n) \tag{A.19}$$

Where $t_n = n\Delta t$, $\Delta t = t_{end}/N$, where t_{end} denotes the final time at which the algorithm will stop, and finally N is the number of nodes chosen for the computation, such that $n = 0, 1, 2...N-1$. By rearranging the terms of the (A.19), we arrive at the discrete equation from which the numerical calculation can start:

$$y_{n+1} = Sin(n\Delta t)\,\Delta t^{\beta}\Gamma(2-\beta) - \sum_{k=1}^{n} b_k^{(\beta)} \left(y_{n-k+1} - y_{n-k}\right) + y_n \tag{A.20}$$

By implementing the algorithm, the numerical solutions are obtained. The following graph shows the analytical solution, black dashed, compared with three curves, cyan, green and orange, at three distinct values of β for the purpose of example:

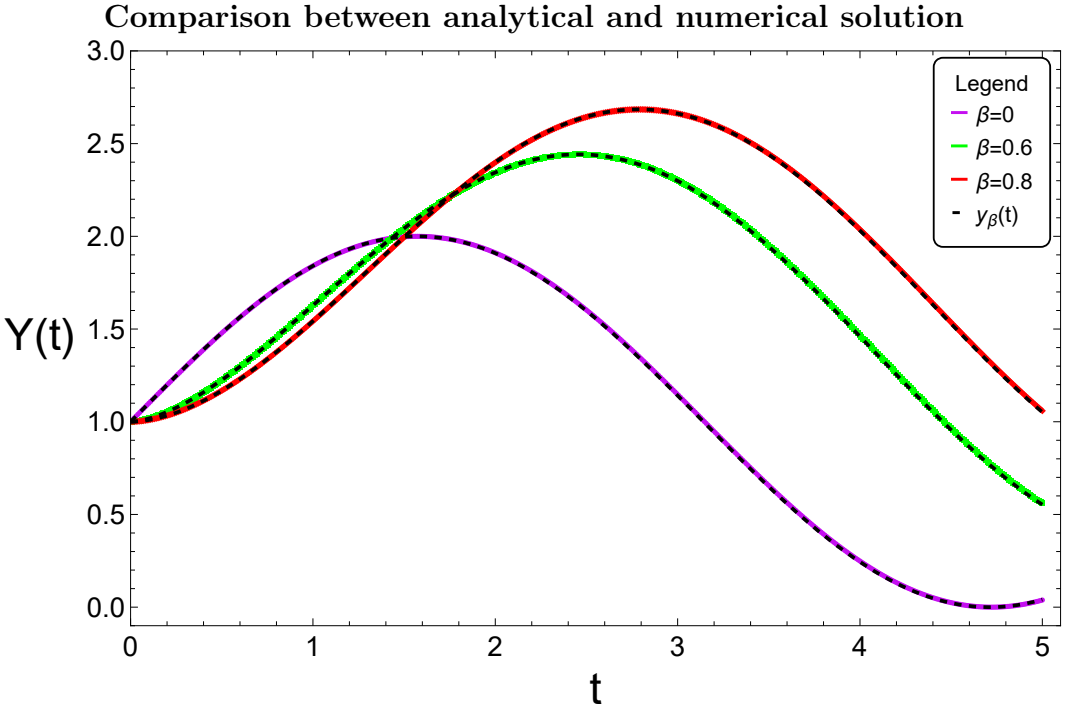

Figure A.1: Comparison between the analytical solution, dashed black, and three numerical solutions, cyan, green and red, at three values of the order of derivation, $\beta = 0$, $\beta = 0.6$ and $\beta = 0.8$ respectively.

Appendix B

Classical Stefan Problem

Stefan problem is a well-known mathematical problem in the literature and still being studied today [87]. This problem consists of a domain composed of two phases, in which one phase expands and the other phase shrinks, such as a block of ice subjected to a heat source that divides the domain into liquid and solid, separated by a moving frontier that widens over time. The final objective for solving Stefan problem is to find the temperature distribution in the two phases and to find out how the moving frontier advances with respect to time [88]. The Stefan problem was introduced by the Slovenian mathematician Josef Stefan in 1890 aiming to study glacier formation, although in fact Franz Ernst Neumann studied the problem as early as 1860, deriving the solution through similarity variable method. However, Neumann's solution was never published until 1901 when Weber reported it in an article. The similarity solution of Stefan's problem and a numerical resolution of it using the variable space grid method will be given below.

B.1 Analytical solution

$T_L(x,t)$ and $T_S(x,t)$ are identified as the temperatures for the liquid side and solid side, respectively, and T_M is the melting temperature; meanwhile $s(t)$ is the position of the moving frontier.

The spatial domain is semi-infinite so from $0 < x < s(t)$ it is occupied by liquid and from $s(t) < x < \infty$ by solid:

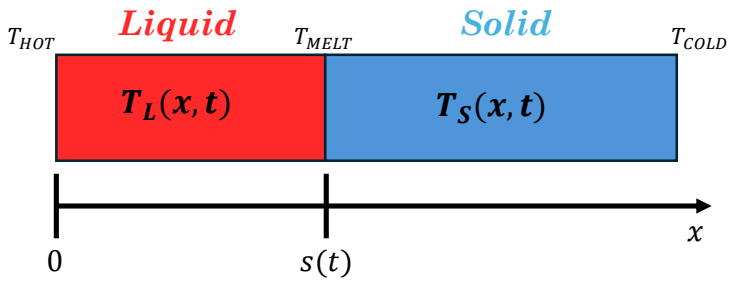

Figure B.1: Schematic representation of the liquid and solid domains withe the frontier involved in Stefan's problem.

In both domains heat diffuses following Fourier law:

$$q_i(x,t) = -k_i \frac{\partial T_i(x,t)}{\partial x} \tag{B.1}$$

Where $i = L(\text{liquid}), i = S(\text{solid})$, k is the thermal conductivity with dimensions $[k_i] = MLT^{-3}K^{-1}$.

Considering the energy conservation law:

$$\varrho c_{p,i} \frac{\partial T_i(x,t)}{\partial t} = -\frac{\partial q_i(x,t)}{\partial x} \tag{B.2}$$

In which ϱ is the density $[\varrho] = ML^{-3}$, while c_p is the specific heat capacity $[c_p] = L^2T^{-2}K^{-1}$.

If we substitute the (B.1) into the (B.2), we obtain the thermal diffusivity equation:

$$\frac{\partial T_i(x,t)}{\partial t} = \alpha_i \frac{\partial^2 T_i(x,t)}{\partial x^2} \tag{B.3}$$

$\alpha_i = k_i \varrho^{-1} c_{p,i}^{-1}$ is called thermal diffusivity $[\alpha] = L^2T^{-1}$.

We can now set the boundary and initial conditions for the two phases.

For the liquid phase, since at time $t = 0$ it does not exist, it is not possible to impose an initial condition, while the two boundary conditions will be one referring to the applied heat source, so we will have a hot temperature greater than the melting temperature $T_L(0,t) = T_H$ and one at the moving frontier equal to the melting temperature $T_L(s(t),t) = T_M$.

The solid at the beginning of the process was at a colder temperature than the melting temperature, so $T_S(x,0) = T_C$, while during the melting process its boundary condition on the left will be equal to the melting temperature $T_S(s(t),t) = T_M$, while on the right we can say that at infinity the temperature remains cold $T_S(x \to \infty, t) = T_C$.

One last thing to do before writing the complete system of partial derivative equations is to write another equation because we have a third unknown that is the moving frontier $s(t)$.

Let us consider two infinitesimal instants of time t_0 and t_1, in which we have two frontier values $s(t_0)$ and $s(t_1)$, as shown:

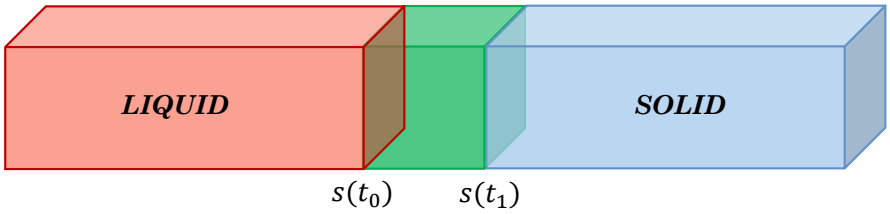

Figure B.2: Liquid and solid phases at two infinitesimal instants of time where the two distinct frontiers correspond. The two frontiers are represented so widely distant for purely illustrative purposes.

From thermodynamics knowledge, we are aware that melting a piece of ice requires heat equal to:

$$Q_1 = V\varrho\lambda = A\left(s\left(t_1\right) - s\left(t_0\right)\right)\varrho\lambda \tag{B.4}$$

Where λ is the latent heat, $[\lambda] = L^2T^{-2}$.

To apply the principle of conservation of energy and thus equalize Q_1 to the liquid and solid flows, they must be integrated twice, first with respect to area and then with respect to time:

$$Q_1 = A\int_{t_0}^{t_1}\left(-k_L\frac{\partial T_L\left(s\left(t\right),t\right)}{\partial x} + k_S\frac{\partial T_S\left(s\left(t\right),t\right)}{\partial x}\right)dt \tag{B.5}$$

We can equalize and perform some simplifications:

$$\left(s\left(t_1\right) - s\left(t_0\right)\right)\varrho\lambda = \int_{t_0}^{t_1}\left(-k_L\frac{\partial T_L\left(s\left(t\right),t\right)}{\partial x} + k_S\frac{\partial T_S\left(s\left(t\right),t\right)}{\partial x}\right)dt \tag{B.6}$$

We divide both members by $(t_1 - t_0)$ and take the limit for $t_1 \to t_0$, since t_0 can be any instant can be replaced with a generic t, so it is obtained:

$$\dot{s}\left(t\right) = -\frac{k_L}{\varrho\lambda}\frac{\partial T_L\left(s\left(t\right),t\right)}{\partial x} + \frac{k_S}{\varrho\lambda}\frac{\partial T_S\left(s\left(t\right),t\right)}{\partial x}$$

This is the so-called *Stefan condition* and binds the temperature gradients of both phases calculated at the frontier to the speed of the moving frontier.

Finally, we can write the complete system separately for the liquid side and the solid side, including the Stefan condition about the frontier:

Liquid Side:

$$\begin{cases} \dfrac{\partial T_L\left(x,t\right)}{\partial t} = \alpha_L\dfrac{\partial^2 T_L\left(x,t\right)}{\partial x^2}, \quad 0 < x < s\left(t\right), t > 0 & \text{(B.7a)} \\ T_L\left(0,t\right) = T_H & \text{(B.7b)} \\ T_L\left(s(t),t\right) = T_M & \text{(B.7c)} \end{cases}$$

Solid Side:

$$\begin{cases} \dfrac{\partial T_S\left(x,t\right)}{\partial t} = \alpha_S\dfrac{\partial^2 T_S\left(x,t\right)}{\partial x^2}, \quad s\left(t\right) < x < \infty, t > 0 & \text{(B.8a)} \\ T_S\left(x,0\right) = T_C & \text{(B.8b)} \\ T_S\left(s(t),t\right) = T_M & \text{(B.8c)} \\ T_S\left(x \to \infty,t\right) = T_C & \text{(B.8d)} \end{cases}$$

Stefan Condition:

$$\begin{cases} \dot{s}\left(t\right) = -\dfrac{k_L}{\varrho\lambda}\dfrac{\partial T_L\left(s\left(t\right),t\right)}{\partial x} + \dfrac{k_S}{\varrho\lambda}\dfrac{\partial T_S\left(s\left(t\right),t\right)}{\partial x} & \text{(B.9a)} \\ s\left(0\right) = 0 & \text{(B.9b)} \end{cases}$$

To find the solutions of (B.7a)-(B.9b) we apply the similarity variable.

The procedure will be carried out for the liquid diffusion equation but is perfectly analogous to the solid one.

Let us introduce the similarity variable:

$$\zeta = \frac{x}{\sqrt{t}} \tag{B.10}$$

And the new unknown function:

$$T_L\left(x,t\right) = f\left(\zeta\left(x,t\right)\right) \tag{B.11}$$

Obtain the derivative with respect to time and the second derivative with respect to space:

$$\frac{\partial T_L\left(x,t\right)}{\partial t} = \frac{df}{d\zeta}\frac{\partial \zeta}{\partial t} = -\frac{x}{2t\sqrt{t}}\frac{df}{d\zeta} = -\frac{\zeta}{2t}\frac{df}{d\zeta} \tag{B.12}$$

$$\frac{\partial^2 T_L\left(x,t\right)}{\partial x^2} = \frac{d^2 f}{d\zeta^2}\left(\frac{\partial \zeta}{\partial x}\right)^2 + \frac{df}{d\zeta}\frac{\partial^2 \zeta}{\partial x^2} = \frac{1}{t}\frac{d^2 f}{d\zeta^2} \tag{B.13}$$

We substitute the two derivatives into the (B.7a):

$$-\frac{\zeta}{2}\frac{df(\zeta)}{d\zeta} = \alpha_L \frac{d^2 f(\zeta)}{d\zeta^2} \tag{B.14}$$

Whose general solution is:

$$f\left(\zeta\right) = c_2 + c_1\sqrt{\pi\alpha_L}\ Erf\left(\frac{\zeta}{2\sqrt{\alpha_L}}\right) \tag{B.15}$$

Where $Erf(y)$ is the error function:

$$Erf\left(y\right) = \frac{2}{\sqrt{\pi}}\int_0^y e^{-t^2}\ dt \tag{B.16}$$

Back to the temperature function of the liquid by resubstituting the (B.10) and (B.11) in the solution:

$$T_L\left(x,t\right) = c_2 + c_1\sqrt{\pi\alpha_L}\ Erf\left(\frac{x}{2\sqrt{\alpha_L t}}\right) \tag{B.17}$$

After applying the (B.7b), by setting the (B.7c) it is clear that we do not yet know the function of $s(t)$, but we can posit that the ratio $s(t)/2\sqrt{\alpha_L t}$ is equal to a dimensionless constant γ so we get:

$$T_L\left(x,t\right) = T_H - \left(\frac{T_H - T_M}{Erf(\gamma)}\right) Erf\left(\frac{x}{2\sqrt{\alpha_L t}}\right) \tag{B.18}$$

$$s\left(t\right) = 2\gamma\sqrt{\alpha_L t} \tag{B.19}$$

Similarly by following the same reasoning for the liquid equation, the solution of the (B.8a) for the temperature distribution in the solid is found:

$$T_S(x,t) = T_C + \left(\frac{T_M - T_C}{Erfc\left(\gamma\frac{\sqrt{\alpha_L}}{\sqrt{\alpha_S}}\right)}\right) Erfc\left(\frac{x}{2\sqrt{\alpha_S t}}\right) \tag{B.20}$$

The only unknown in the problem remains the dimensionless constant γ; to find it we exploit the (B.9a) by substituting in it all previous solutions found:

$$\gamma = \left(\frac{c_{p,L}}{\lambda}\frac{(T_H - T_M)}{\sqrt{\pi}}\right)\frac{e^{-\gamma^2}}{Erf(\gamma)} - \left(\frac{c_{p,L}}{\lambda}\frac{k_S}{k_L}\frac{\sqrt{\alpha_L}}{\sqrt{\alpha_S}}\frac{(T_M - T_C)}{\sqrt{\pi}}\right)\frac{e^{-\frac{\alpha_L}{\alpha_S}\gamma^2}}{Erfc\left(\gamma\frac{\sqrt{\alpha_L}}{\sqrt{\alpha_S}}\right)} \tag{B.21}$$

This is a transcendental equation in the single unknown γ, solvable by numerical method. The set of equations $(B.18) - (B.21)$ compose the solution of Stefan's problem.

B.2 Numerical solution

In the literature, one of the methods for determining temperature distributions and the frontier is carried out by applying the finite difference method.

This method is not applied directly because the spatial grids of the two phases change at each instant, one widening and the other shrinking; the application of simple finite differences is not effective in capturing this phenomenon.

Therefore, two of the methods complement finite differences: the front-fixing method [89] and the variable space grid method [90][91]. The finite differences method with variable space grid will be explained below.

Since we have a time-dependent moving interface, it is logical to think that if we discretize the two domains, the position of the nodes present within them will also be time-dependent.

Taking liquid temperature as an example, one can write:

$$T_L(x(t), t) \tag{B.22}$$

Now we can imagine following a generic node $x(t)$ within the liquid that will have its own path to follow (Figure B.3).

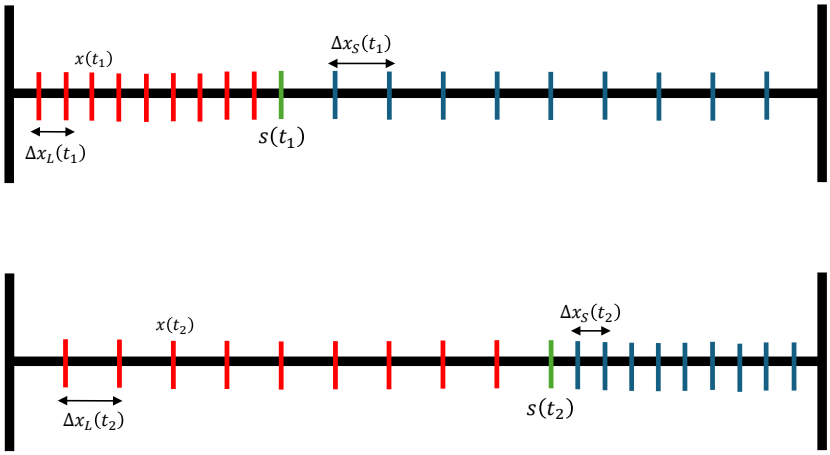

Figure B.3: Schematic representation of how the spatial grid varies for the two liquid (red) and solid (blue) domains, separated by the interface (green), between two instants t_1 and t_2 considering a number of nodes represented by the vertical lines. In the liquid domain, it is possible to observe how a generic node moves between the two moments of time.

At a given instant the node will have a certain temperature, while the next moment it will have a higher temperature. To follow the temperature change along the motion of the node we can apply the total derivative:

$$\frac{dT_L\left(x\left(t\right),t\right)}{dt} = \frac{\partial T_L\left(x\left(t\right),t\right)}{\partial t} + \frac{dx(t)}{dt}\frac{\partial T_L\left(x\left(t\right),t\right)}{\partial x} \tag{B.23}$$

Where the first term represents the temporal change in temperature at fixed point x, while the second term indicates how much the temperature changes in space as a function of the motion of the node with velocity $dx(t)/dt$. Through a simple proportion we can express the velocity of $x(t)$ in function of the frontier:

$$\frac{\frac{dx(t)}{dt}}{x\left(t\right)} = \frac{\frac{ds(t)}{dt}}{s(t)} \tag{B.24}$$

Substituting the proportion in the (B.23) and then this into the (B.7a) we finally obtain the equation to be discretized. Following the same steps, omitted here, the equation of the solid can also be derived:

$$\frac{dT_L\left(x\left(t\right),t\right)}{dt} = \left(\frac{x\left(t\right)}{s(t)}\frac{ds(t)}{dt}\right)\frac{\partial T_L\left(x\left(t\right),t\right)}{\partial x} + \alpha_L\frac{\partial^2 T_L\left(x\left(t\right),t\right)}{\partial x^2} \tag{B.25}$$

$$\frac{dT_S\left(x\left(t\right),t\right)}{dt} = \left(\frac{L-x\left(t\right)}{L-s(t)}\frac{ds(t)}{dt}\right)\frac{\partial T_S\left(x\left(t\right),t\right)}{\partial x} + \alpha_S\frac{\partial^2 T_S\left(x\left(t\right),t\right)}{\partial x^2} \tag{B.26}$$

Where $L >>> s(t)$, L is the extreme right-hand side of the domain of the solid, since it obviously cannot be set infinity at finite differences it will be a sufficiently large number than the value of the frontier.

From the (B.25) it is possible to see that Stefan's problem is degenerate in 0, in fact the numerical computation will not be able to start from s(0)=0, but from an assigned frontier value to which will correspond a temperature vector for the liquid and one for the solid, extrapolated from the analytical solution.

From now on n at superscript, except for the frontier where it will be at subscript, represents a time node at which the function is considered, while J or i at subscript the space node.

The spatial discretization steps for liquid and solid will be:

$$\Delta x_L(n) = \frac{s_n}{N_L}, \quad \Delta x_S(n) = \frac{L - s_n}{N_S} \tag{B.27}$$

Where N_L and N_S are the number of nodes or points in the two domains, while s_n represents a value of the frontier at instant n.

The position of each node J of the liquid and i of the solid will be given by:

$$x_J^n = (J-1)\,\Delta x_L\,(n)\,, \quad x_i^n = (i-1)\,\Delta x_S\,(n) \tag{B.28}$$

For temporal discretization we choose a start time t_{start} and an end time t_{end} in which to make the numerical computation take place and a number of time nodes R, thus:

$$\Delta t = \frac{t_{end} - t_{start}}{R} \tag{B.29}$$

Thus n-th time will be given by $t_n = n\Delta t$ with $n = 1, 2, 3...R-1$.

Denoting the liquid by T_J^n and T_i^n for solid and the speed of the moving frontier with $v(t) = ds(t)/dt$, the implicit dicretization of (B.25),(B.26) is as follows:

$$\frac{\left(T_J^{n+1} - T_j^n\right)}{\Delta t} = \left(\frac{x_J^n}{s_n} v_n\right) \frac{\left(T_{J+1}^{n+1} - T_{J-1}^{n+1}\right)}{2\Delta x_L\,(n+1)} + \alpha_L \frac{\left(T_{J-1}^{n+1} - 2T_J^{n+1} + T_{J+1}^{n+1}\right)}{\left(\Delta x_L\,(n+1)\right)^2} \tag{B.30}$$

$$\frac{\left(T_i^{n+1} - T_i^n\right)}{\Delta t} = \left(\frac{L - x_i^n}{L - s_n} v_n\right) \frac{\left(T_{i+1}^{n+1} - T_{i-1}^{n+1}\right)}{2\Delta x_S\,(n+1)} + \alpha_S \frac{\left(T_{i-1}^{n+1} - 2T_i^{n+1} + T_{i+1}^{n+1}\right)}{\left(\Delta x_L\,(n+1)\right)^2} \tag{B.31}$$

Rearranging and regrouping terms:

$$\begin{aligned} &T_{J-1}^{n+1}\left(-\frac{\alpha_L \Delta t}{\left(\Delta x_L\,(n+1)\right)^2} + \frac{\Delta t}{2\Delta x_L\,(n+1)}\left(\frac{x_J^n}{s_n} v_n\right)\right) \\ &+ T_J^{n+1}\left(1 + 2\frac{\alpha_L \Delta t}{\left(\Delta x_L\,(n+1)\right)^2}\right) \\ &+ T_{J+1}^{n+1}\left(-\frac{\alpha_L \Delta t}{\left(\Delta x_L\,(n+1)\right)^2} - \frac{\Delta t}{2\Delta x_L\,(n+1)}\left(\frac{x_J^n}{s^n} v_n\right)\right) = T_J^n \end{aligned} \tag{B.32}$$

$$
\begin{aligned}
&T_{i-1}^{n+1}\left(-\frac{\alpha_S\Delta t}{\left(\Delta x_L\left(n+1\right)\right)^2}+\frac{\Delta t}{2\Delta x_S\left(n+1\right)}\left(\frac{L-x_i^n}{L-s_n}v_n\right)\right)\\
&+T_i^{n+1}\left(1+2\frac{\alpha_S\Delta t}{\left(\Delta x_L\left(n+1\right)\right)^2}\right)\\
&+T_{i+1}^{n+1}\left(-\frac{\alpha_S\Delta t}{\left(\Delta x_L\left(n+1\right)\right)^2}-\frac{\Delta t}{2\Delta x_S\left(n+1\right)}\left(\frac{L-x_i^n}{L-s_n}v_n\right)\right)=T_i^n
\end{aligned}
\tag{B.33}
$$

To avoid writing too long equations, we name the terms inside round brackets:

$$
T_{J-1}^{n+1}\left(B_{1L}\left(J,n\right)\right)+T_J^{n+1}\left(B_{2L}\left(n\right)\right)+T_{J+1}^{n+1}\left(B_{3L}\left(J,n\right)\right)=T_J^n \tag{B.34}
$$

$$
T_{i-1}^{n+1}\left(B_{1S}\left(i,n\right)\right)+T_i^{n+1}\left(B_{2S}\left(n\right)\right)+T_{i+1}^{n+1}\left(B_{3S}\left(i,n\right)\right)=T_i^n \tag{B.35}
$$

We can set boundary conditions. Those where there is the moving frontier will be placed in the ghost nodes, while the other Dirichlet conditions will be imposed as usual for finite differences, so we will obtain:

Liquid zone:

$$
T_1^n=T_1^{n+1}=T_H \tag{B.36a}
$$

$$
T_{N_L+1}^n=T_{N_L+1}^{n+1}=T_M \tag{B.36b}
$$

Solid zone:

$$
T_0^n=T_0^{n+1}=T_M \tag{B.37a}
$$

$$
T_{N_S}^n=T_{N_S}^{n+1}=T_C \tag{B.37b}
$$

If we apply $J=N_L$ and (B.36b) in the (B.34) with the appropriate steps we arrive at:

$$
T_{N_L-1}^{n+1}\left(B_{1L}\left(N_L,n\right)\right)+T_{N_L}^{n+1}\left(B_{2L}\left(n\right)\right)=T_{N_L}^n-T_M\left(B_{3L}\left(N_L,n\right)\right) \tag{B.38}
$$

While for $i=1$ and (B.37a) in the (B.35) we get:

$$
T_1^{n+1}\left(B_{2S}\left(n\right)\right)+T_2^{n+1}\left(B_{3S}\left(1,n\right)\right)=T_1^n-T_M\left(B_{1S}\left(1,n\right)\right) \tag{B.39}
$$

Stefan's condition (B.9a) instead will be discretized explicitly, the liquid part with finite differences backward and the solid part forward:

$$
v_n=-\frac{k_L}{\varrho\lambda}\frac{T_{N_L+1}^n-T_{N_L}^n}{\Delta x_L\left(n\right)}+\frac{k_S}{\varrho\lambda}\frac{-T_0^n+T_1^n}{\Delta x_S\left(n\right)} \tag{B.40}
$$

Inserting the B.36b and B.37a:

$$
v_n=-\frac{k_L}{\varrho\lambda}\frac{T_M-T_{N_L}^n}{\Delta x_L\left(n\right)}+\frac{k_S}{\varrho\lambda}\frac{-T_M+T_1^n}{\Delta x_S\left(n\right)} \tag{B.41}
$$

Finally, thanks to the speed of the frontier, we can write the following to update the frontier at each time step:

$$s_{n+1} = s_n + v_n \Delta t \tag{B.42}$$

Knowing at time t_{start} the values of s_n, T_L^n and T_S^n, the algorithm loop will be:

1. Calculate $\Delta x_L(n)$, $\Delta x_S(n)$ and consequently (B.28).
2. Calculate v_n with (B.41).
3. Calculate T_L^{n+1} and T_S^{n+1} with (B.34) and (B.35).
4. Calculate s_{n+1} with (B.42) and restart loop.

The data used, by way of example, are those of the Ti6Al4V alloy.

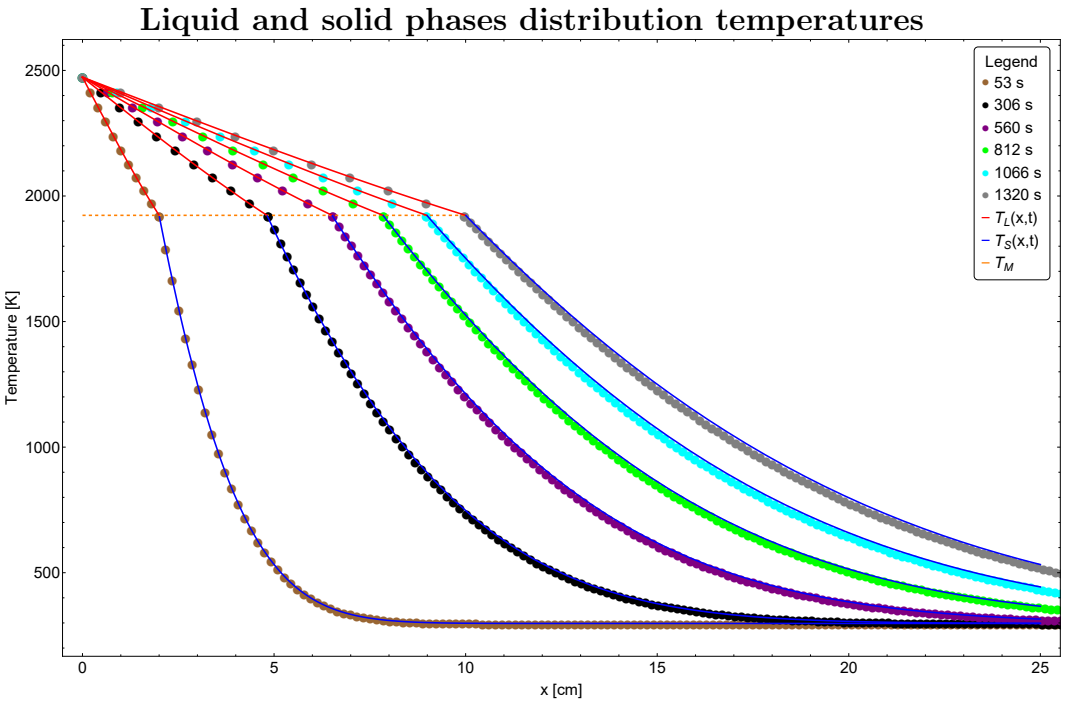

Figure B.4: Illustration of six curves (the first one in brown extrapolated from the analytical solution) resulting from the application of the finite difference method combined with the variable spatial grid.

Figure B.4 shows six curves, the first in brown taken from the analytical solutions, the others are 5 five extrapolated from the result of the algorithm shown above. It can be noticed how well the numerical solutions follow the analytical solutions (red for the temperature distribution of the liquid and blue for the solid). While Figure B.5 shows the performance of the interface in orange compared to the analytical solution in blue.

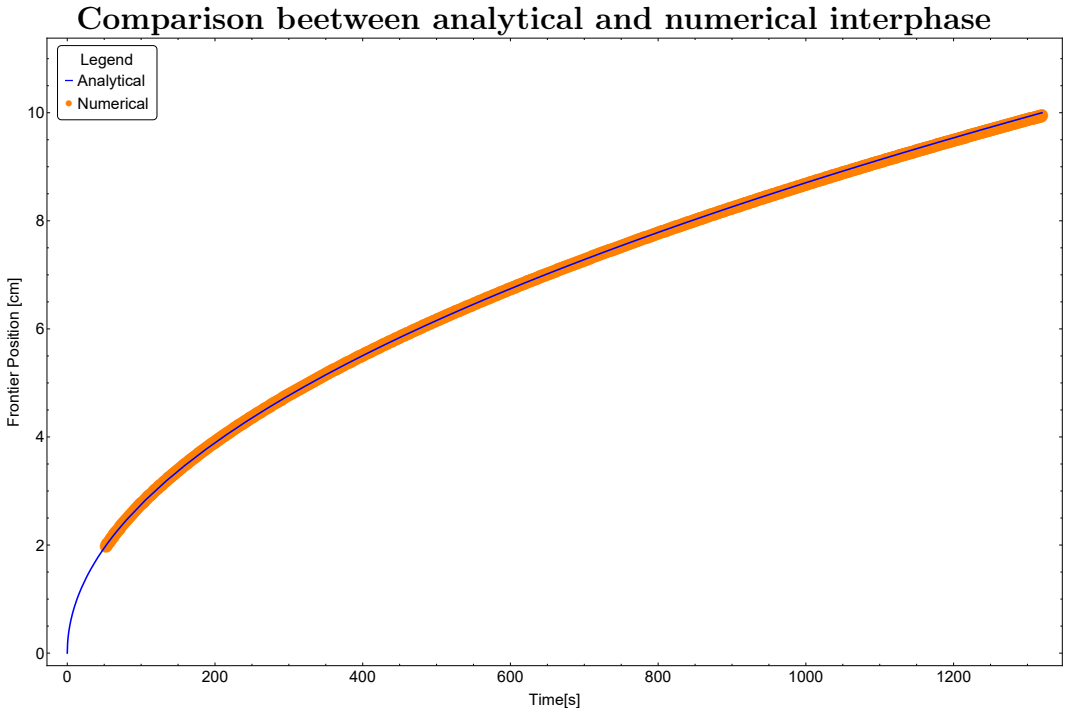

Figure B.5: Comparison between the liquid-solid frontier (orange) and the analytical solution (blue).

Bibliography

[1] Elizabeth Spencer Allman and John A Rhodes. *Mathematical models in biology: an introduction*. Cambridge University Press, 2004. doi:10.1017/CBO9780511790911.

[2] Isabella Ellinger and Peter Pietschmann. Endocytosis in health and disease—a thematic issue dedicated to renate fuchs. *Wiener Medizinische Wochenschrift*, 166:193–195, 2016. doi:10.1007/s10354-016-0454-1.

[3] GJ Russell-Jones. The potential use of receptor-mediated endocytosis for oral drug delivery. *Advanced drug delivery reviews*, 20(1):83–97, 1996. doi:10.1016/0169-409X(95)00131-P.

[4] Robert J. Mashl and Robijn F. Bruinsma. Spontaneous-curvature theory of clathrin-coated membranes. *Biophysical journal*, 74(6):2862–2875, 1998. doi:10.1016/S0006-3495(98)77993-7.

[5] Andrea Remuzzi and Giuseppe Remuzzi. Covid-19 and italy: what next? *The Lancet*, 395(10231):1225–1228, 2020. doi:10.1016/S0140-6736(20)30627-9.

[6] Jun Chen, Hongzhou Lu, Gerry Melino, Stefania Boccia, Mauro Piacentini, Walter Ricciardi, Ying Wang, Yufang Shi, and Tongyu Zhu. Covid-19 infection: the Cina and Italy perspectives. *Cell death & disease*, 11(6):438, 2020. doi:10.1038/s41419-020-2603-0.

[7] Dhanusha Yesudhas, Ambuj Srivastava, and M Michael Gromiha. Covid-19 outbreak: history, mechanism, transmission, structural studies and therapeutics. *Infection*, 49:199–213, 2021. doi:10.1007/s15010-020-01516-2.

[8] Naidi Yang and Han-Ming Shen. Targeting the endocytic pathway and autophagy process as a novel therapeutic strategy in covid-19. *International journal of biological sciences*, 16(10):1724, 2020. doi:10.7150/ijbs.45498.

[9] Oleg O Glebov. Understanding sars-cov-2 endocytosis for covid-19 drug repurposing. *The FEBS journal*, 287(17):3664–3671, 2020. doi:10.1111/febs.15369.

[10] Kristina V Tugaeva, Dorothy EDP Hawkins, Jake LR Smith, Oliver W Bayfield, De-Sheng Ker, Andrey A Sysoev, Oleg I Klychnikov, Alfred A

Antson, and Nikolai N Sluchanko. The mechanism of sars-cov-2 nucleocapsid protein recognition by the human 14-3-3 proteins. *Journal of Molecular Biology*, 433(8):166875, 2021. doi:10.1016/j.jmb.2021.166875.

[11] Shilin Zhou, Panpan Lv, Mingxue Li, Zihui Chen, Hong Xin, Svetlana Reilly, and Xuemei Zhang. Sars-cov-2 e protein: Pathogenesis and potential therapeutic development. *Biomedicine & Pharmacotherapy*, page 114242, 2023. doi:10.1016/j.biopha.2023.114242.

[12] Mauricio Ponga. Quantifying the adhesive strength between the sars-cov-2 s-proteins and human receptor and its effect in therapeutics. *Scientific reports*, 10(1):17538, 2020. doi:10.1038/s41598-020-74189-4.

[13] Xiuyuan Ou, Yan Liu, Xiaobo Lei, Pei Li, Dan Mi, Lili Ren, Li Guo, Ruixuan Guo, Ting Chen, Jiaxin Hu, et al. Characterization of spike glycoprotein of sars-cov-2 on virus entry and its immune cross-reactivity with sars-cov. *Nature Communications*, 11(1):1620, 2020. doi:10.1038/s41467-020-15562-9.

[14] Tiffany Tang, Miya Bidon, Javier A Jaimes, Gary R Whittaker, and Susan Daniel. Coronavirus membrane fusion mechanism offers a potential target for antiviral development. *Antiviral research*, 178:104792, 2020. doi:10.1016/j.antiviral.2020.104792.

[15] Jian Shang, Yushun Wan, Chuming Luo, Gang Ye, Qibin Geng, Ashley Auerbach, and Fang Li. Cell entry mechanisms of sars-cov-2. *Proceedings of the National Academy of Sciences*, 117(21):11727–11734, 2020. doi:10.1073/pnas.2003138117.

[16] Inge Hamming, Wim Timens, MLC Bulthuis, AT Lely, GJ van Navis, and Harry van Goor. Tissue distribution of ACE2 protein, the functional receptor for SARS coronavirus. a first step in understanding SARS pathogenesis. *The Journal of Pathology: A Journal of the Pathological Society of Great Britain and Ireland*, 203(2):631–637, 2004. doi:10.1002/path.1570.

[17] Inge Hamming, Mark E Cooper, Bart L Haagmans, Nighel M Hooper, Ron Korstanje, Albert DME Osterhaus, Wim Timens, AJ Turner, Gerjan Navis, and Harry van Goor. The emerging role of ace2 in physiology and disease. *The Journal of Pathology: A Journal of the Pathological Society of Great Britain and Ireland*, 212(1):1–11, 2007. doi:10.1002/path.2162.

[18] Henrik Garoff and Kai Simons. Location of the spike glycoproteins in the semliki forest virus membrane. *Proceedings of the National Academy of Sciences*, 71(10):3988–3992, 1974. doi:10.1073/pnas.71.10.3988.

[19] Kai Simons and Henrik Garoff. The budding mechanisms of enveloped animal viruses. *Journal of General Virology*, 50(1):1–21, 1980. doi:10.1099/0022-1317-50-1-1.

[20] D Van Effenterre and D Roux. Adhesion of colloids on a cell surface in competition for mobile receptors. *Europhysics Letters*, 64(4):543, 2003. doi:10.1209/epl/i2003-00268-x.

[21] Shelly Tzlil, Markus Deserno, William M Gelbart, and Avinoam Ben-Shaul. A statistical-thermodynamic model of viral budding. *Biophysical journal*, 86(4):2037–2048, 2004. doi:10.1016/S0006-3495(04)74265-4.

[22] Huajian Gao, Wendong Shi, and Lambert B Freund. Mechanics of receptor-mediated endocytosis. *Proceedings of the National Academy of Sciences*, 102(27):9469–9474, 2005. doi:10.1073/pnas.0503879102.

[23] LB Freund and Yuan Lin. The role of binder mobility in spontaneous adhesive contact and implications for cell adhesion. *Journal of the Mechanics and Physics of Solids*, 52(11):2455–2472, 2004. doi:10.1016/j.jmps.2004.05.004.

[24] VB Shenoy and LB Freund. Growth and shape stability of a biological membrane adhesion complex in the diffusion-mediated regime. *Proceedings of the National Academy of Sciences*, 102(9):3213–3218, 2005. doi:10.1073/pnas.0500368102.

[25] Alexei Boulbitch, Zeno Guttenberg, and Erich Sackmann. Kinetics of membrane adhesion mediated by ligand–receptor interaction studied with a biomimetic system. *Biophysical Journal*, 81(5):2743–2751, 2001. doi:10.1016/S0006-3495(01)75917-6.

[26] Z Guttenberg, B Lorz, E Sackmann, and A Boulbitch. First-order transition between adhesion states in a system mimicking cell-tissue interaction. *Europhysics Letters*, 54(6):826, 2001. doi:10.1209/epl/i2001-00328-9.

[27] Xin Yi and Huajian Gao. Kinetics of receptor-mediated endocytosis of elastic nanoparticles. *Nanoscale*, 9(1):454–463, 2017. doi:10.1039/C6NR07179A.

[28] Arijit Mahapatra, Can Uysalel, and Padmini Rangamani. The mechanics and thermodynamics of tubule formation in biological membranes. *The Journal of membrane biology*, 254:273–291, 2021. doi:10.1007/s00232-020-00164-9.

[29] Brian Kobilka. The structural basis of g-protein-coupled receptor signaling (nobel lecture). *Angewandte Chemie (International ed. in English)*, 52(25):6380, 2013. doi:10.1002/anie.201302116.

[30] Angelo R Carotenuto, Laura Lunghi, Valentina Piccolo, Mahnoush Babaei, Kaushik Dayal, Nicola Pugno, Massimiliano Zingales, Luca Deseri, and Massimiliano Fraldi. Mechanobiology predicts raft formations triggered by ligand-receptor activity across the cell membrane. *Journal of the Mechanics and Physics of Solids*, 141:103974, 2020. doi:10.1016/j.jmps.2020.103974.

[31] Gianmarco Nuzzo, Emanuela Bologna, Kaushik Dayal, and Massimiliano Zingales. Fractional diffusion of membrane receptors in endocytosis pathway. *Theor. Appl. Mech. AIMETA*, 2023(26):305–310, 2022. doi:10.21741/9781644902431-50.

[32] Richard Klausner, Jos Van Renswoude, Joe Harford, Carla Wofsy, and Byron Goldstein. Mathematical modeling of receptor-mediated endocytosis. *Endocytosis*, pages 259–279, 1985. doi:10.1007/978-1-4615-6904-6_9.

[33] Kennie U Dee and Michael L Shuler. A mathematical model of the trafficking of acid-dependent enveloped viruses: Application to the binding, uptake, and nuclear accumulation of baculovirus. *Biotechnology and bioengineering*, 54(5):468–490, 1997.

[34] Long Li, Yudie Zhang, and Jizeng Wang. Effects of ligand distribution on receptor-diffusion-mediated cellular uptake of nanoparticles. *Royal Society open science*, 4(5):170063, 2017. doi:10.1098/rsos.170063.

[35] Yudie Zhang, Long Li, and Jizeng Wang. Role of ligand distribution in the cytoskeleton-associated endocytosis of ellipsoidal nanoparticles. *Membranes*, 11(12):993, 2021. doi:10.3390/membranes11120993.

[36] Qingrong Zhang, Siying Li, Yu Yang, Yuping Shan, and Hongda Wang. Studying structure and functions of cell membranes by single molecule biophysical techniques. *Biophysics Reports*, 7(5):384–398, 2021. doi:10.52601/bpr.2021.210018.

[37] Tillmann Wiegold, Sandra Klinge, Robert P Gilbert, and Gerhard A Holzapfel. Numerical simulation of the viral entry into a cell driven by receptor diffusion. *Computers & Mathematics with Applications*, 84:224–243, 2021. doi:10.1016/j.camwa.2020.12.012.

[38] David M Richards and Robert G Endres. Target shape dependence in a simple model of receptor-mediated endocytosis and phagocytosis. *Proceedings of the National Academy of Sciences*, 113(22):6113–6118, 2016. doi:10.1073/pnas.1521974113.

[39] Zhiqiang Shen, Huilin Ye, Xin Yi, and Ying Li. Membrane wrapping efficiency of elastic nanoparticles during endocytosis: Size and shape matter. *ACS nano*, 13(1):215–228, 2018. doi:10.1021/acsnano.8b05340.

[40] Huayuan Tang, Hongwu Zhang, Hongfei Ye, and Yonggang Zheng. Receptor-mediated endocytosis of nanoparticles: roles of shapes, orientations, and rotations of nanoparticles. *The Journal of Physical Chemistry B*, 122(1):171–180, 2018. doi:10.1021/acs.jpcb.7b09619.

[41] Milad Rismanian and Behzad Damirchi. Analytical investigation of nonfickian receptor-mediated endocytosis. *bioRxiv*, page 808212, 2019. doi:10.1101/808212.

[42] Thomas D. Pollard, William C. Earnshaw, Jennifer Lippincott-Schwartz, and Graham T. Johnson. *Cell Biology: Third Edition*. Elsevier Inc., 2016.

[43] Gareth Griffiths, Jean Gruenberg, Mark Marsh, Jens Wohlmann, Arwyn T Jones, and Robert G Parton. Nanoparticle entry into cells; the cell biology weak link. *Advanced Drug Delivery Reviews*, page 114403, 2022. doi:10.1016/j.addr.2022.114403.

[44] Pier Paolo Di Fiore and Mark von Zastrow. Endocytosis, signaling, and beyond. *Cold Spring Harbor perspectives in biology*, 6(8):a016865, 2014. doi:10.1101/cshperspect.a016865.

[45] Sulin Zhang, Huajian Gao, and Gang Bao. Physical principles of nanoparticle cellular endocytosis. *ACS nano*, 9(9):8655–8671, 2015. doi:10.1021/acsnano.5b03184.

[46] John C Charpentier and Philip D King. Mechanisms and functions of endocytosis in t cells. *Cell Communication and Signaling*, 19(1):1–12, 2021. doi:10.1186/s12964-021-00766-3.

[47] Anatoly Zhukov and Valery Popov. Eukaryotic cell membranes: Structure, composition, research methods and computational modelling. *International Journal of Molecular Sciences*, 24(13):11226, 2023. doi:10.3390/ijms241311226.

[48] Wonhwa Cho and Robert V Stahelin. Membrane-protein interactions in cell signaling and membrane trafficking. *Annu. Rev. Biophys. Biomol. Struct.*, 34:119–151, 2005. doi:10.1146/annurev.biophys.33.110502.133337.

[49] S Jonathan Singer and Garth L Nicolson. The fluid mosaic model of the structure of cell membranes: Cell membranes are viewed as two-dimensional solutions of oriented globular proteins and lipids. *Science*, 175(4023):720–731, 1972. doi:10.1126/science.175.4023.720.

[50] Nicole J Yang and Marlon J Hinner. Getting across the cell membrane: an overview for small molecules, peptides, and proteins. *Site-Specific Protein Labeling: Methods and Protocols*, pages 29–53, 2015. doi:10.1007/978-1-4939-2272-7_3.

[51] Garth L Nicolson and Gonzalo Ferreira de Mattos. The fluid–mosaic model of cell membranes: A brief introduction, historical features, some general principles, and its adaptation to current information. *Biochimica et Biophysica Acta (BBA)-Biomembranes*, page 184135, 2023. doi:10.1016/j.bbamem.2023.184135.

[52] John S O'Brien. Cell membranes—composition: structure: function. *Journal of theoretical biology*, 15(3):307–324, 1967. doi:10.1016/0022-5193(67)90140-3.

[53] Mark S Bretscher. The molecules of the cell membrane. *Scientific American*, 253(4):100–109, 1985. doi:10.1038/scientificamerican1085-100.

[54] Lawrence Rajendran and Kai Simons. Lipid rafts and membrane dynamics. *Journal of cell science*, 118(6):1099–1102, 2005. doi:10.1242/jcs.01681.

[55] Tomasz Róg and Ilpo Vattulainen. Cholesterol, sphingolipids, and glycolipids: what do we know about their role in raft-like membranes? *Chemistry and physics of lipids*, 184:82–104, 2014. doi:10.1016/j.chemphyslip.2014.10.004.

[56] LLM Van Deenen. Some structural investigations on phospholipids from membranes. *Journal of the American Oil Chemists Society*, 43:296–304, 1966. doi:10.1007/BF02609677.

[57] Gerrit Van Meer, Dennis R Voelker, and Gerald W Feigenson. Membrane lipids: where they are and how they behave. *Nature reviews Molecular cell biology*, 9(2):112–124, 2008. doi:10.1038/nrm2330.

[58] Williams R Nes. Role of sterols in membranes. *Lipids*, 9(8):596–612, 1974. doi:10.1007/BF02532509.

[59] Dick Hoekstra, Olaf Maier, Johanna M van der Wouden, Tounsia Aït Slimane, and Sven CD van IJzendoorn. Membrane dynamics and cell polarity: the role of sphingolipids. *Journal of lipid research*, 44(5):869–877, 2003. doi:10.1194/jlr.R300003-JLR200.

[60] Elina Ikonen and Xin Zhou. Cholesterol transport between cellular membranes: A balancing act between interconnected lipid fluxes. *Developmental Cell*, 56(10):1430–1436, 2021. doi:10.1016/j.devcel.2021.04.025.

[61] Jennifer A Koenig and J Michael Edwardson. Endocytosis and recycling of G protein-coupled receptors. *Trends in pharmacological sciences*, 18(8):276–287, 1997. doi:10.1016/S0165-6147(97)01091-2.

[62] Gary J Doherty and Harvey T McMahon. Mechanisms of endocytosis. *Annual review of biochemistry*, 78:857–902, 2009. doi:10.1146/annurev.biochem.78.081307.110540.

[63] Portia Gough and Ian A Myles. Tumor necrosis factor receptors: pleiotropic signaling complexes and their differential effects. *Frontiers in immunology*, 11:585880, 2020. doi:10.3389/fimmu.2020.585880.

[64] Johnathan Canton. Macropinocytosis: new insights into its underappreciated role in innate immune cell surveillance. *Frontiers in immunology*, 9:2286, 2018. doi:10.3389/fimmu.2018.02286.

[65] Xiao Peng Lin, Justine D Mintern, and Paul A Gleeson. Macropinocytosis in different cell types: similarities and differences. *Membranes*, 10(8):177, 2020. doi:10.3390/membranes10080177.

[66] Björn Morén, Claudio Shah, Mark T Howes, Nicole L Schieber, Harvey T McMahon, Robert G Parton, Oliver Daumke, and Richard Lundmark. EHD2 regulates caveolar dynamics via ATP-driven targeting and oligomerization. *Molecular Biology of the Cell*, 23(7):1316–1329, 2012. doi:10.1091/mbc.e11-09-0787.

[67] Valerie Legendre-Guillemin, Sylwia Wasiak, Natasha K Hussain, Annie Angers, and Peter S McPherson. ENTH/ANTH proteins and clathrin-mediated membrane budding. *Journal of Cell Science*, 117(1):9–18, 2004. doi:10.1242/jcs.00928.

[68] Jophin G Joseph and Allen P Liu. Mechanical regulation of endocytosis: new insights and recent advances. *Advanced biosystems*, 4(5):1900278, 2020. doi:10.1002/adbi.201900278.

[69] Iris K Jarsch, Frederic Daste, and Jennifer L Gallop. Membrane curvature in cell biology: An integration of molecular mechanisms. *Journal of Cell Biology*, 214(4):375–387, 2016. doi:10.1083/jcb.201604003.

[70] Joshua P Ferguson, Scott D Huber, Nathan M Willy, Esra Aygün, Sevde Goker, Tugba Atabey, and Comert Kural. Mechanoregulation of clathrin-mediated endocytosis. *Journal of Cell Science*, 130(21):3631–3636, 2017. doi:10.1242/jcs.205930.

[71] W Helfrich. Elastic Properties of Lipid Bilayers: Theory and Possible Experiments. *Zeitschrift für Naturforschung C*, 28(11-12):693–703, 1973. doi:10.1515/znc-1973-11-1209.

[72] Gerald Lim H. W., Michael Wortis, and Ranjan Mukhopadhyay. Stomatocyte–discocyte–echinocyte sequence of the human red blood cell: Evidence for the bilayer– couple hypothesis from membrane mechanics. *Proceedings of the National Academy of Sciences*, 99(26):16766–16769, 2002. doi:10.1073/pnas.202617299.

[73] Tobias Baumgart, Samuel Hess, and Watt Webb. Imaging coexisting fluid domains in biomembrane models coupling curvature and line tension. *Nature*, 425:821–4, 11 2003. doi:10.1038/nature02013.

[74] T. Baumgart, S. Das, W.W. Webb, and J.T. Jenkins. Membrane elasticity in giant vesicles with fluid phase coexistence. *Biophysical Journal*, 89(2):1067–1080, 2005. doi:10.1529/biophysj.104.049692.

[75] Masao Doi, Sam F Edwards, and Samuel Frederick Edwards. *The Theory of Polymer Dynamics*, volume 73. Oxford University Press, 1988.

[76] Vincent E Debets, Liesbeth MC Janssen, and Anđela Šarić. Characterising the diffusion of biological nanoparticles on fluid and cross-linked membranes. *Soft Matter*, 16(47):10628–10639, 2020. doi:10.1039/D0SM00712A.

[77] Ping-hung Chen, Huiyu Yao, and Lily Jun-shen Huang. Cytokine receptor endocytosis: new kinase activity-dependent and-independent roles of pi3k. *Frontiers in Endocrinology*, 8:78, 2017. doi:10.3389/fendo.2017.00078.

[78] Paul MP Van Bergen En Henegouwen. Eps15: a multifunctional adaptor protein regulating intracellular trafficking. *Cell Communication and Signaling*, 7:1–11, 2009. doi:10.1186/1478-811x-7-24.

[79] Ali Naji, Alex J Levine, and Philip A Pincus. Corrections to the Saffman-Delbrück mobility for membrane bound proteins. *Biophysical journal*, 93(11):L49–L51, 2007. doi:10.1529/biophysj.107.119222.

[80] Matteo Arricca, Alberto Salvadori, Claudia Bonanno, and Mattia Serpelloni. Modeling receptor motility along advecting lipid membranes. *Membranes*, 12(7):652, 2022. doi:10.3390/membranes12070652.

[81] Vladimir Adrien, Gamal Rayan, Ksenia Astafyeva, Isabelle Broutin, Martin Picard, Patrick Fuchs, Wladimir Urbach, and Nicolas Taulier. How to best estimate the viscosity of lipid bilayers. *Biophysical Chemistry*, 281:106732, 2022. doi:10.1016/j.bpc.2021.106732.

[82] Igor Podlubny. *Fractional Differential Equations: An Introduction To Fractional Derivatives, Fractional Differential Equations, to Methods of their Solution and some of their Applications*. Elsevier, 1998.

[83] Rudolf Gorenflo, Anatoly A Kilbas, Francesco Mainardi, Sergei V Rogosin, et al. *Mittag-Leffler Functions, Related Topics and Applications*. Springer, 2020. doi:10.1007/978-3-662-61550-8.

[84] Diego A Murio. Implicit finite difference approximation for time fractional diffusion equations. *Computers & Mathematics with Applications*, 56(4):1138–1145, 2008. doi:10.1016/j.camwa.2008.02.015.

[85] Changpin Li and Fanhai Zeng. *Numerical Methods for Fractional Calculus*, volume 24. CRC Press, 2015. doi:10.1201/b18503.

[86] Changpin Li and Min Cai. *Theory and numerical approximations of fractional integrals and derivatives*. SIAM, 2019. doi:10.1137/1.9781611975888.

[87] Gianmarco Nuzzo, Fabiana Amiri, Salvatore Russotto, Emanuela Bologna, and Massimiliano Zingales. A fractional-order theory of phase transformation in presence of anomalous heat transfer. *Theor. Appl. Mech. AIMETA*, 2023(26):77–82, 2022. doi:10.21741/9781644902431-13.

[88] Sushil Chandra Gupta. *The classical Stefan problem: basic concepts, modelling and analysis with quasi-analytical solutions and methods*, volume 45. Elsevier, 2017. doi:10.1016/C2017-0-02306-6.

[89] Selçuk Kutluay, AR Bahadir, and A Özdeş. The numerical solution of one-phase classical stefan problem. *Journal of computational and applied mathematics*, 81(1):135–144, 1997. doi:10.1016/S0377-0427(97)00034-4.

[90] William D Murray and Fred Landis. Numerical and machine solutions of transient heat-conduction problems involving melting or freezing: Part I—Method of analysis and sample solutions. *Journal of Heat Transfer*, 81(2):106–112, 1959. doi:10.1115/1.4008149.

[91] Nacer Sadoun, El-Khider Si-Ahmed, Pierre Colinet, and Jack Legrand. On the boundary immobilization and variable space grid methods for transient heat conduction problems with phase change: Discussion and refinement. *Comptes Rendus Mécanique*, 340(7):501–511, 2012. doi:10.1016/j.crme.2012.03.003.


y tea's gone cold, I'm wondering why,
I got out of bed at all
The morning rain clouds up my window
And I can't see at all
And even if I could, it'd all be gray
But your picture on my wall
It reminds me that it's not so bad
It's not so bad

Dido, "Thank you", *No Angel*,
Arista Records, Cheeky Records, 1999.